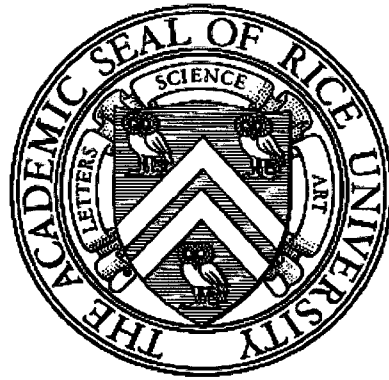


RICE UNIVERSITY



Tests of inter-hotspot motion and of hotspot motion relative to the spin axis

by

Emilia Koivisto

DOCTOR OF PHILOSOPHY

HOUSTON, TEXAS

MAY 2010

UMI Number: 3421148

All rights reserved

INFORMATION TO ALL USERS

The quality of this reproduction is dependent upon the quality of the copy submitted.

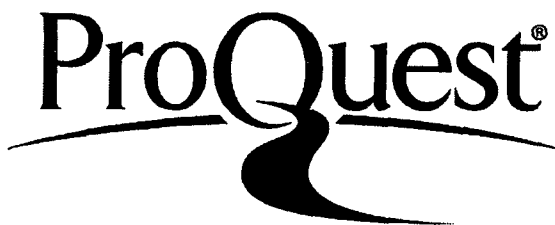
In the unlikely event that the author did not send a complete manuscript and there are missing pages, these will be noted. Also, if material had to be removed, a note will indicate the deletion.



UMI 3421148

Copyright 2010 by ProQuest LLC.

All rights reserved. This edition of the work is protected against unauthorized copying under Title 17, United States Code.



ProQuest LLC
789 East Eisenhower Parkway
P.O. Box 1346
Ann Arbor, MI 48106-1346

RICE UNIVERSITY

Tests of inter-hotspot motion and of hotspot motion relative to the spin axis

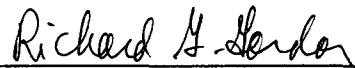
by

Emilia Anna-Liisa Koivisto

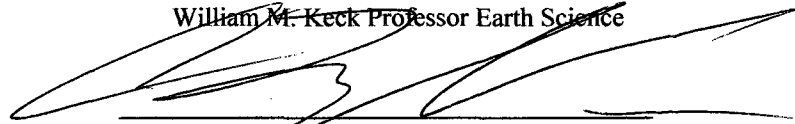
A THESIS SUBMITTED
IN PARTIAL FULFILLMENT OF THE
REQUIREMENTS FOR THE DEGREE

Doctor of Philosophy

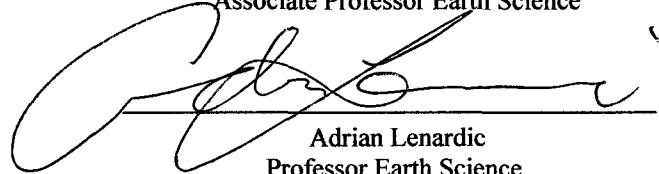
APPROVED, THESIS COMMITTEE:



Richard G. Gordon, Chair
William M. Keck Professor Earth Science



Cin-Ty Lee
Associate Professor Earth Science



Adrian Lenardic
Professor Earth Science



Patricia Reiff
Professor Physics and Astronomy

HOUSTON, TEXAS
MAY 2010

Abstract

Tests of inter-hotspot motion and of hotspot motion relative to the spin axis

by

Emila Koivisto

First, an updated Pacific paleomagnetic skewness pole for chron 32 (72 Ma) is presented. The updated paleomagnetic pole corrects for the spreading-rate dependence of anomalous skewness, a correction which hasn't been applied to Pacific skewness poles before. The presence of anomalous skewness is one of the main factors limiting the accuracy of paleomagnetic poles determined from the skewness data. Thus, successfully correcting for the anomalous skewness, as was done in this study, significantly improves the reliability of the skewness poles. The earlier assertions that the Hawaiian hotspot has shifted southward relative to the spin axis by 13° since ≈ 72 Ma are also confirmed.

Second, updated reconstructions of the Pacific plate relative to the hotspots for the past 68 million years are presented, with the uncertainties in the reconstructions. Plate-circuit reconstructions are used to predict the tracks of some major Indo-Atlantic hotspots (Tristan da Cunha, Réunion and Iceland) from the Pacific-hotspot plate motion and the rates of relative motion between the Pacific and Indo-Atlantic hotspots are estimated. Within the uncertainties, motion between the hotspots is found insignificant for the past 48 million years. For earlier times, a systematic error in the plate circuit used to make the predictions is inferred and which may be due to unmodeled motion between East and West Antarctica. If the observed discrepancy can be shown to correspond to an error in the plate circuit, the southward motion of the Hawaiian hotspot of 13° since ≈ 72 Ma can

likely be attributed to true polar wander. Building on the above-mentioned work, finally, for the first time, a globally self-consistent model of plate motions relative to the global hotspots for the past 48 million years is presented, and the implications of this model to the question of relative hotspot motion discussed. The provided globally self-consistent set of reconstructions can be used as a fixed frame of reference for absolute plate motions, and true polar wander, for the past 48 million years.

Acknowledgements

First, I would like to thank my adviser Dr. Richard Gordon for his patience in guiding me through the Ph.D. I am eternally grateful for his mentoring, I have learned from the best. Thanks also go out to my committee members Dr. Cin-Ty Lee, Dr. Adrian Lenardic and Dr. Patricia Reiff for giving of their time. Thanks to Dr. Katerina Petronotis for supplying the set of spreading rates she estimated for the Pacific plate crossings of anomaly 32 used in Petronotis and Gordon (1999). Thanks to Dr. Jérôme Dyment and Dr. Jafar Arkani-Hamed for their spreading-rate-dependent model of anomalous skewness for anomaly 32 and helpful comments on the work presented in Chapter 1. Also, thanks to David Andrews whose work in Rice in many ways was a starting point to the work presented herein in Chapters 2 and 3. I also thank my friends in Rice, you know who you are, who were a great support to me. Most of all, I am eternally grateful to my husband, and best friend, for his love and support. Finally, I would like to thank my parents for making this all possible, their love has guided me here. Special thanks to U.S. National Science Foundation for support. This material is based upon work supported by the National Science Foundation under Grant No. 0527375. Any opinions, findings, and conclusions or recommendations expressed in this material are those of the author(s) and do not necessarily reflect the views of the National Science Foundation.

Table of Contents

Abstract.....	iii
Acknowledgements.....	v
Introduction.....	1
Chapter 1.....	6
Revised Chron 32 (71.6 to 73.0 Ma) Paleomagnetic Pole for the Pacific Plate Incorporating Spreading-Rate-Dependent Anomalous Skewness.....	6
Summary.....	6
1.1 Introduction.....	7
1.2 Anomalous Skewness.....	8
1.3 Methods.....	11
1.3.1 Anomalous Skewness.....	11
1.3.2 Model Estimation.....	12
1.4 Magnetic Profiles and Spreading Rates.....	14
1.5 Results.....	18
1.6 Discussion.....	22
1.7 Conclusions.....	24
Tables.....	24
Chapter 2.....	29
Tests of Fixity of the Indo-Atlantic Hotspots Relative to Pacific Hotspots.....	29
Summary.....	29
2.1 Introduction.....	29
2.2 Methods and Plate Circuits.....	32
2.3 Hotspot Tracks.....	36
2.4 Results.....	40
2.4.1 Pacific-Hotspot Rotations and Uncertainties Since 68 Ma.....	40
2.4.2 Predicted Tracks.....	41
2.4.3 Summary of the Results.....	46
2.5 Discussion.....	46
2.6 Conclusions.....	48
Tables.....	48
Chapter 3.....	54
A Globally Self-Consistent Model of Plate Motions Relative to the Hotspots for the Past 48 Million Years.....	54
Summary.....	54
3.1 Introduction.....	55
3.2 Methods and Plate Circuits.....	57
3.2.1 Plate-Hotspot Model.....	57
3.2.2 Plate-Circuit.....	58
3.3 Age Progression Along the Hotspot Tracks.....	61
3.3.1 Hawaiian-Emperor and Louisville Tracks.....	62
3.3.2 Tristan da Cunha.....	64
3.3.3 Réunion.....	67
3.3.4 Iceland.....	70

3.4	Results.....	72
3.5	Discussion.....	81
3.6	Conclusions.....	82
	Tables.....	83
	Conclusions.....	90
	Appendix A.....	92
	References.....	102

Introduction

Hotspots are volcanic anomalies, either in an intraplate setting or in the form of excessive volcanism along the plate boundaries, not explained by classic plate tectonics. In the early 70's, along with a deep mantle origin, hotspots were proposed to move so slowly relative to one another such that they could be used as a reference frame fixed in the deep mantle for describing plate motions in an "absolute" sense (e.g. Morgan, 1972). In this scenario, the stationary plumes leave trails of age-progressive volcanism on the plates as the plates move over them. These trails can then be used to track the history of absolute global plate motions. Ever since the idea was first introduced, however, the rates of relative hotspot motion, and thus the limits of the hotspot frame of reference, have remained a source of heated debate with suggestions ranging from apparent fixity (e.g. Morgan, 1971; 1972; Duncan, 1981; Müller et al., 1993; and also our position) to rapid motion (e.g. Molnar and Stock (1987) and up to 80 mm a^{-1} by Raymond et al. (2000)) between the hotspots.

The question of inter-hotspot motion is closely related to the estimation of true polar wander—rotation of the whole solid earth relative to the spin axis. A fundamental problem of global tectonics and paleomagnetism is determining which part of apparent polar wander—the apparent movement of age-progressive paleomagnetic poles relative to the continent in question—is due to plate motion, and which part is due to true polar wander. One approach for separating these is available if the hotspots are indeed tracking the motion of the mantle beneath the asthenosphere and are moving slowly relative to one another. In this case, a model of plate motion relative to the hotspots can be used to

predict the positions of past paleomagnetic poles relative to the spin axis and thus estimate the amount of true polar wander.

The Pacific plate provides an excellent opportunity to study these questions because it hosts two of the most prominent and best sampled hotspot tracks, the Hawaiian-Emperor and Louisville chains, and paleomagnetic poles can be estimated from skewness of the marine magnetic anomalies. Thus, to make progress on answering these questions, high-quality paleomagnetic poles for the Pacific plate are needed, as well as estimates of the Pacific plate motion relative to the hotspots, along with the uncertainties in such motion. This thesis presents new results that address all these questions.

First, in Chapter 1, we present an updated high-quality Pacific paleomagnetic pole for chron 32 (≈ 72 Ma) determined from the skewness of magnetic anomaly 32 (Petronotis and Gordon, 1999). In the absence of oriented rock samples, as is often the case for oceanic plates, paleomagnetic poles can be determined from asymmetry (skewness) of marine magnetic anomalies. The updated paleomagnetic pole corrects for the spreading-rate dependence of anomalous skewness (Dyment and Arkani-Hamed, 1995), a correction which hasn't been applied to Pacific skewness poles before. Anomalous skewness can be thought of as the systematic difference between the observed skewness and the skewness predicted by a simple magnetization model with rectangular two-dimensional layer 2A prisms of alternating polarity separated by vertical boundaries. The presence of anomalous skewness is one of the main factors limiting the accuracy of paleomagnetic poles determined from the skewness data. Thus, successfully correcting for the anomalous skewness, as was done in this study, significantly improves

the reliability of the skewness poles. We also confirm the earlier assertions that the Hawaiian hotspot has shifted southward relative to the spin axis by 13° since ≈ 72 Ma.

We believe that many of the discrepancies in the suggested rates of relative hotspot motion can be attributed to shortcomings in the methods used in the previous studies, in particular to shortcomings in quantifying the inherent uncertainties.

Additionally, recent improvements in the age progression along the hotspot tracks (e.g. Sharp and Clague, 2006; Koppers et al., 2004) and geomagnetic reversal time scale, lead to significant changes in results. In Chapter 2, we build on a new method for objectively estimating plate-hotspot rotations and their uncertainties (Andrews et al., 2006), and present updated reconstructions of the Pacific plate relative to the hotspots for the past 68 million years with the uncertainties in the reconstructions. To investigate the question of relative hotspot motion, we use plate-circuit reconstructions to predict the tracks of some major Indo-Atlantic hotspots (Tristan da Cunha, Réunion and Iceland) from our Pacific-hotspot rotations and estimate the rates of relative motion between the Pacific and Indo-Atlantic hotspots. Appendix A provides a detailed discussion on the choices made for the plate circuit. Besides the uncertainties in plate-hotspot rotations, uncertainties in relative plate motions are accumulated through the plate circuit to obtain the final uncertainty (in the form of two-dimensional 95 per cent confidence regions) in the predicted positions. We find that the predicted and observed tracks agree much better than found previously, for the past 48 million years, and that within the uncertainties, motion between the hotspots is insignificant. For the discrepancy observed at earlier times, we suggest a systematic error in the plate circuit used to make the predictions, most likely unmodeled motion between East and West Antarctica. If the observed discrepancy can be shown to

correspond to an error in the plate circuit, the southward motion of the Hawaiian hotspot of 13° since ≈ 72 Ma, as indicated in Chapter 1, can likely be attributed to true polar wander.

In line with the conclusions of the above mentioned work, in Chapter 3 we present a globally self-consistent model of plate motions relative to the hotspots for the past 48 million years and discuss the implications of this model to the question of relative hotspot motion. In this study, we use the most up-to-date reconstructions together with radiometric dates along the major hotspot tracks to derive a plate motion model relative to the major hotspots in the Pacific, Atlantic and Indian Oceans. We use the tracks of Hawaiian, Louisville, Tristan da Cunha, Réunion, and Iceland hotspots. We also present plate-circuit reconstructions for the Hawaiian, Louisville, Tristan da Cunha, Réunion, and Iceland hotspots assuming them to be fixed relative to a global hotspot reference frame, and plate-circuit reconstructions for the Hawaiian and Louisville hotspots assuming them to be fixed relative to an Indo-Atlantic hotspot reference frame. Finally, we compare the different hotspot frames of reference and make a note that they are not significantly different from each other for the past 48 million years, and thus, show that the provided set of reconstructions can be used as a fixed frame of reference for plate motions. The new set of rotations presented here provide a firm basis for estimating absolute plate motions for the past 48 million years and, in particular, can be used to separate paleomagnetically determined apparent polar wander into the component due to plate motion and the component due to true polar wander.

As a final note, we must acknowledge what is referred to as the Great Plume Debate. Even though the deep mantle plume hypothesis successfully predicts many

observed characteristics of hotspot volcanism (e.g. age-progression along the tracks, flood basalts at the ends of the tracks, topographic swells associated with the hotspots etc.; Campbell, 2007), some of the observed variety in volcanism remains to be resolved (e.g. short vs. long-lived hotspot tracks etc.). Over the years, a number of other attempts to explain hotspot volcanism (e.g. the idea of propagating cracks expounded by Don Anderson) have surfaced, curiously resulting in a division of the Earth Science community into pro-plume and anti-plume camps. Studies in between these two camps (e.g. Courtillot et al., 2003) emphasize the need to develop a variety of models to fit the observations, suggesting deep mantle origin to only a handful of hotspots. Some of the confusion contributing to large inter-hotspot drift rates found in previous studies may be understood if hotspots with different origins have been erroneously combined. However, even though the fixed hotspot approximation originally relies on stationary deep mantle plumes, the work herein does not, in itself, make any deeper assumptions about the origin of hotspots as it merely concentrates on the kinematic side of the story, that is, on estimating the rates of relative motion between the hotspots. The observed fixity of the hotspots (Hawaii, Louisville, Tristan da Cunha, Réunion and Iceland as used in this study), at least for the past 48 million years, however, is not easily explained by any other proposed mechanism than the presence of relatively stationary deep mantle plumes.

Chapter 1

Revised Chron 32 (71.6 to 73.0 Ma) Paleomagnetic Pole for the Pacific Plate Incorporating Spreading-Rate-Dependent Anomalous Skewness

Summary

Paleomagnetic poles for the Pacific plate have important implications for estimating the motion of the Pacific plate relative to the spin axis, for testing plate reconstructions, for estimating the motion of Pacific hotspots relative to the spin axis, and for estimating the motion of hotspots relative to one another. Skewness estimates of the shapes of marine magnetic anomalies due to seafloor spreading have been successfully used before to estimate Pacific plate paleomagnetic poles. The presence of spreading-rate-dependent anomalous skewness may limit the accuracy of such poles, however. Here we test a previously proposed model for spreading-rate-dependent anomalous skewness with a set of 108 skewness estimates previously used to estimate the chron 32 (71.6–73.0 Ma) paleomagnetic pole for the Pacific plate. The resulting revised paleomagnetic pole lies only 0.2° to 1.3° from the prior pole depending on the set of spreading rates used for the spreading-rate-dependent correction for anomalous skewness. Additional spreading-rate-independent adjustments to anomalous skewness beyond those predicted by the spreading-rate-dependent model insignificantly reduce the misfit to the data. The results support the assertion that Pacific plate poles determined from low-paleolatitude skewness data are insensitive to anomalous skewness. They also support the validity of the

spreading-rate-dependent model for anomalous skewness. The revised pole, as was the case for the original pole, shows that the Hawaiian hotspot has shifted southward relative to the spin axis by 13° since ≈ 72 Ma.

1.1 Introduction

Paleomagnetic poles for the Pacific plate have important implications for estimating the motion of the Pacific plate relative to the spin axis, for testing plate reconstructions, for estimating the motion of Pacific hotspots relative to the spin axis, and for estimating the relative motion of Pacific hotspots relative to non-Pacific hotspots. Because fully oriented samples cannot be easily collected on oceanic plates, apparent polar wander (APW) paths for oceanic plates are mainly estimated by methods other than laboratory analysis of oriented rock samples. Marine magnetic anomalies over the oceanic plates provide a record of the paleomagnetic field from Late Jurassic time to the present. The relative ages of these anomalies are well known. Skewness (asymmetry) data from these anomalies have the potential to provide an APW path with fine age resolution. In prior studies, several Pacific plate paleomagnetic poles have been determined in whole or in part from skewness data and have provided strong evidence for southward motion of Pacific hotspots relative to the spin axis (Gordon, 1982; Acton and Gordon, 1991; Petronotis et al., 1992; 1994; Petronotis and Gordon, 1999).

A possible weakness of these earlier results is that they do not account for the spreading-rate dependence of anomalous skewness (Roest et al., 1992; Dyment et al., 1994). Here we focus on the Pacific plate pole determined for anomaly 32 (71.6–73.0

Ma for the time scale of Cande and Kent (1995), which is used throughout this chapter) and the possible effect of spreading-rate-dependent anomalous skewness on its estimated location. We explicitly account for this dependence and show its consistency with Pacific plate anomaly 32 skewness data (Petronotis and Gordon, 1999). This consistency supports the validity of the model of Dyment and Arkani-Hamed (1995). We find a revised paleomagnetic pole for the Pacific plate that differs little (by 0.2° to 1.3°) from the original and confirm that the Hawaiian hotspot has shifted 13° southward relative to the spin axis since ≈ 72 Ma (Petronotis and Gordon, 1999).

1.2 Anomalous Skewness

In a simple model with vertical polarity boundaries, the skewness of an anomaly in total magnetic field intensity depends on the ambient field direction, the remanent magnetization direction, and the strike of the magnetic lineations (Schouten and McCamy, 1972; Blakely and Cox, 1972; Schouten and Cande, 1976). Skewness is quantified as the phase shift that best transforms an observed magnetic anomaly to a shape expected from a simple model of sea-floor magnetization (i.e. the rectangular two-dimensional layer 2A prisms with vertical reversal boundaries and vertical magnetization with alternating polarity). This simple oceanic crustal magnetization model is only a first-order representation, however, and does not account for the details of the source of marine magnetic anomalies. The difference between the observed skewness and the skewness that is predicted by the simple magnetization model is called anomalous

skewness. Its presence may limit the accuracy of paleomagnetic poles determined from skewness data.

Early applications of skewness analysis demonstrated the existence of anomalous skewness (Cande, 1976). The size of anomalous skewness was estimated from the discrepancy between the skewness of anomalies on one plate compared with that of their counterparts on another plate across a mid-ocean ridge. Anomalous skewness is more difficult to estimate, though, when the counterparts have been subducted, as is the case for many anomalies on the Pacific plate. Petronotis et al. (1992) presented a solution to this problem. They assumed that anomalous skewness is independent of spreading rate and simultaneously estimated anomalous skewness and a best-fitting paleomagnetic pole from skewness data from a single plate. Their spreading-rate-independent method has been applied to some key Pacific plate anomalies, including anomalies 25r and 32 (Petronotis et al., 1994; Petronotis and Gordon, 1999).

In disagreement with the spreading-rate independence assumed by Petronotis et al. (1992), however, Roest et al. (1992) and Dyment et al. (1994) showed that the size of anomalous skewness varies with spreading rate. Thus, the question remained if a correction for the spreading-rate dependence of anomalous skewness would result in significant changes to the poles determined by Petronotis et al. (1994) and Petronotis and Gordon (1999).

Several models have been proposed to explain anomalous skewness including temporal variations of the geomagnetic field intensity within a given chron (Cande, 1978), tectonic rotation of the source layer (Cande, 1978; Verosub and Moores, 1981), acquisition of a secondary magnetization in crustal layer 2A (Raymond and LaBrecque,

1987; Beske-Diehl, 1989), and magnetization of the deep crust and uppermost mantle controlled by the thermal structure of the oceanic lithosphere (Blakely, 1976; Cande, 1976; Kidd, 1977; Harrison, 1987; Arkani-Hamed, 1988; 1989). But none of these models account for the tendency of anomalous skewness to decrease with increasing spreading rate and to become negligible above spreading half rates of $\approx 50 \text{ mm a}^{-1}$ (e.g. Roest et al., 1992; Dyment et al., 1994). A model based on spreading-rate-dependent thermo-viscous remanent magnetization of oceanic crustal layer 3 and the uppermost mantle successfully explains these characteristics of anomalous skewness (Dyment and Arkani-Hamed, 1995; Dyment et al., 1997). In the model the magnetic structure of the oceanic lithosphere depends on spreading rate with parameters adjusted to fit the observed spreading-rate dependence of anomalous skewness. At a given spreading rate, the anomalous skewness is different for different anomalies. This is related to the effect of unevenly distributed neighboring magnetic sources on the skewness of these anomalies, which Dyment and Arkani-Hamed (1995) refer to as the sequence effect.

At intermediate and slow spreading rates, the magnetization polarity boundaries of the lower crust and uppermost mantle are non-vertical and curved, flattening with distance from the ridge axis, and are responsible for the anomalous skewness. The transition occurs at a spreading half rate of $\approx 50 \text{ mm a}^{-1}$ (above which anomalous skewness is negligible) and is probably controlled by the percolation of hydrothermal fluids, which controls the serpentinization of layer 3 and the uppermost mantle (Harrison, 1987; Dyment et al., 1997). That is, the percolation of hydrothermal fluids to layer 3 and the upper mantle is negligible at half rates above $\approx 50 \text{ mm a}^{-1}$ and increases with decreasing spreading rate at half rates below $\approx 50 \text{ mm a}^{-1}$.

In apparent conflict with the observed spreading-rate dependence of anomalous skewness (Dyment et al., 1994), Petronotis and Gordon (1999) found little, if any, dependence of anomalous skewness on spreading half rate over the range of ≈ 20 to ≈ 75 mm a^{-1} (as corrected for the time scale of Cande and Kent (1995)). If anomalous skewness was assumed to increase with decreasing spreading rate in their analysis, the data were fit worse than if no dependence on spreading rate was assumed.

To explore this apparent conflict more deeply, here we explicitly apply the model of Dyment and Arkani-Hamed (1995) to independently estimate anomalous skewness for crossings of anomaly 32 on the Pacific plate. We then use the anomalous-skewness-corrected skewness estimates to determine a revised paleomagnetic pole for the Pacific plate. Because the anomalous-skewness correction depends on spreading rate, we test different sets of spreading rates to examine the sensitivity of the estimated pole position to uncertainty in the spreading rates. We use previously determined skewness estimates of anomaly 32 (Petronotis and Gordon, 1999).

1.3 Methods

1.3.1 Anomalous Skewness

Anomalous skewness is the difference between the observed skewness and the skewness expected from the simple (i.e., vertical reversal boundaries) magnetization model of oceanic lithosphere. From an experimentally determined phase shift, θ , one can calculate the apparent effective remanent inclination, I_a^{eff} , which gives a biased estimate of the true

effective remanent inclination, I_r^{eff} . The bias is hereinafter called anomalous skewness, θ_a , where

$$I_a^{eff} = I_r^{eff} - \theta_a = -\theta - I_s^{eff} + 180^\circ . \quad (1.1)$$

I_s^{eff} is the ambient effective field inclination (Schouten and Cande, 1976; Petronotis et al., 1992), given by

$$\tan I_s^{eff} = \frac{\tan I}{\sin(A - D)} , \quad (1.2)$$

where A is the azimuth of the strike of the magnetic lineation at the site, measured 90° clockwise from the direction in which the seafloor becomes younger. I and D are the inclination and declination of the ambient geomagnetic field. I_s^{eff} is estimated from a geomagnetic reference field model for a given latitude, longitude and lineation azimuth.

1.3.2 Model Estimation

Best-fitting values of pole latitude, pole longitude, and, when desired, anomalous skewness are estimated by weighted least squares from observed apparent effective remanent inclinations (Gordon and Cox, 1980; Gordon, 1982; Petronotis et al., 1992).

Ninety five per cent confidence limits for these parameters are determined both from a constant chi-square boundary and by linear propagation of errors.

We use the method of Petronotis et al. (1992), but first correct for spreading-rate-dependent anomalous skewness. Thus the true effective remanent inclinations can presumably be directly calculated from the skewness data (eq. 1.1). The spreading-rate-dependent values of anomalous skewness for anomaly 32 are predicted from the model of Dyment and Arkani-Hamed (1995) (Table 1.1; Fig. 1.1).

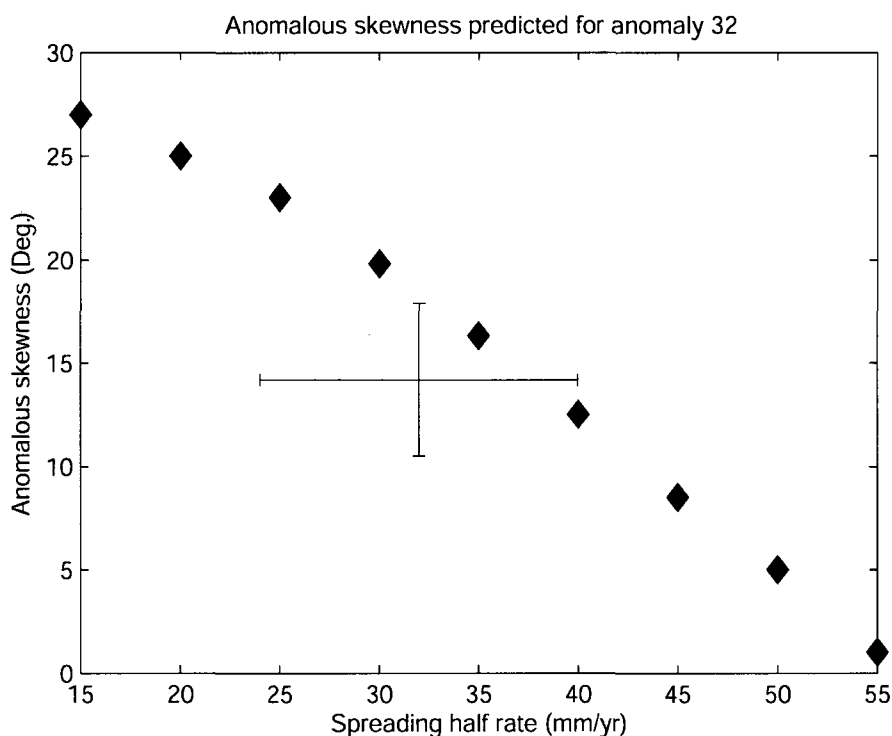


Figure 1.1. Anomalous skewness predicted by the model of Dyment and Arkani-Hamed (1995) for anomaly 32 (blue symbols) and the value of spreading-rate-independent anomalous skewness ($14.2^{\circ} \pm 3.7^{\circ}$ (95 per cent confidence limit)) estimated by Petronotis and Gordon (1999) versus spreading half rates. Most of the skewness estimates of Petronotis and Gordon (1999) come from profiles with half rates between 24 and 40 mm a^{-1} , which is the range of the horizontal bar.

1.4 Magnetic Profiles and Spreading Rates

Anomalous-skewness corrections are applied to 108 skewness estimates of anomaly 32 (Fig. 1.2): 19 recording Pacific-Kula spreading, 55 Pacific-Farallon spreading, 3 Pacific-Aluk spreading, 11 Pacific-Bellingshausen spreading, and 20 Pacific-Antarctic spreading (Petronotis and Gordon, 1999). The profiles collected over seafloor produced by Pacific-Farallon spreading are further subdivided into three groups: northern (36 profiles north of 22°N), central (15 profiles between the equator and 22°N) and southern (4 profiles south of 5°S).

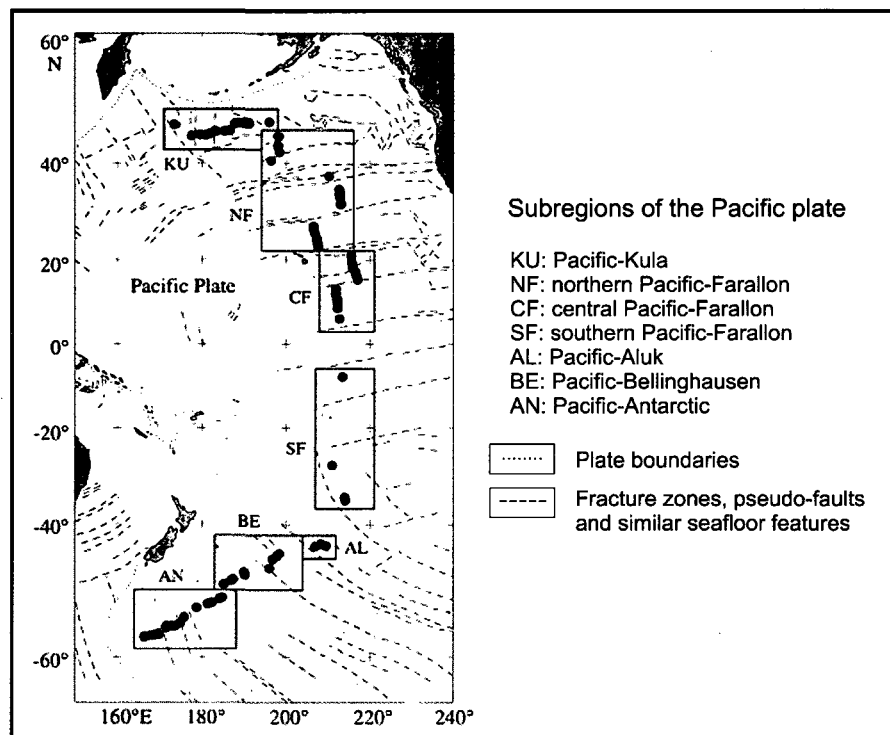


Figure 1.2. Map of the Pacific basin showing the locations of crossings of anomaly 32. Dotted lines show plate boundaries. The dashed lines show the locations of fracture zones, pseudo-faults, similar seafloor features, and the Pacific-Farallon-Aluk triple junction trace. Seven sub-regions of the Pacific plate are indicated and labeled as follows: KU, Pacific-Kula; NF, northern Pacific-Farallon; CF, central Pacific-Farallon; SF southern Pacific-Farallon; AL, Pacific-Aluk; BE, Pacific-Bellingshausen; AN, Pacific-Antarctic.

Using the Cande and Kent (1992) time scale, Petronotis and Gordon (1999) estimated the spreading rate appropriate for each crossing of anomaly 32 by comparing the observed sequence of anomalies 30 to 33 with synthetic magnetic-anomaly profiles. When no rate estimate was available for an individual crossing, they used an average for the subregion (cf. Fig. 1.2). We have revised their rates to consistency with the time scale of Cande and Kent (1995), which results in rates that are $\approx 15\%$ lower than before (Fig. 1.3, Table 1.2).

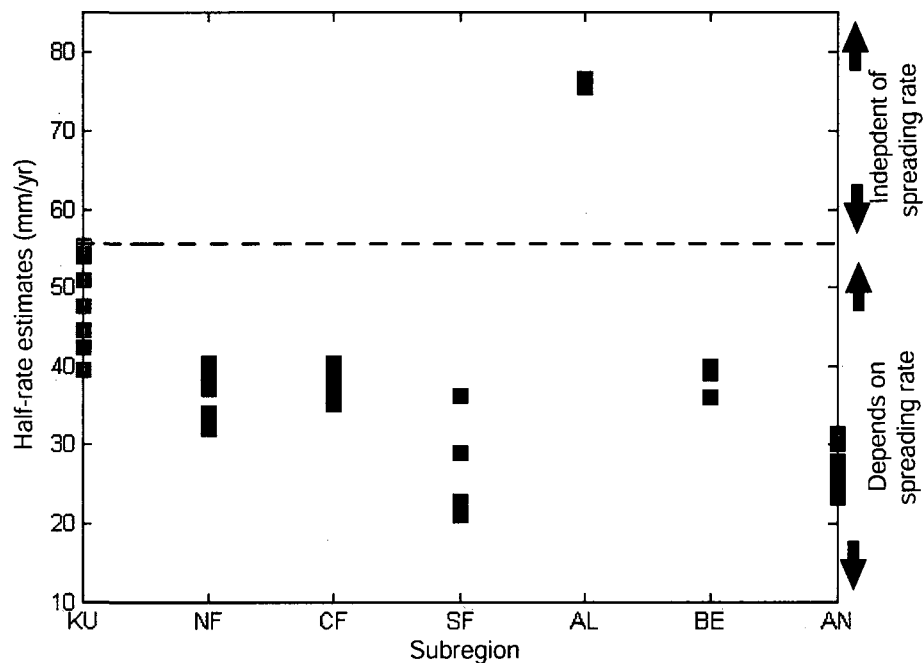


Figure 1.3. Range of spreading half rates estimated for the different crossings by Petronotis and Gordon (1999). Herein their rates have been corrected to the time scale of Cande and Kent (1995), which results in $\approx 15\%$ lower rates than those from the Cande and Kent (1992) time scale used by Petronotis and Gordon (1999). The two-letter codes denote the seven geographical subgroups of data as in Fig. 1.2.

We also estimated some spreading rates from published stage poles and angles (Table 1.3) using updated ages from the time scale of Cande and Kent (1995) (Table 1.4). The rates of Petronotis and Gordon (1999) for Pacific-Farallon spreading are similar to

those calculated from the anomaly 34 to 25 stage pole and angle of Engebretson et al. (1984), and also to those calculated from the anomaly 32a to 30/31 stage pole and angle of Rosa and Molnar (1988) (Fig. 1.4). The Pacific-Kula rates of Petronotis and Gordon (1999) are higher than the rates inferred from the anomaly 32 to 31 stage pole and angle of Engebretson et al. (1984), and considerably higher than the rates inferred from the anomaly 32a to 30/31 stage pole and angle of Rosa and Molnar (1988) (Fig. 1.4). These differences in estimated rates can cause differences of up to $\approx 15^\circ$ in estimated anomalous-skewness correction (Figs. 1.1 and 1.5). Because Pacific-Kula spreading slowed from 72 Ma to 56 Ma (Engebretson et al., 1984), the stage poles and angles from Engebretson et al. (1984) and of Rosa and Molnar (1988) give spreading rates that may be biased toward lower than appropriate values for anomaly 32. Thus, the true uncertainty in anomalous-skewness correction may be smaller than implied by the large range of spreading rates that we use. Because published stage poles are only available for Pacific-Farallon and Pacific-Kula profiles, rate estimates of Petronotis and Gordon (1999) were used for other regions in all cases.

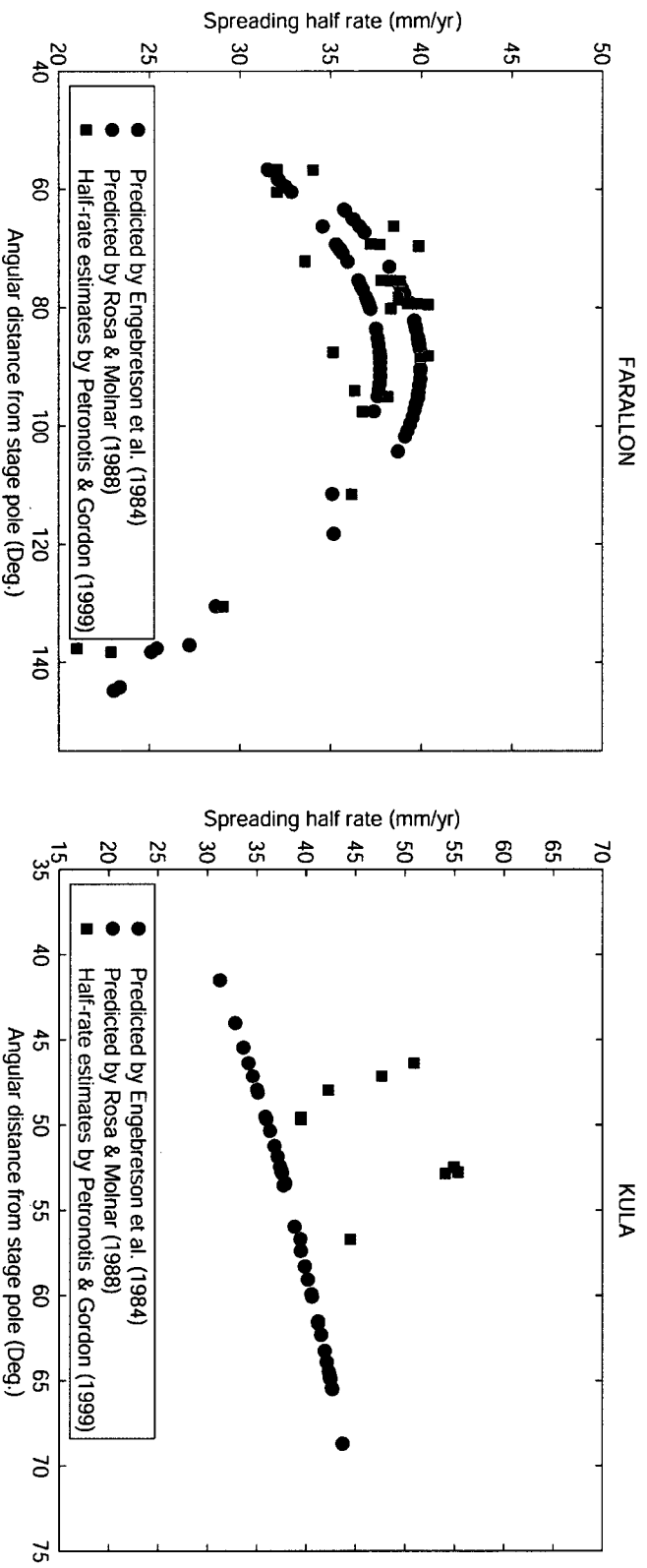


Figure 1.4. On the left, observed [red squares: revised from Petronotis and Gordon (1999)] and predicted spreading half rates versus distance from the stage pole of rotation for Pacific-Farallon profiles [black circles: calculated from the anomaly 34–25 stage pole and angle of Engebretson et al. (1984); blue circles: calculated from the anomaly 32–30/31 stage pole and angle of Rosa and Molnar (1988)]. On the right, observed [red squares: revised from Petronotis and Gordon (1999)] and predicted spreading half rates versus distance from the stage pole of rotation for Pacific-Kula profiles [black circles: calculated from the anomaly 32–31 stage pole and angle of Engebretson et al. (1984); blue circles: calculated from the anomaly 32–30/31 stage pole and angle of Rosa and Molnar (1988)]. For a comparison the observed half rates are shown as angular distance from the stage poles of Rosa and Molnar (1988) (for Pacific-Farallon and Pacific-Kula profiles, respectively).

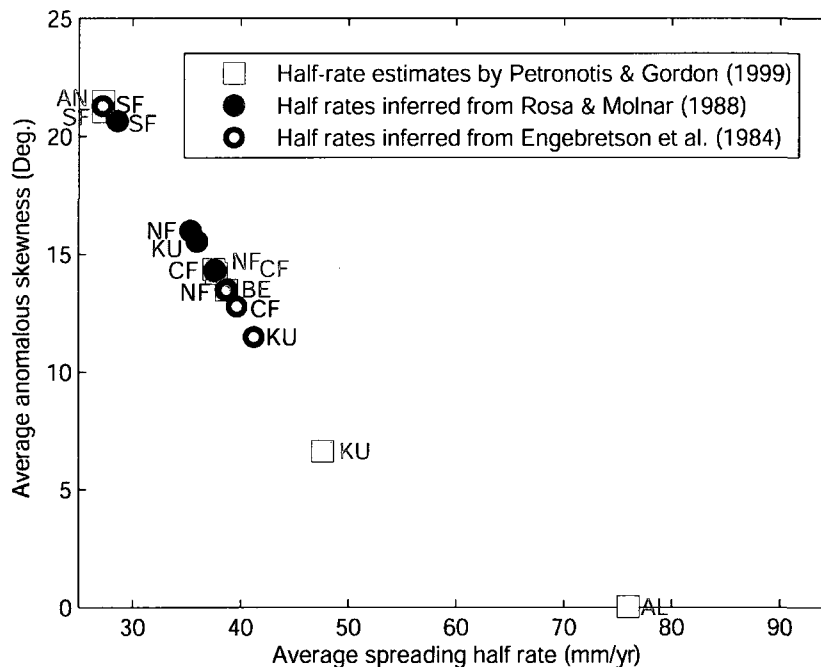


Figure 1.5. Average of the different half-rate estimates used for each subgroup of crossings and corresponding anomalous skewness predicted by the model for anomaly 32 (Fig. 1.1) [red squares calculated from the half-rate estimates of Petronotis and Gordon (1999); black circles calculated from the stage pole and angle of Engebretson et al. (1984) for Pacific-Farallon and Pacific-Kula crossings; blue circles calculated from the stage pole and angle of Rosa and Molnar (1988) for Pacific-Farallon and Pacific-Kula crossings]. The two-letter codes denote the geographical subgroups of data as in Fig. 1.2.

1.5 Results

If no correction is made for anomalous skewness, the sum-squared normalized misfit, r , is 165.2 (Petronotis and Gordon, 1999). With the spreading-rate-dependent anomalous-skewness corrections derived from the spreading rates of Petronotis and Gordon (1999) (Fig. 1.3; Table 1.2), the best-fitting pole is located at 71.8°N , 23.0°E (95 per cent confidence ellipse: 4.2° major semi-axis oriented 96° clockwise from north and 1.5° minor semi-axis) with $r=137.7$ (Fig. 1.6). This reduction in misfit is generally supportive

of the model for spreading-rate-dependent skewness, although the improvement in fit is not statistically significant ($F=1.20$ with 106 versus 106 degrees of freedom; the probability, p , of finding a value of F this large or larger, if the two distributions have identical variances, is 17%). If anomalous skewness is allowed to adjust in the inversion (after the spreading-rate-dependent anomalous-skewness correction has already been applied), the best-fitting pole is located at 71.7°N , 22.9°E , and the best-fitting value of additional anomalous skewness is $-0.6^\circ \pm 3.7^\circ$ (95 per cent confidence limits).

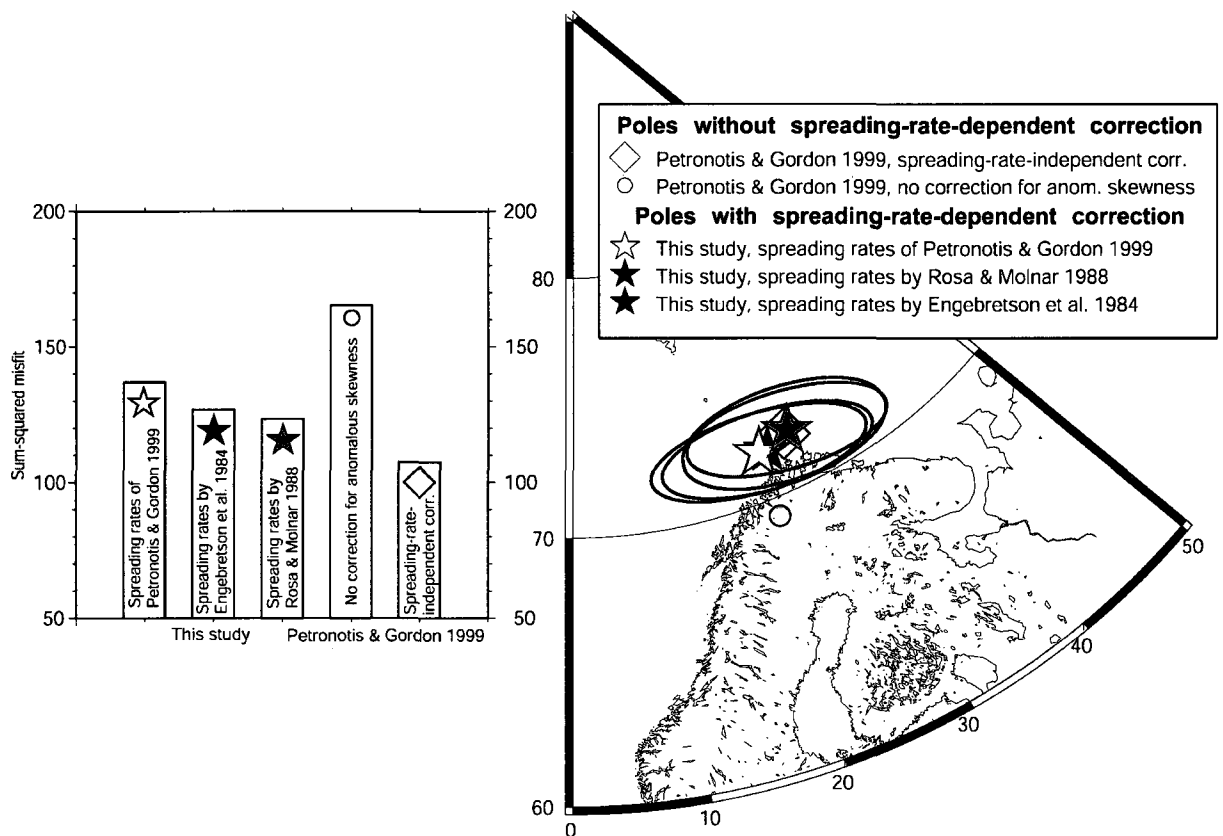


Figure 1.6. Different pole positions and sum-squared misfits for different sets of spreading half rates used: Yellow diamond, 72.1°N , 26.8°E , $r=108.7$; red circle, 69.3°N , 22.5°E , $r=165.2$; red star, 71.8°N , 23.0°E , $r=137.7$; black star, 71.8°N , 24.1°E , $r=126.9$; blue star (new preferred pole position), 72.2°N , 27.3°E , $r=123.6$.

When anomalous-skewness corrections determined from the rates of Engebretson et al. (1984) are applied, the chron 32n paleomagnetic pole is located at 71.8°N , 24.1°E (95

per cent confidence ellipse: 4.1° major semi-axis oriented 97° clockwise from north and 1.5° minor semi-axis) with $r=126.9$ (Fig. 1.6). If anomalous skewness is allowed to adjust in the inversion, the best-fitting pole is located at 71.5°N , 23.7°E , and the best-fitting value of additional anomalous skewness is $-1.6^\circ \pm 3.7^\circ$ (95 per cent confidence limits).

For the rates of Rosa and Molnar (1988), the pole position is 72.2°N , 27.3°E (95 per cent confidence ellipse: 4.0° major semi-axis oriented 98° clockwise from north and 1.7° minor semi-axis) with $r=123.6$ (Fig. 1.6). If anomalous skewness is allowed to adjust in the inversion, the best-fitting pole is located at 71.6°N , 26.5°E , and the best-fitting value of additional anomalous skewness is $-3.0^\circ \pm 3.7^\circ$ (95 per cent confidence limits).

Thus, in all three cases, if anomalous skewness is allowed to adjust, no significant additional anomalous skewness is indicated. The three new poles lie very near one another and the pole of Petronotis and Gordon (1999) (Fig. 1.6).

The corrections derived from the rates from available stage poles reduce the misfit more than does the use of the spreading rates of Petronotis and Gordon (1999). None of the spreading-rate-dependent corrections reduce the misfit as much, however, as when anomalous skewness is treated solely as a spreading-rate-independent adjustable parameter ($r=108.7$; Petronotis and Gordon, 1999). Because the model of Dymant and Arkani-Hamed (1995) seems to explain the anomalous skewness in the data set, we interpret these conflicting results as indicating that the true dispersion of the data may be greater than originally estimated by Petronotis and Gordon (1999) from their spreading-rate-independent estimate of anomalous skewness.

Because the rates from Rosa and Molnar (1988) result in the smallest misfit and agree reasonably well with Petronotis and Gordon's (1999) estimates of Pacific-Farallon spreading rates, we consider the pole obtained using their rates to be the new preferred pole (Fig. 1.6). In Fig. 1.7 each observed remanent effective inclination (calculated from the phase shifts using the spreading-rate-dependent anomalous-skewness correction) is compared with its corresponding model effective inclination (calculated from the new preferred pole position). Both are plotted against site paleolatitude. Near the paleo-equator, effective inclination changes rapidly with paleolatitude and gives the best constraints for determining the pole. The largest information contribution thus unsurprisingly comes from the profiles near the paleo-equator (Fig. 1.8).

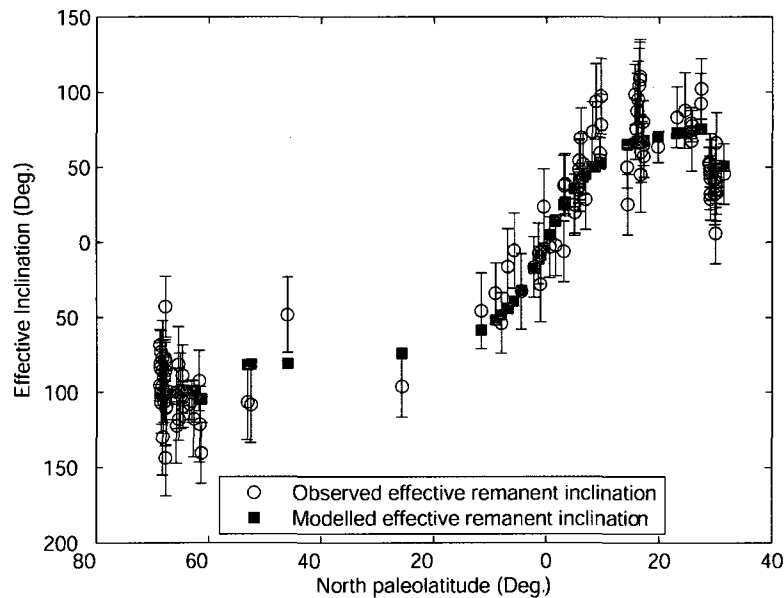


Figure 1.7. Observed (blue open circles) and calculated (black squares) effective remanent inclinations versus paleolatitude for the new preferred pole position (at 72.2°N , 27.3°E). The observed effective remanent inclinations are calculated from the phase shifts after the spreading-rate-dependent anomalous-skewness correction is applied.

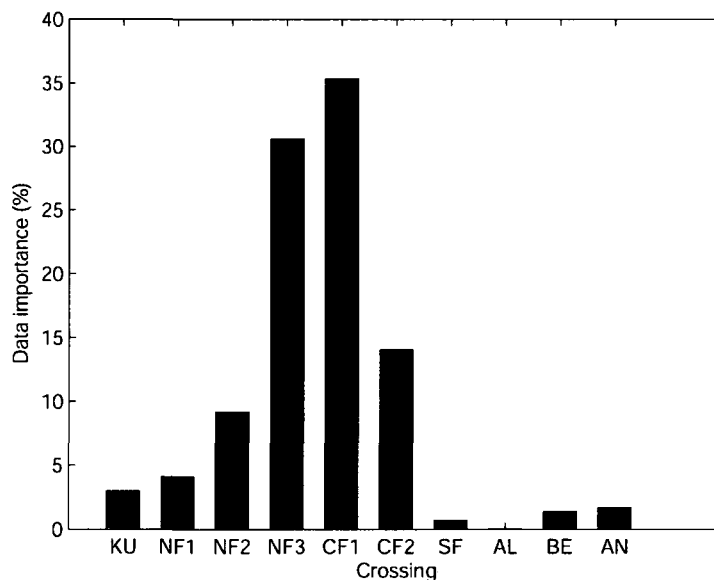


Figure 1.8. Data importance from the different subgroups of the data for the new preferred pole position (at 72.2°N , 27.3°E) found using spreading-rate-dependent anomalous-skewness correction. All 108 skewness estimates were inverted after a spreading-rate-dependent anomalous-skewness correction was applied, for rates inferred from the stage poles and angles of Rosa and Molnar (1988) for the Pacific-Farallon and Pacific-Kula profiles and rate estimates of Petronotis and Gordon (1999) for other profiles. The two-letter codes denote the seven geographical subgroups of data as in Fig. 1.2. Northern Pacific-Farallon (NF) and central Pacific-Farallon (CF) crossings were furthermore subdivided into three and two geographic groups, respectively (Petronotis and Gordon, 1999). Data importance measures the information contribution of each skewness estimate and depends on the site location and distribution, as well as the strike of the magnetic lineations.

1.6 Discussion

The first main issue addressed by this chapter is testing the consistency of the spreading-rate-dependent anomalous skewness model of Dyment and Arkani-Hamed (1995) with the set of Pacific plate anomaly 32 skewness estimates of Petronotis and Gordon (1999).

The data provide strong support for the model. First, use of the model corrections reduces the sum-squared-normalized misfit by 17% to 25%, depending on the set of

spreading rates used, relative to an inversion with no correction for anomalous skewness. Second, no significant additional spreading-rate-independent anomalous skewness is indicated by the data if first corrected for spreading-rate-dependent anomalous skewness. Thus, Pacific plate skewness data for anomaly 32 are consistent with the model of Dyment and Arkani-Hamed (1995).

The second main issue addressed herein is how much, if any, does spreading-rate-dependent anomalous skewness alter the chron 32 paleomagnetic pole obtained by Petronotis and Gordon (1999) and potentially alter other poles determined using spreading-rate-independent adjustments for anomalous skewness. The results indicate that the pole position obtained from the Pacific plate anomaly 32 skewness data of Petronotis and Gordon (1999) is robust with respect to the treatment of anomalous skewness as the revised pole lies merely 0.2° to 1.3° (depending on the set of spreading rates used for the spreading-rate-dependent correction for anomalous skewness) from the prior pole.

The same may not be true for other data sets, however. Given that the spreading-rate-dependence of anomalous skewness is well established, we think that it is important to apply this correction in future work estimating paleomagnetic poles from skewness data. It seems especially important to apply the correction when the data set does not include many crossings at low paleolatitudes across lineations that strike close to paleo-north-south.

1.7 Conclusions

The anomaly 32 skewness data for the Pacific plate are consistent with, and generally supportive of, the model for spreading-rate-dependent anomalous skewness of Dymant and Arkani-Hamed (1995). The largest uncertainties in anomalous-skewness correction are due to uncertainties in spreading rates. Paleomagnetic poles estimated from the anomaly 32 data set of Petronotis and Gordon (1999) are robust with respect to the method of estimating anomalous skewness. The conclusions of Petronotis and Gordon (1999), in particular the inferred $13^{\circ} \pm 3^{\circ}$ (95 per cent confidence limits) southward shift of the Hawaiian hotspot since ≈ 72 Ma, are strongly supported by the revised pole determined using a spreading-rate-dependent correction for anomalous skewness.

Tables

Table 1.1: Predicted anomalous skewness for anomaly 32 from the method and results of Dymant and Arkani-Hamed (1995).

Spreading Half Rate (mm/yr)	Anomalous Skewness
15	27°
20	25°
25	23°
30	19.8°
35	16.3°
40	12.5°
45	8.5°
50	5°
55	1°

Table 1.2: Spreading half rates and corresponding anomalous skewness estimated for the crossings of anomaly 32 using the model of Dymant and Arkani-Hamed (1995).

Profile	Lat (°N)	Lon (°E)	Half Rate (mm/yr)	Anom. Skewness (°)
Pacific-Kula				
c1108	46.92	173.45	47.63	6.66
c1008	45.06	177.50	47.63	6.66
si932005.a	45.24	179.52	47.63	6.66
v2006	45.18	180.83	50.90	4.28
pol6971	45.41	181.89	47.65	6.65
gecs-bmv	45.85	183.04	42.25	10.70
cmappi5a	45.84	183.25	47.63	6.66
c1109.a	45.85	185.33	39.51	12.87
pol6829.c	45.88	185.52	39.51	12.87
pol6829.d	45.98	186.50	47.63	6.66
cmapsu5a	47.12	187.78	47.63	6.66
c1220	47.23	188.72	47.63	6.66
c1010	47.20	189.58	54.93	1.06
pol6829.a	47.25	189.99	47.63	6.66
kh7002.a	47.29	190.04	55.36	0.00
l878np	47.16	190.15	54.07	1.74
pol6829.b	47.23	190.98	47.63	6.66
pol7103.m	47.11	191.09	47.63	6.66
v2112	47.33	195.85	44.48	8.92
Pacific-northern Farallon				
c1109.b	45.04	198.04	32.05	18.37
yaq701	44.95	198.19	34.02	16.99
kh7002.b	43.37	197.96	37.54	14.37
si932005.b	43.32	198.05	37.54	14.37
pptu11wt	43.22	198.02	37.54	14.37
pol7004	42.16	198.36	37.54	14.37
pol7103.a	40.62	196.34	32.05	18.37
pol7201	37.62	210.24	38.48	13.66
lusi01ar	35.03	212.64	37.19	14.64
indp01wt	34.98	212.68	37.71	14.24
pol7103.b	34.77	212.70	39.85	12.61
pol7103.c	34.57	212.71	39.85	12.61
pol7103.d	34.44	212.82	37.54	14.37
nova01ar	34.29	212.64	37.54	14.37
pol7103.e	34.25	212.64	37.54	14.37
pol7103.f	34.09	212.70	37.54	14.37
pol7103.h	33.92	212.70	37.54	14.37
pol7103.j	33.77	212.81	37.54	14.37
pol7103.g	33.58	212.79	37.54	14.37
pol7103.i	33.42	212.85	37.54	14.37
pol7103.k	32.13	213.01	33.59	17.29
gecs-amv	32.07	213.11	33.59	17.29
elt30	27.47	206.43	37.79	14.18

pol7103.l	27.42	206.58	38.31	13.78
c1301.a	27.32	206.49	38.82	13.40
jpyn01bd	26.51	206.64	37.54	14.37
v2004	25.92	206.83	37.54	14.37
rndb01wt.b	24.76	207.33	38.74	13.46
si933010	24.32	207.33	38.74	13.46
erdc01wt	23.90	207.40	39.25	13.07
c1301.b	23.66	207.44	39.25	13.07
dsdp18gc	23.65	207.46	39.76	12.68
um6503-a	23.63	207.47	39.76	12.68
78070800	23.51	207.57	40.36	12.21
dsdp55gc.b	22.84	207.67	38.31	13.78
scan05ar	22.80	207.68	38.31	13.78
Pacific-central Farallon				
c2002	20.99	215.53	37.78	14.19
78123001	20.78	215.60	37.78	14.19
76101000	20.72	215.59	37.78	14.19
71042612	19.30	215.71	37.78	14.19
elt31	18.23	215.82	37.78	14.19
um6503-b	17.13	216.65	35.14	16.19
epll01wt	16.54	216.71	40.36	12.21
dpsn01wt	16.21	216.79	39.93	12.55
72081900	15.40	217.03	37.78	14.19
v2113	13.27	211.87	37.78	14.19
swan-1ar	11.99	211.91	37.78	14.19
scan02ar	10.82	212.10	37.78	14.19
87001611	9.66	212.28	36.34	15.28
nova06ho	8.64	212.31	38.14	13.91
dsdp08gc	6.12	212.69	36.76	14.96
pptu03wt	-8.01	213.44	36.16	15.42
Pacific- southern Farallon				
elt29	-28.22	210.99	29.05	20.41
pol6702	-34.84	214.03	21.00	24.60
c0905	-35.46	214.14	22.88	23.85
Pacific-Aluk				
elt20	-43.79	209.58	76.06	0.00
c1212	-43.49	208.34	76.61	0.00
v3601	-43.93	207.00	75.50	0.00
Pacific-Bellinghausen				
cf.a409	-45.17	198.38	38.71	13.48
v3602.a	-45.64	197.75	38.71	13.48
v3602.b	-46.16	196.89	38.71	13.48
elt33	-47.57	195.94	39.08	13.20
cf.a408n	-48.64	190.09	38.71	13.48
elt19	-48.21	189.99	35.91	15.61
kh6804-c	-48.26	189.91	38.71	13.48
elt25	-49.29	187.33	39.93	12.55
cf.odf6	-49.50	186.90	38.71	13.48
cf.v16	-50.08	185.34	38.71	13.48
um66-b	-50.13	185.18	39.93	12.55

Pacific-Antarctica				
cf.odf8	-52.10	184.8	27.29	21.53
cf.w	-52.24	184.33	27.29	21.53
um6402-b	-52.83	182.56	30.85	19.20
end.t	-52.79	182.41	31.28	18.90
gecs-gmv	-52.86	182.18	30.85	19.20
mons06ar.a	-53.03	181.44	27.29	21.53
elt43	-53.00	181.30	27.29	21.53
elt27	-53.55	178.76	29.99	19.81
end.k	-54.91	175.85	27.85	21.18
elt52	-55.72	174.95	24.51	23.20
end.q	-56.11	173.71	24.42	23.23
end.b	-56.09	172.91	25.19	22.88
cf.v	-56.10	171.80	27.29	21.53
cf.a707	-56.32	171.64	27.29	21.53
end.n	-57.14	169.87	23.31	23.68
elt34	-57.21	169.93	27.29	21.53
mons06ar.b	-57.26	169.20	26.74	21.89
end.r	-57.37	168.02	25.19	22.88
cp7808.a	-57.49	166.72	27.29	21.53
cp7808.b	-57.52	166.49	27.29	21.53

When no half rate estimate was available, an average for the subregion is used (subregions as in Fig. 1.2).

Table 1.3. Stage poles.

	From Anomaly	To Anomaly	Rotation pole		Finite Angle Deg.
			Latitude °N	Longitude °E	
Pacific-Farallon					
Engebretson	34	25	66	64	20.7±1.2
Rosa & Molnar	32a	30/31	71.89	73.76	-1.2
Pacific-Kula					
Engebretson	32b	31	18	111	4.3±1.4
Rosa & Molnar	32a	30/31	27.5	126.25	-1.5

Engebretson: Engebretson et al. (1984);
Rosa & Molnar: Rosa and Molnar (1988)

Table 1.4. Ages for the magnetic anomalies.

Magnetic anomaly	Used in this study*	Age, Ma	
		Used in Engebretson et al. (1984)**	Used in Rosa and Molnar (1988)***
25	56.15 ^a	55.97	58.94
30/31	67.67 ^b		68.47
31	68.24 ^c	67.4	
32a	71.2 ^d	69.6	71.51
32b	73.33 ^e	71.8	
34	84.9 ^f	84.9	

*Source of ages is Cande and Kent (1995)

**Source of ages is Harland et al. (1982)

***Source of ages is Berggren et al. (1985)

^a Mean age for chron C25n.

^b Mean age for chron C30r.

^c Mean age for chron C31n.

^d 32a is the anomaly corresponding to chron C32n.1n. This age is the mean age for C32n.1.

^e 32b refers to the polarity chron C32r.1n. This age is the mean age for C32r.1n.

^f The mean age for the positive anomaly near the young end of chron C34n

Chapter 2

Tests of Fixity of the Indo-Atlantic Hotspots Relative to Pacific Hotspots

Summary

The rates of inter-hotspot motion, and thus the limits of the hotspot frame of reference, have remained as a matter of debate over decades. Recent improvements to the methods, age along the hotspot tracks and geomagnetic reversal time scale lead to significant changes in previous results. Herein we present updated predictions for the tracks of Tristan da Cunha, Réunion and Iceland hotspots assuming them to be fixed relative to a Pacific hotspot reference frame. It is found that the Indo-Atlantic hotspots have had no significant motion relative to Pacific hotspots since 48 Ma. Prior to 48 Ma, however, the apparent rates of inter-hotspot motion increase to about $45\text{-}55 \pm 20 \text{ mm a}^{-1}$. Uncertainties allow some motion between Pacific and Indo-Atlantic hotspots (up to $\approx 10 \text{ mm a}^{-1}$) for the past 48 million years, but based on this study the fixed hotspot approximation cannot be excluded. A possible cause for the pre-48 Ma apparent motion is a systematic error in the global plate circuits used to make the predictions.

2.1 Introduction

Hotspots are sites of intraplate volcanism or of excessive volcanism along plate boundaries. Morgan (1971) proposed hotspots to be the surface manifestations of

relatively stationary deep mantle plumes, which leave tracks of age-progressive volcanism on the plates as the plates move over them. These tracks are used to determine the history of plate motion relative to the deep mantle. Despite considerable effort, how fast hotspots move relative to another continues to be debated. The results have ranged from apparent fixity (e.g. Morgan, 1971; 1972; Duncan, 1981; Müller et al., 1993) to substantial and rapid motion between Pacific and Indo-Atlantic hotspots (e.g. relative speeds up to 80 mm a^{-1} by Raymond et al. (2000)). Rising plumes in a convecting mantle cannot be completely fixed, so the question is a matter of degree rather than of kind. Some models of mantle flow indicate that the motions of hotspots may be predictable, at least in direction (e.g. Steinberger and O'Connell, 1998). Depending on the mantle viscosity profile used in the modeling, however, the rates are unknown by an approximately constant multiplicative factor (e.g. O'Neill et al., 2005).

Given the motion of one plate (e.g. the Pacific plate) over its hotspots, relative plate reconstructions can be used to predict the positions of hotspots under other plates, which can be compared with the observed track of the hotspots. If the plates are rigid, if all the ancient plate boundaries have been recognized and properly incorporated, and if the hotspots are fixed relative to one another, the predicted track should coincide with the known trace (within uncertainties). Inconsistencies, on the other hand, give an estimate of the relative motion between hotspots (or indicate plate non-rigidity or neglected plate boundaries).

In an important study, Molnar and Stock (1987) used this approach to estimate average velocities of 10 to 20 mm a^{-1} between Hawaiian and Indo-Atlantic hotspots for the past 68 million years, concluding that hotspots do not define a fixed reference frame.

More than two decades of new age dates (e.g. Duncan and Keller, 2004; Sharp and Clague, 2006), updated plate reconstructions, updated geomagnetic reversal time scale (e.g. Cande and Kent, 1995), and updated methods for estimating plate reconstructions relative to the hotspots and their uncertainties (e.g. Andrews et al., 2006) requires a new analysis. Thus, we present updated plate-circuit reconstructions for the past 68 million years for Tristan da Cunda, Réunion and Iceland hotspots assuming them to be fixed relative to Pacific hotspots. We build on a new method for objectively estimating plate-hotspot rotations and their uncertainties (Andrews et al., 2006). Besides the uncertainties in plate-hotspot rotations, uncertainties in relative plate motions are accumulated through the plate circuit to obtain the final uncertainty (in the form of two-dimensional 95 per cent confidence regions) in the predicted positions. Predictions are made for ages corresponding to those of magnetic anomalies commonly used in global plate reconstructions: 10.9 Ma (C5o; old end of anomaly 5), 20.1 Ma (C6o; old end of anomaly 6), 33.5 Ma (C13o; old end of anomaly 13), 39.3 Ma (C18; center of anomaly 18), 47.9 Ma (C21o; old end of anomaly 21), 56.1 Ma (C25; center of anomaly 25) and 67.7 Ma (C30/31; center of the reversed polarity interval between anomalies 30 and 31). We find that the predicted tracks agree with the observed tracks much better for the past 48 million years than found before. For reconstructions for 56.1 Ma and 67.7 Ma, however, the predicted and observed tracks of Indo-Atlantic hotspots diverge.

2.2 Methods and Plate Circuits

To establish a model for Pacific plate motion relative to the hotspots, along with proper uncertainty estimates over the past 68 million years, we use the N-hotspot method of Andrews et al. (2006). This method allows the use of any number of hotspot tracks and elliptical uncertainties of arbitrary sizes for both ancient and current locations of hotspots in estimating the rotation that minimizes the summed squared normalized misfit. It is useful to be able to use elliptical uncertainties because the location of an ancient hotspot track is often better constrained in the direction perpendicular to the track, than it is along the track because of uncertainties and gaps in the age progression along a volcanic chain. Once a best-fitting rotation for a given age has been found, a covariance matrix describing the uncertainties in the rotation is determined (Andrews et al., 2006).

The sum squared normalized misfit, r , is expected to be approximately chi-square distributed (Andrews et al., 2006). The Hawaiian-Emperor and Louisville tracks both limit two degrees of freedom and a rotation is specified by three parameters, thus resulting in an over-determined problem with one degree of freedom. Values of r exceeding 3.84 are unacceptably large at the 5 per cent significance level, and values of r less than 0.004 are unacceptably small at the 5 per cent significance level.

A global relative plate motion circuit over the past 68 million years is also needed. Relative motion between two plates can be estimated if the plates share a mid-ocean ridge, and marine magnetic anomalies and fracture zones can be used to determine the history of seafloor spreading. The plate circuit (through Antarctica) used in this study is shown in Fig. 2.1 and described in detail in Table 2.1. Most of the relative plate motion

rotations adopted herein were taken from analyses using Hellinger's (1981) criterion for goodness of fit, associated with covariance matrix values describing the uncertainties in the rotations based on the statistical approach developed by Chang (1988). Because rotations may not be available for the age of interest, some rotations were interpolated from the two published rotations closest to the age of interest (Table 2.1). Rotations were assigned ages according to the time scale of Cande and Kent (1995). If a covariance matrix for a particular rotation was not available, we estimated it from partial uncertainty rotations, i.e. from partial uncertainty rotations of McQuarrie et al. (2003) and Acton (1999) (Table 2.2). For some of the older rotations, neither covariance matrices nor partial uncertainty rotations were available. For these rotations, we used the closest (in age) available uncertainty estimate for the same plate pair (Table 2.2). To obtain the final uncertainty in the predicted positions (shown in figures as two-dimensional 95 per cent confidence regions, all uncertainties discussed here are two-dimensional 95 per cent confidence limits), the uncertainties in relative plate motions were accumulated through the plate circuit (for details see Chang, 1988; Chang et al., 1990; Royer and Chang, 1991; Kirkwood et al., 1999).

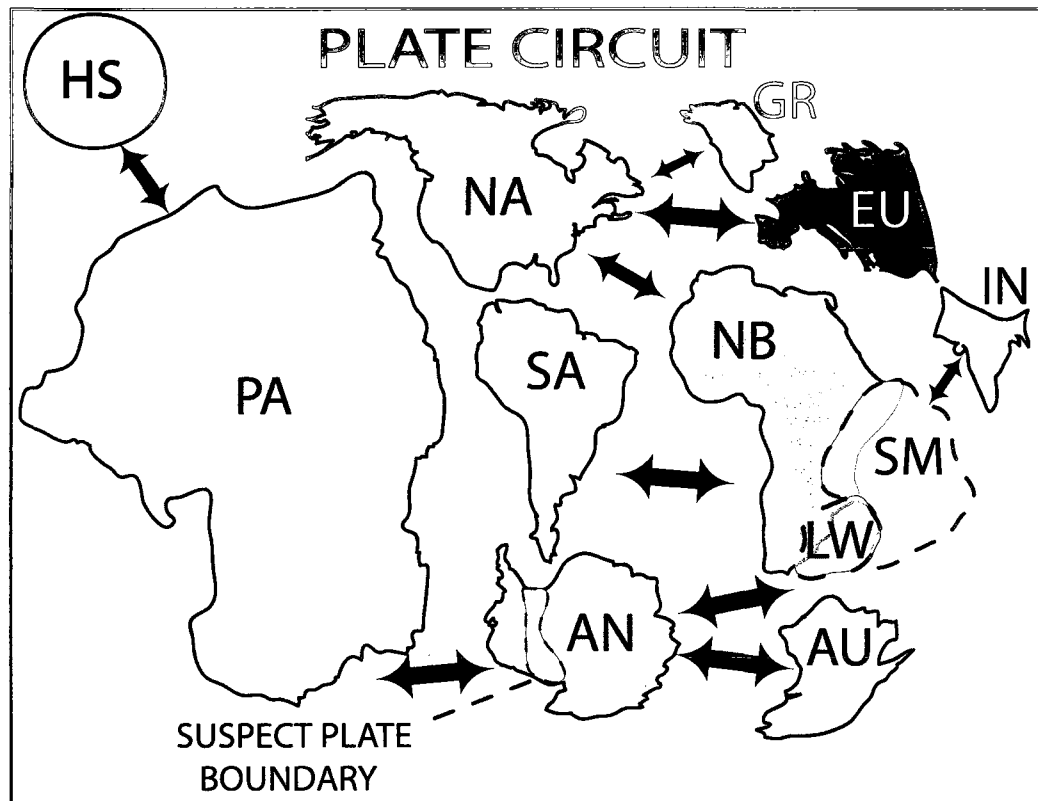


Figure 2.1. Main components and layout of the global plate circuit through mid-ocean ridges (as used in this study). Arrows represent motion on mid-ocean ridges.

Before making the final choices for our plate circuit rotations, we tested how much different available rotations affect the final predicted positions. In particular, we tested how different estimates of motion within Africa (e.g. Royer et al., 2006; Horner-Johnson et al., 2007 etc.) change the predicted tracks. The timing of motion between the Nubia (West Africa) and Somalia (East Africa) plates is uncertain and the location of the boundary between these two plates has not been fully resolved. The hypothesized existence of the Lwandle plate (Hartnady, 2002; Horner-Johnson et al., 2007) between the Nubia and Somalia plates adds to the puzzle. Horner-Johnson et al. (2007) found that their data are better fit if a Lwandle plate lies along the Africa side of the Southwest Indian Ridge between the Nubia and Somalia plates. If so, published rotations for “Africa-Antarctica” motion may represent Nubia-Antarctica motion, Lwandle-Antarctica

motion, Somalia-Antarctica, or some combination of, or compromise between, two or more of these (Horner-Johnson et al., 2007). In our preferred model, we account for motion between the Nubia and Lwandle plates. We take the estimates for East Antarctica-Somalia or East Antarctica-Africa motion (e.g. Royer and Chang, 1991; Molnar et al., 1988; Bernard et al., 2005) to represent East Antarctica-Lwandle motion because most of the data used to constrain these estimates of motion are from the portion of the Southwest Indian Ridge separating Antarctica from the hypothesized Lwandle plate.

Motion between Nubia and Somalia began no earlier than ≈ 30 Ma (Burke, 1996). We considered alternative models with motion beginning either at 30 Ma or at 10 Ma. For both models the finite rotations were found by extrapolating the current Nubia-Lwandle and Nubia-Somalia angular velocities (Horner-Johnson et al., 2007). We found that the results are insensitive to these alternative assumptions, and indeed change little if motion between Nubia and Lwandle is instead neglected (see Appendix A for more).

Tests using other alternative rotations for the plate pairs are described in the supplementary material (Appendix A of this thesis). Generally, the predicted locations are similar to our preferred rotations. In the case of Iceland, however, the predicted position for 68 Ma is somewhat sensitive to the choice of East Antarctica-Lwandle rotations. The choices for ages older than c13 were between the rotations of Royer and Chang (1991) combined with the rotation of Molnar et al. (1988) for c31 and the rotations of Bernard et al. (2005). Use of the rotations by Bernard et al. (2005) moves the predicted position for c31 130 km north-eastwards from the position obtained using the rotation of Molnar et al. (1988) for c31. Nonetheless, all the predicted tracks lie within the 95 per cent uncertainty limits of our preferred model. Our preferred rotations for describing

motion before c13 (33.3 Ma) between the East Antarctica and Lwandle plates are those of Royer and Chang (1991) combined with the rotation of Molnar et al. (1988) for c31. For the younger times we use the rotation of Lemaux et al. (2002) for c5 and the rotations of Patriat et al. (2008) for c6 and c13.

Sources for the other links are given in Table 2.1.

2.3 Hotspot Tracks

For estimating Pacific-hotspots rotations for the past 68 Ma, we use the tracks of the Hawaii and Louisville hotspots because they are the least ambiguous tracks on the Pacific plate. Relatively dense age dates are available along them (Table 2.3) and both hotspots have been active throughout the time interval of the analysis. Although the Hawaiian-Emperor and Louisville chains are the temporally best defined Pacific plate tracks, there is still room for more age determinations. For example, the Louisville chain has very few samples along the younger part of the chain, only one dated sample (13.2 Ma; Koppers et al., 2004) between the youngest dated volcanism (one sample dated for 1.1 Ma; Koppers et al., 2004) and the dated sample for 36.5 Ma (Koppers et al., 2004). Both chains are best sampled between ≈ 33 and 50 Ma (Sharp and Clague, 2006; Koppers et al., 2004).

Table 2.4 lists the locations with assigned uncertainties (two-dimensional 95 per cent confidence regions) corresponding to c5 (10.9 Ma), c6 (20.1 Ma), c13 (33.5 Ma), c18 (39.3 Ma), c21 (47.9 Ma), c25 (56.1 Ma) and c31 (67.7 Ma) along the chains (Figs. 2.2a and b) and used as input to the N-hotspot method. We take the current location of the Hawaiian hotspot to be at Kilauea at 19.6°N , 204.5°E ; it was assigned a circular

uncertainty with a radius of 95 per cent confidence of 100 km. The current location of the Louisville hotspot, which we take it to be at -50.9°N , 221.9°E as suggested by Lonsdale (1988), is less certain and was assigned a circular uncertainty region with a radius of 200 km. Generally, the uncertainties assigned for the ancient locations along the Louisville chain are larger than those assigned along the Hawaiian-Emperor chain (Table 2.4) because the age data are sparser along the Louisville chain. Both chains are spatially well constrained in the direction perpendicular to the volcanic chain and thus the assigned uncertainty is smaller in this direction.

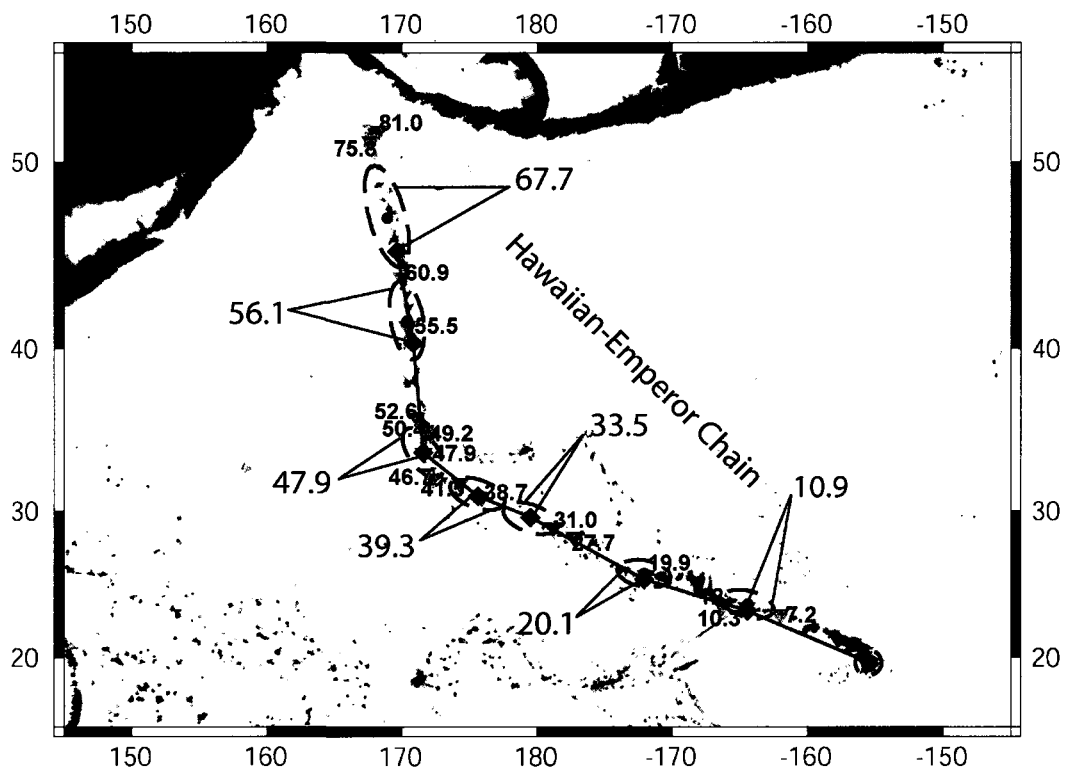


Figure 2.2a. Map showing the Hawaiian-Emperor hotspot track, input and resulting model using the N-hotspot numerical method (Andrews et al., 2006). Red inverted triangles show locations of dated igneous rock samples with ages (Darlymple et al., 1974; 1977; 1981; Sharp and Clague, 2006; Duncan and Keller, 2004). Black circles with ages and accompanying ellipses (two-dimensional 95 per cent confidence regions) show the input into the N-hotspot method for determining rotations. Blue diamonds show the model's calculated track. All ages are in millions of years before present.

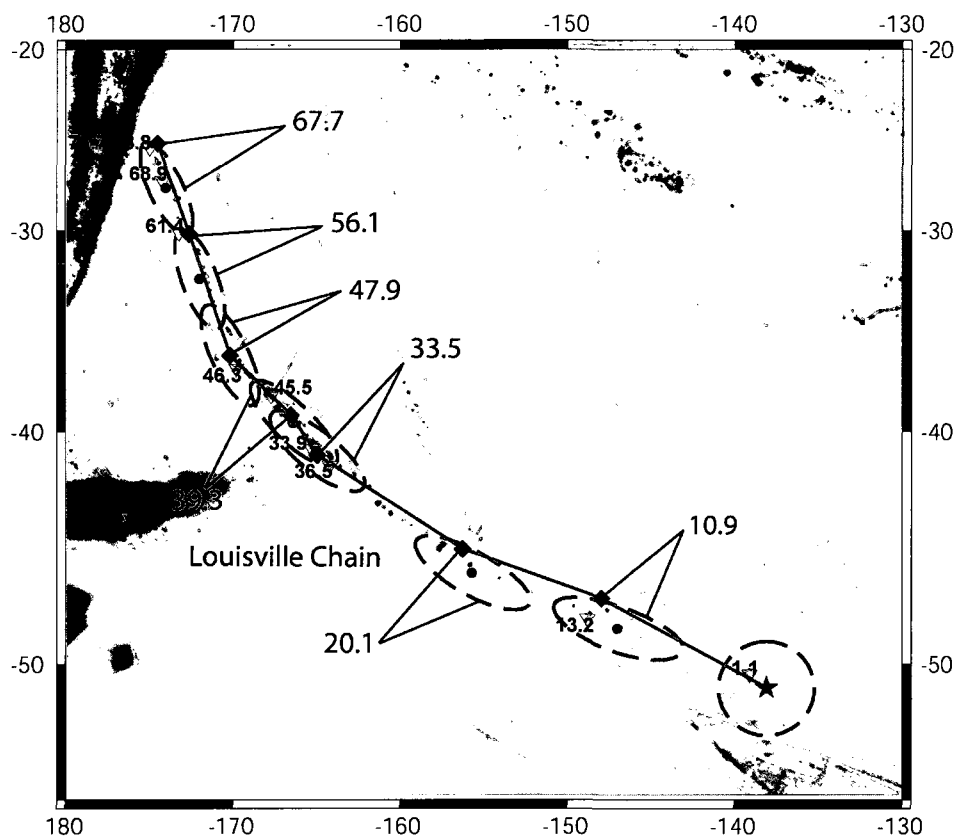


Figure 2.2b. Map showing the Louisville hotspot track, input and resulting model using the N-hotspot numerical method (Andrews et al., 2006). Red inverted triangles show locations of dated igneous rock samples with ages (Koppers et al., 2004). Black circles with ages and accompanying ellipses (two-dimensional 95 per cent confidence regions) show the input into the N-hotspot method for determining rotations. Blue diamonds show the model's calculated track. All ages are in millions of years before present.

Tristan da Cunha hotspot has a well established age progression along its track and provides a critical test for hotspot fixity for it has remained beneath the Nubia plate for the past 70 Ma (O'Connor and Duncan, 1990). The Tristan da Cunha hotspot track comprises the Walvis Ridge on the Nubia plate and the Rio Grande Rise on the South America plate. Etendeka Flood Basalts in Africa and Parana Flood Basalts in South America can be tracked at the ends of these features, and are thought to have erupted at ~131-133 Ma (e.g. Renne et al., 1992; Renne et al., 1996) indicating the arrival of the Tristan da Cunha plume head at this time. Age data have demonstrated a clear age

progression on Walvis Ridge for the past ≈ 80 million years (O'Connor and Duncan, 1990; O'Connor and le Roex, 1992; Table 2.3). The current position of the Tristan da Cunha hotspot is taken as -37.5°N , 347.5°E on Tristan da Cunha Island, and assigned a circular two-dimensional 95 per cent confidence region with a radius of 150 km. The current location of the Tristan da Cunha is thought to be fairly well constrained beneath the island, best estimate for the age of volcanism on the Tristan da Cunha Island ranges from 0.64-1.3 Ma (0.64 Ma for isochron age and 1.3 Ma for plateau age; O'Connor and le Roex, 1992).

The tracks for Réunion and Iceland hotspots are more complicated because of the interaction of each hotspot with the mid-ocean ridge as the ridge approaches the hotspot.

Réunion hotspot track comprises the Chagos-Laccadive Ridge on the India plate, and Mascarene Plateau-Nazareth Bank-Mascarene Island group on the Somalia plate (Duncan and Hargraves, 1990). The Deccan flood basalts are attributed to the arrival of the Réunion plume head beneath India at 65.5 Ma (e.g. Hoffmann et al., 2000). The current position of the Réunion hotspot is taken as -21.1°N , 55.5°E on Réunion Island. Réunion Island has experienced ongoing volcanism since 2 Ma (Duncan and Hargraves, 1990; McDougall, 1971) and Duncan (1990) notes that a large seamount currently 160 km west of Réunion may actually represent the most recent activity of the hotspot. Thus, the current location of the Réunion hotspot is assigned a circular uncertainty with a radius of 200 km to include this possible shift of the current location of the hotspot.

The location of Iceland hotspot on the axis of the Mid-Atlantic Ridge gives a unique role to it. As a consequence of the plume-ridge interaction, a lack of simple time-progressive volcanic track complicates the tests of hotspot fixity. However, Vink's

(1984) simple geometric model with a fixed hotspot and channeling of asthenosphere to the closest section of the rise crest uniquely predicts a location, orientation, and age progression for the Greenland-Faeroe and Voring Plateaus. These features are used to constitute the Iceland hotspot track and the ocean floor isochrons are used to indicate the location of the hotspot at different times. The current position of the Iceland hotspot is taken as 64°N , 344°E (Lawver and Mueller, 1994) and assigned a circular uncertainty region with a radius of 200 km.

All the hotspots used in this study are widely accepted as being among the most likely candidates for a deep mantle origin (e.g. Courtillot et al., 2003).

2.4 Results

2.4.1 Pacific-Hotspot Rotations and Uncertainties Since 68 Ma

Fig. 2.3 shows the resulting poles of rotation, which are listed in Table 2.5 with sum squared misfits and covariance matrix parameters. The uncertainty regions shown in Fig. 2.3 are two-dimensional 95 per cent confidence regions. The uncertainties appear to get smaller with increasing age. This, however, does not indicate decreasing uncertainty with time but is an artifact caused by projecting uncertainties of rotations onto a spherical surface (Chang et al. 1990). The poles of Andrews et al. (2006) are similar to ours and are within the uncertainty limits of our new poles of rotation. Andrews et al. (2006) obtained their poles using the same method as in this study but with older age data along the chains. Our uncertainty regions also include the poles of Wessel and Kroenke (2008), except their model WK08-A pole for 47.9 Ma.

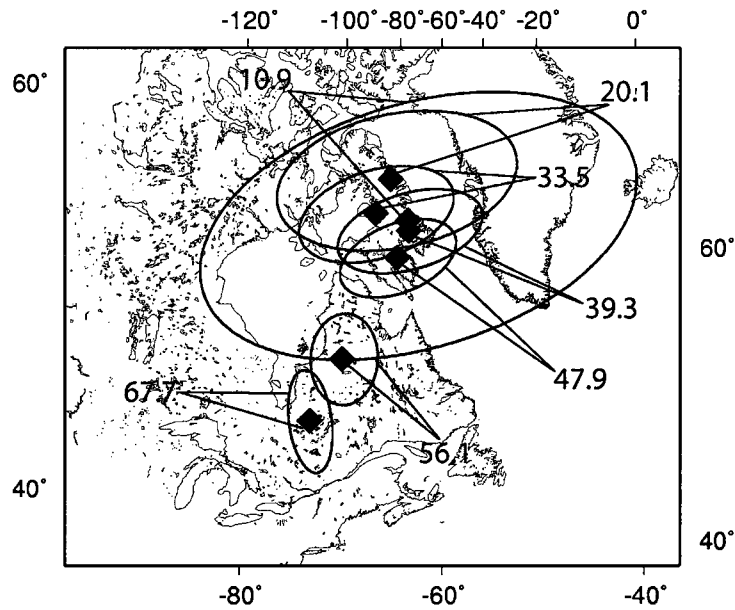


Figure 2.3. Pacific-hotspot poles of rotation (blue diamonds). Ellipses are the corresponding two-dimensional 95 per cent confidence regions.

Misfits for 10.9 Ma, 20.1 Ma, 33.5 Ma, 39.3 Ma and 47.9 Ma fall within the acceptable limits, as discussed above in the section on methods, but misfits for 56.1 Ma and 67.7 Ma exceed 3.84 (Table 2.5) and are larger than found by Andrews et al. (2006) for their corresponding poles of rotation.

2.4.2 Predicted Tracks

Tristan da Cunha

The predicted and observed Tristan da Cunha tracks have no significant differences for the past 48 million years (Fig. 2.4). This contradicts earlier results, in particular the results of Molnar and Stock (1987). For example, Molnar and Stock's (1987) predicted location for 48 Ma is ≈ 950 km (± 500 km) from the coeval dated volcanism (46,52 Ma location; Table 2.3) on the Walvis Ridge, whereas the misfit found herein is ≈ 250 km (± 350 km), or in terms of rates 5 ± 6 mm a^{-1} . Although the predicted and observed tracks are

significantly different for 56 Ma and 68 Ma, the misfits are less than found by Molnar and Stock (1987). The misfit between the predicted and observed locations for 68 Ma (c31) is $\approx 900 \pm 400$ km. If this misfit occurred entirely between 68 and 48 Ma, it gives an early Tertiary rate of motion between the Tristan da Cunha hotspot and Pacific hotspots of 45 ± 20 mm a⁻¹.

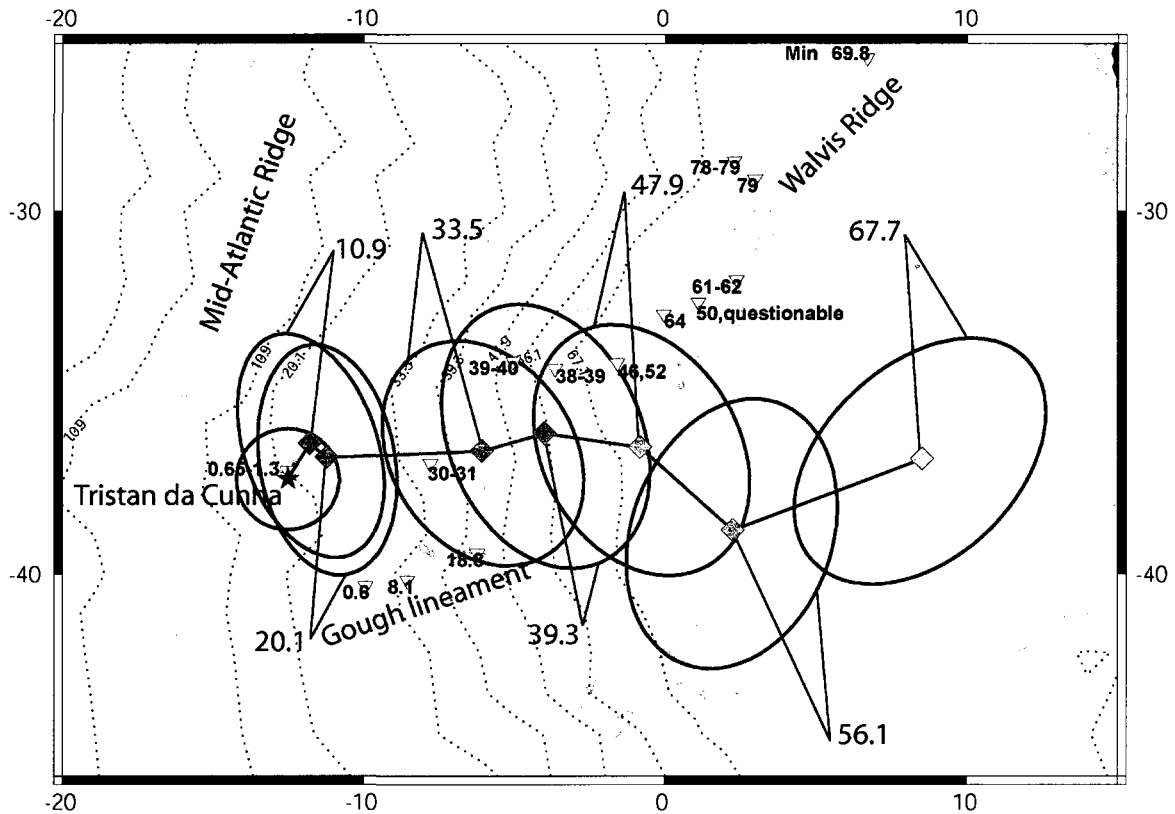


Figure 2.4. Predicted positions of the Tristan da Cunha hotspot relative to the Nubia plate (shown with green diamonds) assuming that the Tristan da Cunha hotspot is stationary relative to Pacific hotspots. Red inverted triangles show locations for age dates of O'Connor and Duncan (1990) and O'Connor and le Roex (1992). The point labeled “46, 52” has a plateau age of 46 Ma and a total fusion age of 52 Ma. The ages for Gough lineament are also shown (O'Connor and le Roex, 1992). Ellipses (two-dimensional 95 per cent confidence regions) show uncertainties propagated from the uncertainties in the motion of the Pacific plate relative to the Hawaiian and Louisville hotspots and relative plate motion uncertainties, combined with the uncertainty in the current location of the Tristan da Cunha hotspot. The black star is the current location of the Tristan da Cunha hotspot (at -37.5°N , 347.5°E). Dotted lines are synthetic isochrons from Mueller et al. (2008) with ages (Ma) as labeled. All ages are in millions of years before present.

Réunion

The predicted track is shown relative to the Somalia plate for times 11 Ma (c5) through 39 Ma (c18) and relative to the India plate for earlier times (Fig. 2.5). We find that the predicted and observed tracks agree since 48 Ma. The 48 Ma (c21) reconstruction lies about 100 ± 300 km from ODP site 713, dated as 49 Ma (Duncan and Hargraves, 1990). This corresponds to a rate of motion of 2 ± 6 mm a⁻¹. The 68 Ma (c31) reconstructed point lies $\approx 900 \pm 400$ km from a central location on the Deccan flood basalt province that has been dated between 64 and 69 Ma (Duncan and Pyle, 1988; Courtillot et al., 1988; 65.5 Ma by Hofmann et al., 2000). If this misfit occurred entirely between 48 Ma and 68 Ma, it gives an early Tertiary rate of motion between the Réunion hotspot and Pacific hotspots of 45 ± 20 mm a⁻¹.

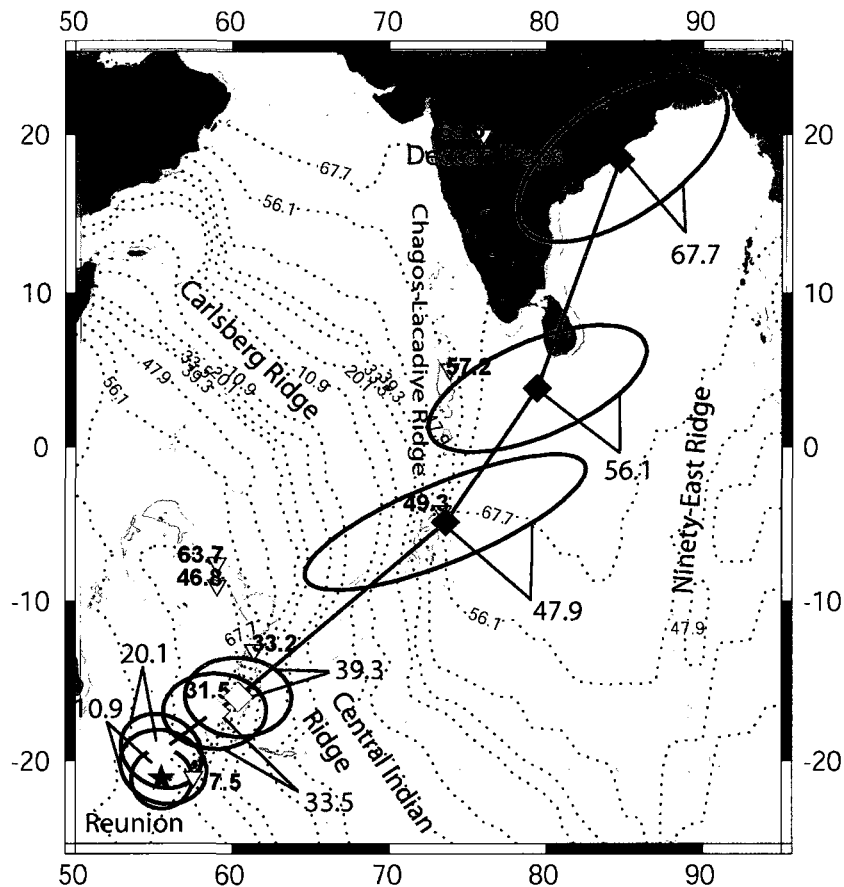


Figure 2.5. Predicted positions of the Réunion hotspot relative to the Somalia plate for times 10.9 Ma through 39.3 Ma (yellow diamonds) and relative to the India plate for earlier times (purple diamonds) assuming that the Réunion hotspot is stationary relative to Pacific hotspots. Red inverted triangles show locations for age dates of Duncan and Hargraves (1990). Ellipses (two-dimensional 95 per cent confidence regions) show uncertainties propagated from the uncertainties in the motion of the Pacific plate relative to the Hawaiian and Louisville hotspots and relative plate motion uncertainties, combined with the uncertainty in the current location of the Réunion hotspot. The black star is the current location of the Réunion hotspot (at -21.1°N , 55.5°E). Dotted lines are synthetic isochrons from Mueller et al. (2008) with ages (Ma) as labeled. All ages are in millions of years before present.

Iceland

In Fig. 2.6 the predicted track is shown relative to the Eurasia plate for 10.9 Ma and relative to the Greenland plate for earlier times. These reconstructed points are made with the constraint that they always lay on seafloor older than the reconstruction age. The observed and predicted Iceland hotspot tracks agree for the past 48 million years (Fig.

2.6). The 48 Ma reconstructed point lies ≈ 250 km (± 300 km) from mafic intrusions dated as ≈ 47 -50 Ma (Tegner et al., 1998; Tegner et al., 2008), corresponding to a rate of 5 ± 6 mm a⁻¹ since 48 Ma. The 68 Ma (c31) reconstructed point lies $\approx 1100 \pm 400$ km from the oldest lavas on the West Coast of Greenland (estimated as about 60.9-61.3 Ma by Storey et al. (1998); the earlier estimate for this spans a little longer). If this misfit occurred entirely between 68 Ma and 48 Ma, it gives an early Tertiary rate of motion between the Iceland hotspot and Pacific hotspots of 55 ± 20 mm a⁻¹.

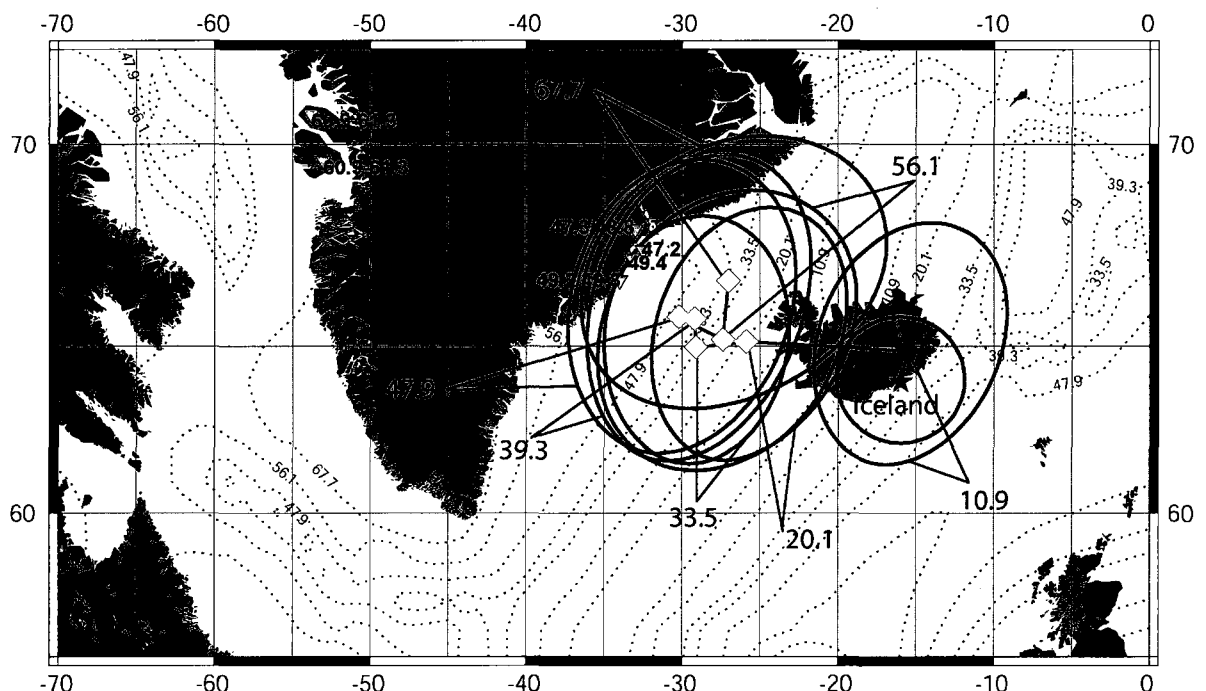


Figure 2.6. Predicted positions of the Iceland hotspot relative to the Eurasia plate for 10.9 Ma (blue diamonds) and relative to the Greenland plate for earlier times (turquoise diamonds) assuming that the Iceland hotspot is stationary relative to Pacific hotspots. Reconstructed points are made with the constraint that they always lay on seafloor older than the reconstruction age. Red inverted triangles show locations for age dates of Tegner et al (1998), Tegner et al. (2008) and Storey et al. (1998). Ellipses (two-dimensional 95 per cent confidence regions) show uncertainties propagated from elliptical uncertainties in the motion of the Pacific plate relative to the Hawaiian and Louisville hotspots and relative plate motion uncertainties, combined with the uncertainty in the current location of the Iceland hotspot. The black star is the current location of Iceland hotspot (at 64° N, 344° E). Dotted lines are synthetic isochrons from Mueller et al. (2008) with ages (Ma) as labeled. All ages are in millions of years before present.

2.4.3 Summary of the Results

Tristan da Cunha, Réunion, and Iceland hotspots are shown to have no significant motion relative to Pacific hotspots since 48 Ma (≈ 2 to 5 ± 6 mm a⁻¹). Prior to 48 Ma, however, the inter-hotspot rates of motion increase to between 45 and 55 ± 20 mm a⁻¹. This result is in contrast with those found by Molnar and Stock (1987) and Raymond et al. (2000), who both suggest significant inter-hotspot motion between the Pacific and Indo-Atlantic hotspots (with rates up to ≈ 80 mm a⁻¹). The results are consistent for all the hotspots examined here (insignificant inter-hotspot motion since 48 Ma, and dramatically higher rates for earlier times) which suggests the possibility of a common cause for the observed pre-48 Ma misfits, a reason other than high rates of inter-hotspot motion.

2.5 Discussion

When establishing the plate circuit we implicitly assume that there were no additional plate boundaries active during the time span of the analysis. The idea of a missing plate boundary, however, has been long suggested (e.g. Molnar et al., 1975; Morgan, 1981; Gordon and Cox, 1981; Duncan, 1981). Especially paleomagnetic data have suggested a missing plate boundary, particularly within Antarctica (e.g. Acton and Gordon, 1994). Here we have shown that, unlike many of the previous studies have concluded, within our uncertainty limits the fixed hotspot hypothesis cannot be excluded for the past 48 Ma. In line with the long standing search for a missing plate boundary, we believe that a plausible cause for the apparent pre-48 Ma inter-hotspot motion is unmodeled motion

across Antarctica, a region whose large-scale tectonic history prior to 48 Ma is unclear. Cande et al. (2000) note that the timing and magnitude of the plate motion in the West Antarctic rift system remain poorly known because of a lack of magnetic anomaly and fracture zone constraints on seafloor spreading.

Until recently, the bend in the Hawaiian-Emperor chain was believed to be ≈ 43 Ma old and in the absence of any major plate reorganization the timing was used as one of the lines of evidence to point towards moving hotspots. New age dates affect these conclusions. Sharp and Clague (2006) and Duncan and Keller (2004) have recently reported new incremental heating $^{40}\text{Ar}/^{39}\text{Ar}$ ages for the Hawaiian-Emperor chain. In particular, Sharp and Clague (2006) show that the initiation of the Hawaiian-Emperor bend at ≈ 50 Ma B. P. coincided with a major reorganization of northern Pacific spreading centers (Atwater, 1989) and initiation of magmatism in the Izu-Bonin-Mariana arc system, consistent with the formation of the bend by changed Pacific plate motion (Atwater, 1989; Norton, 2000). (The initiation of the bend has also been linked to chron 21 reorganizations in the southern Pacific (e.g. Wessel et al., 2006; Cande et al., 1982; Cande et al., 1995) and recently Whittaker et al. (2007) reported a major plate reorganization event between Australia and Antarctica 50-53 million years ago, linking all the above mentioned together.)

As the formation of the bend has thus been linked to plate reorganizations, not to change in motion of the plume itself, and the hotspots have been herein demonstrated to, within the uncertainties, remain stationary relative to one another for the past 48 million years, a fault in the plate circuit used to make the predictions remains an attractive option to explain the systematic pre-48 Ma increase in the rates of inter-hotspot motion.

2.6 Conclusions

We show that the Indo-Atlantic hotspots have had no significant motion relative to Pacific hotspots since 48 Ma. Prior to 48 Ma, however, the apparent rates of inter-hotspot motion increase to about $45\text{-}55 \pm 20 \text{ mm a}^{-1}$. Uncertainties allow some motion between Pacific and Indo-Atlantic hotspots (up to $\approx 10 \text{ mm a}^{-1}$) for the past 48 million years, but based on this study the fixed hotspot approximation cannot be excluded.

A possible cause for the pre-48 Ma apparent motion is a systematic error in the global plate circuits used to make the predictions. A potential candidate for the error is pre-48 Ma motion across Antarctica.

Tables

Table 2.1. Preferred rotations used to quantify the global plate circuit in making hotspot track predictions. pa refers to the Pacific plate, wa is the West Antarctica, ea East Antarctica, lw Lwandle, sm Somalia, nb Nubia, na North America, eu Eurasia, gr Greenland and in India plate. The ages shown are given in the timescale of Cande and Kent (1995) and (y), (o), and (m), refer to young and old ends and middle of polarity chron, respectively. Rotations for the plate pairs are given as motion of the first plate relative to the second.

Plate pair	Source age	Age (Ma)	Lat ($^{\circ}$ N)	Lon ($^{\circ}$ E)	Angle ($^{\circ}$)	Source
pa-wa	C5n.2n(o)	10.9	70.36	-77.81	9.48	Croon et al. 2008
pa-wa	C6n(o)	20.1	74.00	-70.16	16.73	Croon et al. 2008
pa-wa	C13n(o)	33.5	74.48	-64.02	27.40	Croon et al. 2008
pa-wa	C18n.1n(y)	38.4	74.86	-56.21	31.41	Croon et al. 2008
pa-wa	C18n.2n(o)	40.1	74.87	-54.46	32.62	Croon et al. 2008
pa-wa	C21n(o)	47.9	74.52	-50.19	37.64	Cande et al. 1995
pa-wa	C24n.3n(o)	53.4	73.62	-52.50	40.03	Cande et al. 1995
pa-wa	C27n(m)	61.1	71.38	-55.57	44.90	Cande et al. 1995
pa-wa	C28r(m)	63.8	70.55	-55.72	47.00	Eagles et al. 2004*
pa-wa	C30r(o)/C31n(y)	67.7	68.94	-55.52	49.60	Eagles et al. 2004*
Plate pair	Source age	Age (Ma)	Lat ($^{\circ}$ N)	Lon ($^{\circ}$ E)	Angle ($^{\circ}$)	Source
ea-wa	C8n.2n(o)	26.6	0.00	0.00	0.0	Cande et al. 2000
ea-wa	C13n(o)	33.5	-18.15	-17.85	-0.7	Cande et al. 2000
ea-wa	C20n(o)	43.8	-18.15	-17.85	-1.7	Cande et al. 2000

Plate pair	Source age	Age (Ma)	Lat (°N)	Lon (°E)	Angle (°)	Source
ea-lw	C5n.2n(o)	10.9	14.6	-49.1	1.53	Lemaux et al. 2002
ea-lw	C6n(o)	20.1	10.8	-46.0	2.70	Patriat et al. 2008
ea-lw	C13n(m)	33.3	16.2	-44.7	5.66	Patriat et al. 2008
ea-lw	C26n(o)	57.9	8.8	-42.6	10.83	Royer and Chang 1991
ea-lw	reversed polarity interval between 30/31 (m)	67.7	2.22	-40.74	12.5	Molnar et al. 1988
Plate pair	Polarity Chron	Age (Ma)	Lat (°N)	Lon (°E)	Angle/Ma (°/Ma)	Source
nb-lw	angular velocity vector		-37.2	-23.1	0.04	Horner-Johnson et al. 2007
lw-nb		30	-37.2	-23.1	1.2	
Plate pair	Source age	Age (Ma)	Lat (°N)	Lon (°E)	Angle (°)	Source
nb-na	C6n(m)	19.6	81.1	56.5	-5.21	McQuarrie et al. 2003
nb-na	C13n(m)	33.3	76.3	2.2	-9.96	McQuarrie et al. 2003
nb-na	C18n(m)	39.3	-74.8	177.1	12.48	McQuarrie et al. 2003
nb-na	C21n(m)	47.1	73.7	-6.1	-15.46	McQuarrie et al. 2003
nb-na	C25n(m)	56.1	80.0	-0.7	-18.11	McQuarrie et al. 2003
nb-na	30/31r	67.7	82.5	-0.6	-20.96	McQuarrie et al. 2003
Plate pair	Source age	Age (Ma)	Lat (°N)	Lon (°E)	Angle (°)	Source
na-eu	c5n.2n(o)	10.9	67.75	133.17	2.62	Merkouriev and DeMets 2008
na-eu	c6n(o)	20.1	68.62	131.76	5.03	Merkouriev and DeMets 2008
na-eu	C13n(m)	33.3	63.6	137.1	7.38	McQuarrie et al. 2003
na-eu	C18n(m)	39.3	57.8	140.3	8.48	McQuarrie et al. 2003
na-eu	C21n(m)	47.1	52.8	142.3	9.82	McQuarrie et al. 2003
na-eu	C25n(m)	56.1	46.6	145.5	12.83	McQuarrie et al. 2003
na-eu	30/31r	67.7	58.4	145.9	16.31	McQuarrie et al. 2003
Plate pair	Source age	Age (Ma)	Lat (°N)	Lon (°E)	Angle (°)	Source
gr-na		35	0.00	0.00	0.00	Roest and Srivastava 1989
gr-na	C21n	48	62.80	-91.95	-2.61	Roest and Srivastava 1989
gr-na	C24n.3n	54	55.86	-104.55	-4.44	Roest and Srivastava 1989
gr-na	C25n	58	24.48	-137.25	-3.12	Roest and Srivastava 1989
gr-na	C27n	62	27.36	-149.41	-3.72	Roest and Srivastava 1989
gr-na	C31n	68	43.94	-145.31	-4.92	Roest and Srivastava 1989
Plate pair	Source age	Age (Ma)	Lat (°N)	Lon (°E)	Angle/Ma (°/Ma)	Source
sm-lw	angular velocity vector		-27.9	52.2	0.066	Horner-Johnson et al. 2007
lw-sm		30	-27.9	52.2	1.98	
Plate pair	Source age	Age (Ma)	Lat (°N)	Lon (°E)	Angle (°)	Source
sm-in	c5n.2n(o)	10.9	23.98	29.71	4.34	Demets et al. 2004
sm-in	c6n(o)	20.1	24.52	31.20	8.59	Demets et al. 2004
sm-in	c13n(m)	33.3	21.80	35.00	14.39	Royer and Chang 1991
sm-in	c21n(y)	46.3	18.64	43.37	22.56	Royer et al. 2002
sm-in	c22n(y)	49.0	18.94	39.62	23.20	Royer et al. 2002
sm-in	c25n(y)	55.9	19.41	29.02	30.11	Royer et al. 2002
sm-in	c27n(y)	60.9	18.83	24.86	35.41	Royer et al. 2002
sm-in	c33n(o)	79.1	20.32	21.39	51.30	Molnar et al. 1988

*from Stock et al. (unpublished manuscript)

Table 2.2. Covariance matrix values used for the relative plate motions. Covariance matrix values are given in the reference frame fixed to the second plate in the plate pair.

Plate pair	Used for	Source	Source	a	b	c	d	e	f	g
pa-wa	c5	c5	Croon et al. 2008	2.52	0.662	3.49	2.72	3.92	10.6	8
pa-wa	c6	c6	Croon et al. 2008	2.00	0.848	2.37	1.13	1.54	4.65	8
pa-wa	c13	c13	Croon et al. 2008	5.29	3.16	0.72	2.68	3.37	6.19	8
pa-wa	c18	c18	Croon et al. 2008	1.48	1.04	1.61	0.982	1.34	2.24	7
pa-wa	c21	c24	*	49.5	4.10	75.1	2.10	4.60	119	7
pa-wa	c25	c27	*	19.3	-1.10	31.0	0.30	-1.8	50.9	7
pa-wa	c31	c31	*	76.0	-3.42	109	1.33	-2.67	167	7
Plate pair	Used for	Source	Source	a	b	c	d	e	f	g
ea-wa	c13-c31	c13	Cande et al. 2000	2.19	0.0039	5.74	0.0041	0.0083	15.1	5
Plate pair	Used for	Source	Source	a	b	c	d	e	f	g
ea-lw	c5	c5	Lemaux et al. 2002	0.221	0.236	-0.092	0.304	-0.167	0.245	6
ea-lw	c6	c6	Patriat et al. 2008	1.028	0.883	-0.234	1.759	-1.347	2.237	6
ea-lw	c13	c13	Patriat et al. 2008	0.856	0.673	-0.166	0.69	-0.374	0.582	5
ea-lw	c18-c31	c26	Royer and Chang 1991	0.15	0.12	-0.09	0.11	-0.07	0.11	3
Plate pair	Used for	Source	Source	a	b	c	d	e	f	g
lw-nb	c5-c31	**	Horne-Johnson et al. 2007	73.116	49.887	-95.766	41.736	-67.68	132.657	8
Plate pair	Used for	Source	Source	a	b	c	d	e	f	g
nb-na	c5, c6	c6	***	0.5773	-0.4609	0.4223	0.4724	-0.3969	0.3577	5
nb-na	c13	c13	***	0.5686	-0.4835	0.433	0.5206	-0.434	0.3841	5
nb-na	c18	c18	***	0.1231	-0.1092	0.0959	0.1207	-0.0987	0.0884	4
nb-na	c21	c21	***	0.1119	-0.1155	0.0822	0.1484	-0.0991	0.0694	4
nb-na	c25	c25	***	0.1243	-0.1491	0.1024	0.1948	-0.1287	0.0886	4
nb-na	c31	c31	***	0.6503	-0.6436	0.4545	0.9357	-0.5599	0.4392	5
Plate pair	Used for	Source	Source	a	b	c	d	e	f	g
na-eu	c5	c5	Merkouriev and DeMets 2008	0.0779	-0.0133	0.0925	0.0572	-0.1141	0.2978	5
na-eu	c6	c6	Merkouriev and DeMets 2008	0.5661	-0.1278	0.6896	0.0758	-0.2358	0.9895	5
na-eu	c13	c13	***	0.0807	-0.0254	0.1078	0.023	-0.0409	0.1648	4
na-eu	c18	c18	***	0.1835	-0.0559	0.2449	0.0455	-0.0876	0.3697	4
na-eu	c21	c21	***	0.3029	-0.1202	0.3823	0.0778	-0.1658	0.5122	4
na-eu	c25	c25	***	0.2476	-0.0822	0.2974	0.0704	-0.1206	0.3834	4
na-eu	c31	c31	***	0.1968	-0.0683	0.249	0.0301	-0.088	0.3216	3
Plate pair	Used for	Source	Source	a	b	c	d	e	f	g
gr-na	c18, c21	c21	****	0.1574	-0.1967	0.3899	0.2499	-0.4923	0.9775	4
gr-na	c25	c25	****	0.0657	-0.094	0.1778	0.1394	-0.2607	0.495	4
gr-na	c31	c31	****	0.0863	-0.13	0.2396	0.2012	-0.3678	0.6796	4
Plate pair	Used for	Source	Source	a	b	c	d	e	f	g
lw-sm	c5-c31	**	Horne-Johnson et al. 2007	65.004	63.732	-79.782	78.783	-80.493	114.321	8
Plate pair	Used for	Source	Source	a	b	c	d	e	f	g
sm-in	c21	c23	Royer and Chang 1991	42900	77300	19900	139400	35800	9300	7
sm-in	c25, c31	c26	Royer and Chang 1991	13700	28300	9200	58800	19100	6300	7

*Personal communication with Stock 1997

**Extrapolated from the values for angular velocity vector

***Calculated from partial uncertainty rotations of McQuarrie et al. 2003

****Calculated from Acton's unpublished partial uncertainty rotations

$$\text{Covariance matrix} = \begin{pmatrix} a & b & c \\ b & d & e \\ c & e & f \end{pmatrix} \times 10^{-8} \text{ radians}^2$$

Table 2.3. Radiometric age dates used along the Hawaiian-Emperor, Louisville, Tristan da Cunha, Réunion and Iceland tracks.

HAWAII				
Age (Ma)	Lat (°N)	Lon (°E)	Source	Comments
0 ^{a)}	19.6	204.5		At Kilauea
7.2	23.0	198.0	Darlympe et al. 1974	*
10.3	23.5	195.5	Darlympe et al. 1974	*
12	23.6	193.7	Darlympe et al. 1974	*
19.9	25.7	188.0	Darlympe et al. 1981	*
27.7	28.3	182.7	Darlympe et al. 1977	*
31	28.9	181.2	Sharp and Clague 2006	Unnamed seamount; Shield and postshield stage
38.7	30.9	175.9	Sharp and Clague 2006	Colahan seamount; Shield stage
41.5	31.8	174.3	Sharp and Clague 2006	Abbott seamount; Postshield stage
46.7	32.1	172.3	Sharp and Clague 2006	Diakakuji seamount; Postshield stage
47.9	33.7	171.6	Sharp and Clague 2006	Kimmei seamount; Shield stage
50.4	35.1	171.7	Sharp and Clague 2006	Koko (south); Shield stage
52.6	35.9	171.1	Sharp and Clague 2006	Koko (north); Rejuvenated
60.9	44.0	170.0	Sharp and Clague 2006	Suiko seamount; Postshield stage
49.2	34.9	172.2	Duncan and Keller 2004	Site 1206; Koko Seamount; Shield stage
55.5	41.3	170.4	Duncan and Keller 2004	Site 1205; Nintoku seamount; Shield stage
75.8	51.0	167.7	Duncan and Keller 2004	Site 1203; Detroit seamount; Shield stage
81	51.5	168.3	Keller et al. 1995	Detroit north
*Age dates for the younger part of the chain are not comparable in quality to the newer ages along the older part of the chain.				
LOUISVILLE				
Age (Ma)	Lat (°N)	Lon (°E)	Source	Comments
0 ^{a)}	-50.9	221.9	Londsdale 1988	
1.11	-50.4	220.9	Koppers et al. 2004	Sample MTHN-7D1
13.2	-48.2	211.2	Koppers et al. 2004	Sample MTHN-6D1
36.5	-41.6	195.8	Koppers et al. 2004	Sample VG-3a/MSN110-1; Valerie seamount
33.9	-40.8	194.7	Koppers et al. 2004	Sample VM36-02
45.5	-38.3	192.3	Koppers et al. 2004	Sample VM36-03
46.3	-37.0	190.2	Koppers et al. 2004	Sample VM36-04
61.4	-30.1	186.8	Koppers et al. 2004	Sample SOTW-9-48-2; Currituck seamount
68.9	-27.3	185.8	Koppers et al. 2004	Sample SOTW-9-52-1
76.7/78.7	-25.5	185	Koppers et al. 2004	Samples SOTW-9-58-1a and SOTW-9-58-7; Osborn seamount
TRISTAN DA CUNHA				
Age (Ma)	Lat (°N)	Lon (°E)	Source	Comments
0 ^{a)}	-37.5	347.5	O'Connor and le Roex 1992	On Tristan da Cunha island; best age estimate ranges 0.64-1.3 Ma
Walvis Ridge				
30*	-37.1	-7.8	O'Connor and Duncan 1990	Comments from O'Connor and Duncan (1990): Best estimate for the age of this site is 30-31 Ma
39-40	-34.3	-5.0	O'Connor and Duncan 1990	Best estimate for the crystallization age is 39-40 Ma
38-39	-34.5	-3.6	O'Connor and Duncan 1990	Best estimate for the age of this volcano is 38-39 Ma

46,52/~50**	-34.3	-1.6	O'Connor and Duncan 1990	Total fusion age of 52 Ma and plateau age of 46.2
64	-33.0	0.0	O'Connor and Duncan 1990	Apparent age of this sample is 64 Ma
50	-32.6	1.1	O'Connor and Duncan 1990	Questionable sample V29-9-1; we omit this age
61-62	-32.0	2.4	O'Connor and Duncan 1990	Crystallization age of this site is between 61-62 Ma
79	-29.1	3.0	O'Connor and Duncan 1990	Best estimate for the age of the basement is 79 Ma
78-79	-28.5	2.3	O'Connor and Duncan 1990	Best estimate of the crystallization age at this site is between 78-79 Ma
Min 69.8	-25.4	6.7	O'Connor and Duncan 1990	Questionable sample, minimum age provided

*concordant sample with 30 Ma average

**Baksi (1999) estimates ~50 Ma based on high temperature step ages

We omit the ages along the Gough Lineament

REUNION

Age (Ma)	Lat (°N)	Lon (°E)	Source	Comments
0 ^{a)}	-21.1	55.5	McDougall 1971	on Réunion Island
7.5	-21.0	57.5	Duncan and Hargraves 1990; McDougall 1971	
31.5*	-16.0	60.5	Duncan and Hargraves 1990	Industry well NB-1
33.2*	-13.1	61.4	Duncan and Hargraves 1990	ODP site 706
49.3*/50	-4.2	73.4	Duncan and Hargraves 1990	ODP site 713; Baksi (2005) estimates 50±2 Ma
57.2*	5.1	73.8	Duncan and Hargraves 1990	ODP site 715
~65.5	~20.0	~76.0	Hoffmann et al. 2000	Deccan traps, within 1 Ma

*age is the average of weighted isochron and plateau ages

ICELAND

Age (Ma)	Lat (°N)	Lon (°E)	Source	Comments
0 ^{a)}	64.0	344.0	Lawver and Muller 1994	

West Greenland

Storey et al. 1998 estimate that 80% of the lavas erupted between 60.9 and 61.3 Ma

East Greenland

49.4	67.3	-33.2	Tegner et al. 2008	Sample SA-1; Plateau age
47.2	67.5	-32.5	Tegner et al. 2008	Sample P-175; Total fusion age
49.2/49.8	66.7	-34.0	Tegner et al. 1998	Samples 416822 and 416804; Plateau and isochron age
47.3/48.8	68.0	-33.0	Tegner et al. 1998	Samples PCT-75 and KEH-302; Plateau ages

^{a)}Current location of the hotspot

Table 2.4. Locations and uncertainties used as input into the N-hotspot method. Azimuth is the azimuth of the major axis of the uncertainty ellipse associated with the input location.

HAWAII					
Age (Ma)	Lat (°N)	Lon (°E)	Major axis (km)	Minor axis (km)	Azimuth (CW from N)
0	19.6	204.5	100	100	0
10.9	23.7	195.6	200	100	-75
20.1	25.8	187.9	200	100	-80
33.5	29.5	179.5	200	100	-70
39.3	31.1	175.6	200	100	-70
47.9	33.7	171.6	200	100	-35
56.1	41.6	170.4	250	100	-10
67.7	47.2	169.0	300	100	-15
LOUISVILLE					
Age (Ma)	Lat (°N)	Lon (°E)	Major axis (km)	Minor axis (km)	Azimuth (CW from N)
0	-50.9	221.9	200	200	0
10.9	-48.6	213.0	300	100	-70
20.1	-46.3	204.3	300	100	-60
33.5	-40.9	195.0	300	100	-50
39.3	-39.6	193.6	300	100	-45
47.9	-36.3	189.8	300	100	-25
56.1	-32.5	188.0	300	100	-20
67.7	-27.7	186.0	300	100	-25

Table 2.5. Rotations and uncertainties of the Pacific plate relative to the hotspots as determined by the N-hotspot method (Andrews et al., 2006). 'r' is the sum squared normalized misfit.

AGE (Ma)	Best-fit rotation				Covariance matrix values					
	Lat (°N)	Lon (°E)	Angle (°)	r	a	b	c	d	e	f
10.9	67.55	-66.85	9.56	1.50	0.2734	0.1753	-0.0456	0.2587	0.0223	0.1327
20.1	70.55	-71.89	17.49	0.93	0.3012	0.1690	-0.1115	0.2306	-0.0249	0.1636
33.5	67.70	-73.53	26.58	0.04	0.3000	0.1537	-0.0455	0.2050	0.0166	0.1405
39.3	66.77	-66.49	29.90	0.10	0.3311	0.1764	-0.0658	0.2121	-0.0012	0.1408
47.9	64.56	-67.99	34.29	0.005	0.2876	0.1496	-0.0344	0.2027	0.0201	0.1432
56.1	56.03	-73.79	37.96	5.02	0.0947	0.0751	-0.1284	0.3334	-0.0718	0.4016
67.7	50.82	-76.15	41.65	6.00	0.0757	-0.0553	-0.0103	0.4193	-0.0781	0.5928

$$\text{Covariance matrix} = \begin{pmatrix} a & b & c \\ b & d & e \\ c & e & f \end{pmatrix} \times 10^{-3} \text{ radians}^2$$

Chapter 3

A Globally Self-Consistent Model of Plate Motions Relative to the Hotspots for the Past 48 Million Years

Summary

A fundamental problem of global tectonics and paleomagnetism is determining what part of apparent polar wander is due to plate motion and what part is due to true polar wander. One approach for separating these is available if the hotspots can be used as a reference frame fixed in the deep mantle. Building on recent results that have demonstrated no significant motion between the Pacific and Indo-Atlantic hotspots since 48 Ma, we herein present a globally self-consistent model of plate motions relative to the hotspots for the past 48 million years. To obtain the model, we use the tracks of the Hawaiian, Louisville, Tristan da Cunha, Réunion and Iceland hotspots. The new set of plate reconstructions presented here provide a firm basis for estimating absolute plate motions for the past 48 million years and, in particular, can be used to separate paleomagnetically determined apparent polar wander into the part due to plate motion and the part due to true polar wander.

3.1 Introduction

The hotspot frame of reference has been widely used for absolute plate motion models, to infer true polar wander and to study the driving forces of plate motion and mantle convection. The question of how fast hotspots actually move relative to one another, however, has remained as a matter of debate since Morgan (1971) proposed that the hotspots could be used a reference frame fixed in the deep mantle. Over the years, suggestions for the rates of inter-hotspot motion have ranged from apparent fixity (e.g. Morgan, 1971) to rapid motion between the hotspots (e.g. up to 80 mm a^{-1} by Raymond et al. (2000)). Recently, Andrews et al. (2006) challenged the methods used in many of the previous studies on inter-hotspot motion and presented a new method for objectively estimating plate-hotspot rotations and their uncertainties.

In Chapter 2 of this thesis, we have built on the method of Andrews et al. (2006) to obtain a new Pacific-hotspot model for the past 68 million years and have reported that the predicted hotspot tracks for three major hotspots in the Indo-Atlantic (Tristan da Cunha, Réunion, and Iceland) are in better agreement with the observed tracks for the past 48 million years than found before. Accordingly, as shown in Chapter 2, we found no significant motion between the Pacific and Indo-Atlantic hotspots since 48 Ma. In line with the conclusions of Chapter 2, we herein present a globally self-consistent model of plate motions relative to the hotspots for the past 48 million years. The provided set of reconstructions can be used as a fixed frame of reference for absolute plate motions, and true polar wander, for the past 48 million years.

In this study, we use the most up-to-date reconstructions for the past 48 million years together with radiometric dates along the hotspot tracks to derive a plate motion model relative to the major hotspots in the Pacific, Atlantic and Indian Oceans. Specifically, we use the tracks of the Hawaiian, Louisville, Tristan da Cunha, Réunion and Iceland hotspots. All the hotspot tracks used in this analysis are among the most widely accepted candidates for a deep mantle origin (e.g. Courtillot et al., 2003). The poles of rotation are estimated for ages corresponding to some key magnetic anomalies used in plate reconstructions: 10.9 Ma (c5; old end of anomaly 5), 20.1 Ma (c6; old end of anomaly 6), 33.5 Ma (c13; old end of anomaly 13), 39.3 Ma (c18; centre of anomaly 18) and 47.9 Ma (c21; old end of anomaly 21). The time scale of Cande and Kent (1995) is used throughout this chapter.

We also present plate-circuit reconstructions for the Hawaiian, Louisville, Tristan da Cunha, Réunion and Iceland hotspots assuming them to be fixed relative to a global hotspot reference frame and furthermore, we present plate-circuit reconstructions for the Hawaiian and Louisville hotspots assuming them to be fixed relative to an Indo-Atlantic hotspot reference frame. Besides the uncertainties in plate-hotspot rotations, uncertainties in relative plate motions are accumulated through the plate circuit to obtain the final uncertainty (in the form of two-dimensional 95 per cent confidence regions) in the predicted positions. In Chapter 2 of this thesis, we presented plate-circuit reconstructions for the Tristan da Cunha, Réunion and Iceland hotspots assuming them to be fixed relative to a Pacific hotspot reference frame. In this chapter, we will finally compare the different hotspot frames of reference, and predicted tracks, and make a note that they are not significantly different from each other for the past 48 million years.

3.2 Methods and Plate Circuits

3.2.1 Plate-Hotspot Model

We build on the N-hotspot method of Andrews et al. (2006) for objectively estimating plate-hotspot rotations and their uncertainties. The N-hotspot method allows for the use of any number of hotspot tracks and elliptical uncertainties of arbitrary sizes for both ancient and current locations of hotspots in estimating the rotation that minimizes the summed squared normalized misfit. Elliptical uncertainties are useful because the location of an ancient hotspot is due to gaps and uncertainties in the ages along the chain generally much more uncertain in the direction parallel to the volcanic chain than in the direction perpendicular to the volcanic chain. Additionally, other factors, such as the presence of a mid-ocean ridge that might have complicated the track, can be taken into account when assigning the uncertainty. Once a best-fitting rotation for the age in question has been found, a covariance matrix describing the uncertainties in the rotation is calculated from the corresponding eigenvectors and values, found by another grid search (see Andrews et al., 2006 for more).

The sum squared normalized misfit, r , is expected to be approximately chi-square distributed (Andrews et al., 2006). The five hotspot tracks each limit two degrees of freedom and a rotation is specified by three parameters, thus resulting in an over-determined problem with seven degrees of freedom. Values of r exceeding 14.07 are unacceptably large at the 5 per cent significance level, and values of r less than 2.17 are unacceptably small at the 5 per cent significance level.

We use the tracks of the Hawaiian, Louisville, Tristan da Cunha, Réunion and Iceland hotspots in this work. Age data used to establish age progression along the chains is listed in Table 3.1 and the coeval dated points picked along the chains corresponding to c5 (10.9 Ma), c6 (20.1 Ma), c13 (33.5 Ma), c18 (39.3 Ma) and c21 (47.9 Ma) are listed in Table 3.2, along with the assigned uncertainties (two-dimensional 95 per cent confidence limits). These choices are discussed in detail for each hotspot track in Section 3.3. Since the hotspot tracks fall on different plates (Hawaiian and Louisville tracks on the Pacific plate, Tristan da Cunha on the Nubia plate, Réunion track on the Somalia and India plates and the Iceland hotspot track on the Eurasia and Greenland plates), the dated locations and uncertainty regions need to be rotated onto a common reference frame, in this case onto one attached to the Pacific plate. The current locations of the hotspots remain unchanged.

3.2.2 Plate-Circuit

A quantified global plate circuit over the desired time span needs to be established to rotate the dated locations onto a common reference frame and to predict the hotspot tracks. The plate circuit (through Antarctica) used in this study is shown in Fig. 3.1, and our choices for the plate circuit rotations are listed in Table 3.3 and, are discussed in more detail below. Because the published rotations were not necessarily readily available for the ages of our interest, coeval rotations were interpolated from the two published rotations closest to the age of interest. Published rotations were assigned ages according to the time scale of Cande and Kent (1995). To obtain the final uncertainty in the input

positions, the uncertainties in relative plate motions were accumulated through the plate circuit. The reader is referred to Chang (1988), Chang et al. (1990), Royer and Chang (1991) and Kirkwood et al. (1999) for more details. Table 3.4 lists the covariance matrix parameters for the relative plate motion data used in this study. If no covariance matrix for a particular rotation was available, it was estimated from partial uncertainty rotations, i.e. from partial uncertainty rotations of McQuarrie et al. (2003) for their rotations and from unpublished partial uncertainty rotations of Acton (1999) for reconstructing Greenland to North America.

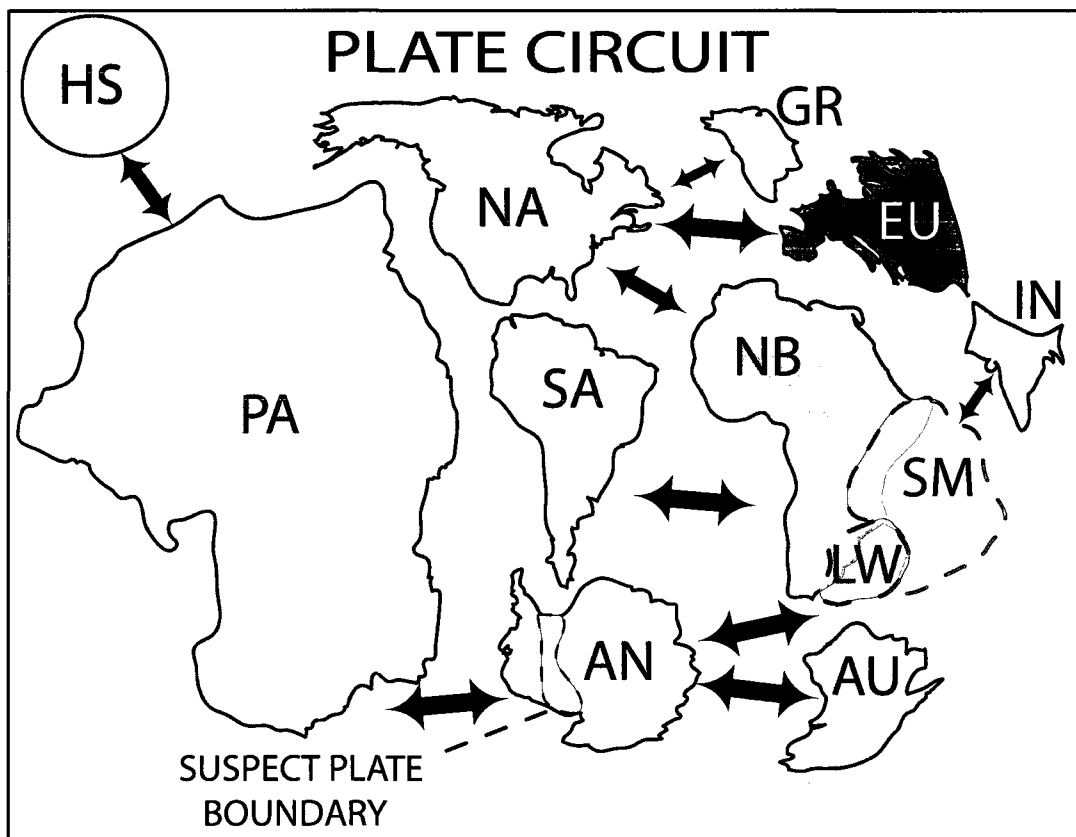


Figure 3.1. Main components and layout of the global plate circuit through mid-ocean ridges (as used in this study). Arrows represent motion on mid-ocean ridges. See text and Table 3.3 for more details.

We have used the most up-to-date rotations in the plate circuit, preferably with published uncertainty estimates. Our circuit links Pacific to West Antarctica with the rotations from Croon et al. (2008) for the past ≈ 40 million years and with a rotation by Cande et al. (1995) for c21. For the motion between East and West Antarctica, the best estimate comes from Cande et al. (2000). From East Antarctica, the circuit moves to Nubia through the Lwandle plate (Horner-Johnson et al., 2007) and, we assume motion between the Nubia, Somalia and Lwandle plates since 30 Ma. The exact timing of motion between the Nubia (West Africa) and Somalia (East Africa) plates is still an open question and the boundary between these two plates has not been fully resolved. To explain some of the observed discrepancy, Lwandle plate has been suggested to lie between the Nubia and Somalia plates (Hartnady, 2002; Horner-Johnson et al., 2007). Following this suggestion, we account for the Lwandle plate. Accordingly, we take the estimates for East Antarctic-Somalia motion (e.g. Lemaux et al., 2002; Patriat et al., 2008; Royer and Chang, 1991) to actually represent East Antarctic-Lwandle motion because most of the data used to constrain these estimates of the relative motion actually come from the portion of the Southwest Indian Ridge on the boundary of the East Antarctic and hypothesized Lwandle plates. For reconstructing Nubia relative to North America, we use the rotations of McQuarrie et al. (2003) and for North America to Eurasia, the recent detailed study by Merkuriev and Demets (2008) for the past 20 million years, and the parameters by McQuarrie et al. (2003) for earlier times. For the motion between Greenland and North America, we rely on the work of Roest and Srivastava (1989). And, for reconstructing the India plate relative to the Somalia plate for c21, a rotation from Royer et al. (2002).

The circuit used in this study is the same as was used in Chapter 2 of this thesis, and a more detailed discussion of the choices can be found in Appendix A.

3.3 Age Progression Along the Hotspot Tracks

Age data along the hotspot tracks are of varying quality. As new age determinations over the past few years have become available for the Pacific, it has become clear that the older age estimates are not comparable to the new age estimates obtained with improved methods. In particular, the new age data has changed our understanding of the age progression along Hawaiian-Emperor and Louisville chains (e.g. Sharp and Clague, 2006; Koppers et al., 2004), key examples of hotspot volcanism in the Pacific. Baksi (1999; 2005) has reanalyzed some old sets of age data from the Atlantic, Indian and Pacific Oceans (including data along Tristan da Cunha and Réunion tracks) and has concluded that many of the old data used to temporally define hotspot tracks are invalid as proper estimates for crystallization age. The early ages include many conventional K-Ar total fusion ages and $^{40}\text{Ar}/^{39}\text{Ar}$ total fusion analyses on whole rocks that lack internal reliability criteria, making their accuracy difficult to assess. As we have recently seen significant changes in the age progression along the Hawaiian-Emperor and Louisville chains, it is to be expected that as more new age determinations become available, our understanding of the age progression along the Indo-Atlantic hotspot tracks will be prone to change, too. If we, however, apply the very strict analysis criteria of Baksi (1999; 2005), we are left with almost no data along the Indo-Atlantic hotspot tracks. It is spatially clear, however, where the tracks lie (the tracks can be clearly distinguished in

topography and gravity anomaly maps) and the old age data do establish clear age progressions. Thus, we simply take the ambiguity in ages into account by introducing large uncertainties where applicable. Even if currently unknown errors would be present in ages, the likelihood of the new dated locations lying outside our uncertainty regions is small.

3.3.1 Hawaiian-Emperor and Louisville Tracks

We take the current location of the Hawaiian hotspot as 19.6°N , 204.5°E , at Kilauea. The current location of the Hawaiian hotspot is well documented and thus, we assign a circular uncertainty with a radius of only 100 km (95 per cent confidence region) to it. The current location of the Louisville hotspot is taken to be at -50.9°N , 221.9°E (Lonsdale, 1988) at a seamount in the close vicinity of a seamount with recent volcanism (dated 1.1 Ma by Koppers et al. (2004)). The Louisville hotspot is assigned a circular uncertainty region with a radius of 200 km. The Louisville hotspot has not left an easily traceable track for the recent past and considerably different, more southern, present-day locations have been suggested and used (such as -53.6°N 219.4°E by Morgan and Morgan (2007) in their recent analysis of the current motions of the plates relative to the hotspots). However, we have chosen to use the current location as suggested by Lonsdale (1988), as it is commonly used in plate-hotspot reconstructions and seems to follow the ancient trend of the Louisville track better than the other suggested current locations.

For most part of their history, both the Hawaiian and Louisville hotspots have produced a rather simple track. Because more age data is available along the Hawaiian-Emperor chain, the major axes of the uncertainty ellipses along the chain are assigned smaller values than for the Louisville chain (see Tables 3.1 and 3.2 for more details). Inputs to the N-hotspot method are also shown in Figs. 3.2a and b.

Input locations herein are the same as were used in Chapter 2 of this thesis to obtain the Pacific-hotspot rotations.

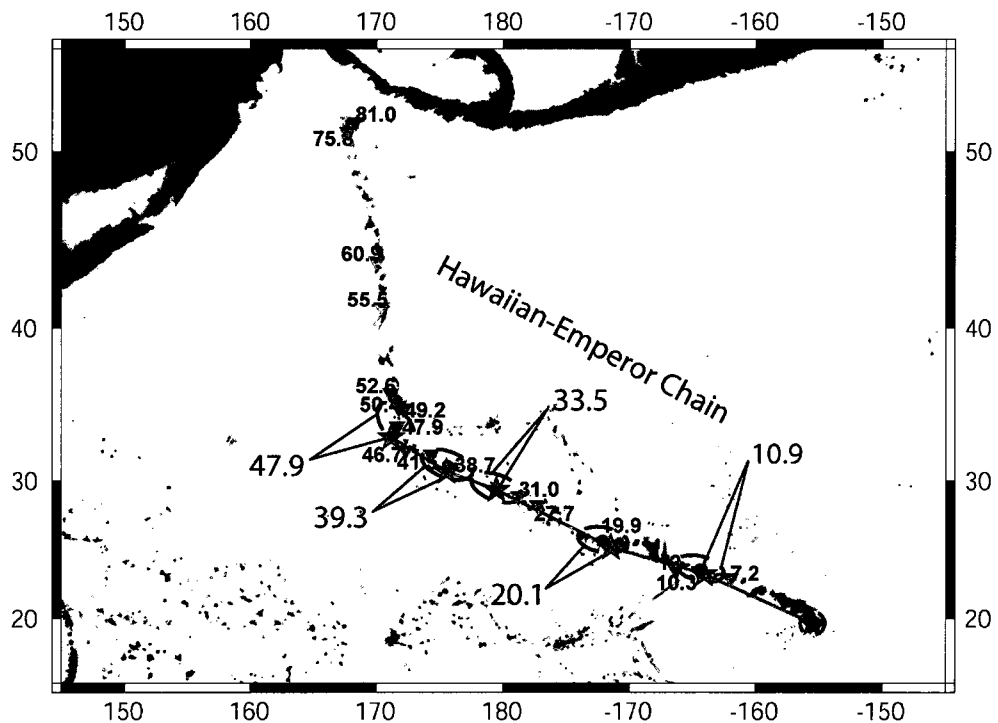


Figure 3.2a. Map showing the Hawaiian-Emperor hotspot track, input (black small circles with the two-dimensional 95 per cent confidence ellipses shown with dashed line) to the N-hotspot numerical method and resulting model (red stars) obtained using all five hotspot tracks as input. Red inverted triangles accompanied with small numerals show locations of dated igneous rock samples with ages (see references in Table 3.1). All ages are in millions of years before present.

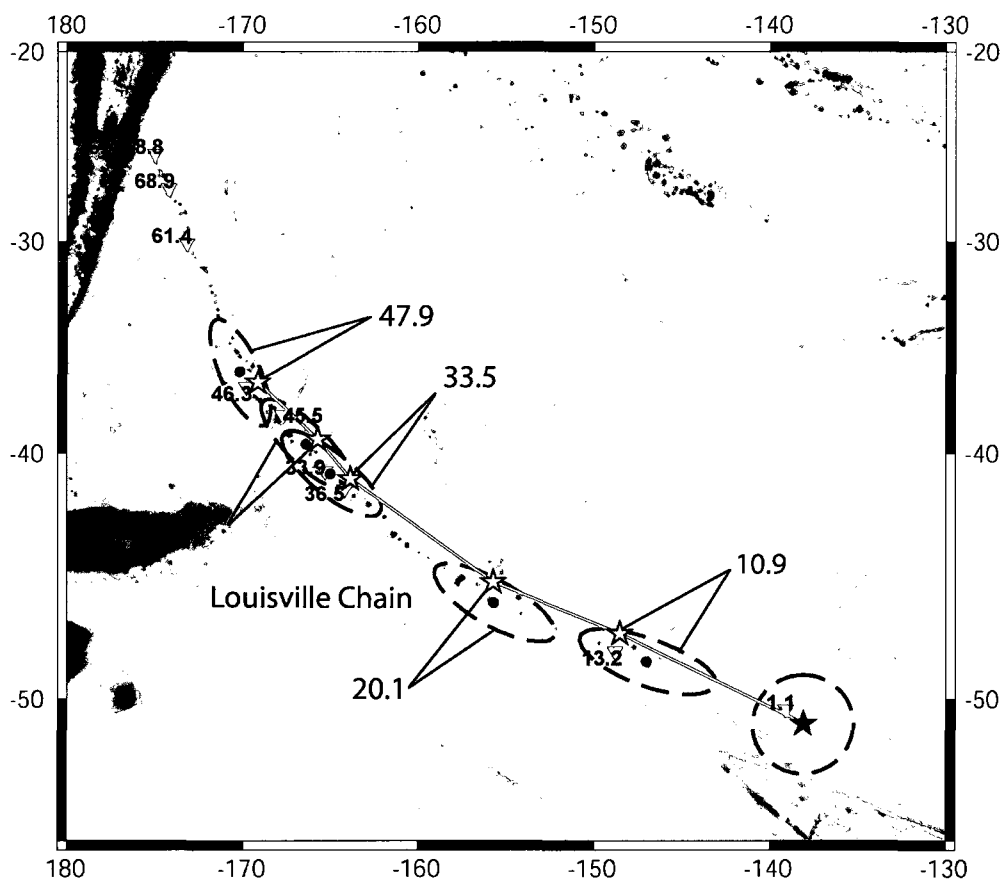


Figure 3.2b. Map showing the Louisville hotspot track, input (black small circles with the two-dimensional 95 per cent confidence ellipses shown with dashed line) to the N-hotspot numerical method and resulting model (red stars) obtained using all five hotspot tracks as input. Red inverted triangles accompanied with small numerals show locations of dated igneous rock samples with ages (see references in Table 3.1). All ages are in millions of years before present.

3.3.2 Tristan da Cunha

Tristan da Cunha hotspot track comprises the Walvis Ridge on the Nubia plate and the Rio Grande Rise on the South America plate. Age data has demonstrated a clear age progression on the Walvis Ridge for the past ~80 million years (O'Connor and Duncan, 1990; O'Connor and le Roex, 1992; Table 3.1), with active volcanism currently occurring on both Tristan da Cunha and Gough Islands, ~400 km apart. Etendeka Flood Basalts in

Africa and Parana Flood Basalts in South America can be tracked at the ends of the Walvis Ridge and the Rio Grande Rise. The peak event of volcanism is dated at ~131-133 Ma (Renne et al., 1992; Renne et al., 1996) indicating the arrival of the Tristan da Cunha plume head at this time. Unfortunately, only one age estimate exists along the Rio Grande Rise (O'Connor and Duncan, 1990), but, the Walvis Ridge has been fairly well covered (O'Connor and Duncan, 1990). Two distinct age progressions can be followed for the Tristan da Cunha and Gough lineaments (O'Connor and Duncan, 1990; O'Connor and le Roex, 1992). The mechanism which produces this type of dual age progression is still unclear (other examples of such systems are for example, Madeira and Canary, and Easter and Crough). However, Tristan da Cunha has been widely accepted as the primary hotspot location in the system (e.g. Courtillot et al., 2003) and age progression established on the Walvis Ridge can be associated to Tristan da Cunha. Thus, herein, we omit the ages along the Gough lineament.

The current position of the Tristan da Cunha hotspot is taken as -37.5°N , 347.5°E on Tristan da Cunha Island and is assigned a circular two-dimensional 95 per cent confidence region with a radius of 150 km. The best estimate for the age of volcanism on the Tristan da Cunha Island ranges from 0.64-1.3 Ma (0.64 Ma for isochron age and 1.3 Ma for plateau age; O'Connor and le Roex, 1992). We also assign a circular uncertainty for 10.9 Ma and 20.1 Ma because the topographic expression of the hotspot track for these times is not as prominent as for the earlier times. Elliptical uncertainties are assigned for ages 33.5 Ma and 39.3 Ma, with 200-km-long major semi axes and 150-km-long minor semi axes. The uncertainty region for 39.3 Ma includes all the dated samples for ages 38-40 Ma (see Table 3.1). For estimating the 47.9 Ma location on the chain, we

have used the dated volcanism for ~ 38 Ma and ~ 64 Ma along the chain. The uncertainty region (elliptical uncertainty region with 200-km-long major semi axis and 150-km-long minor semi axis) includes the dated volcanism for ≈ 50 Ma, but, we haven't used this location primarily because the original age estimate for the location resulted in discordant total fusion and plateau ages of 52 and 46 Ma, respectively (O'Connor and Duncan, 1990). Furthermore, O'Connor and Duncan (1990) actually give their best age estimate as a minimum age of 52 Ma. There is another sample dated ≈ 50 Ma along the northern segment of the chain, but this age estimate has been reported as questionable (O'Connor and Duncan, 1990) and thus we omit it.

The input into the N-hotspot method is shown in Fig. 3.2c. Actual input uncertainties for the Tristan da Cunha hotspot are larger than discussed above because we need to add the uncertainties in the relative plate motions when the dated locations are rotated onto a common reference frame attached to the Pacific plate (in Fig. 3.2c the final uncertainties, as well as the originally picked uncertainties along the chain, are shown in the reference frame attached to the Nubia plate). These differences are not visible for c5 and c6, but the combined final uncertainties become increasingly bigger for c13, c18 and c21, as the uncertainties in relative plate motions increase.

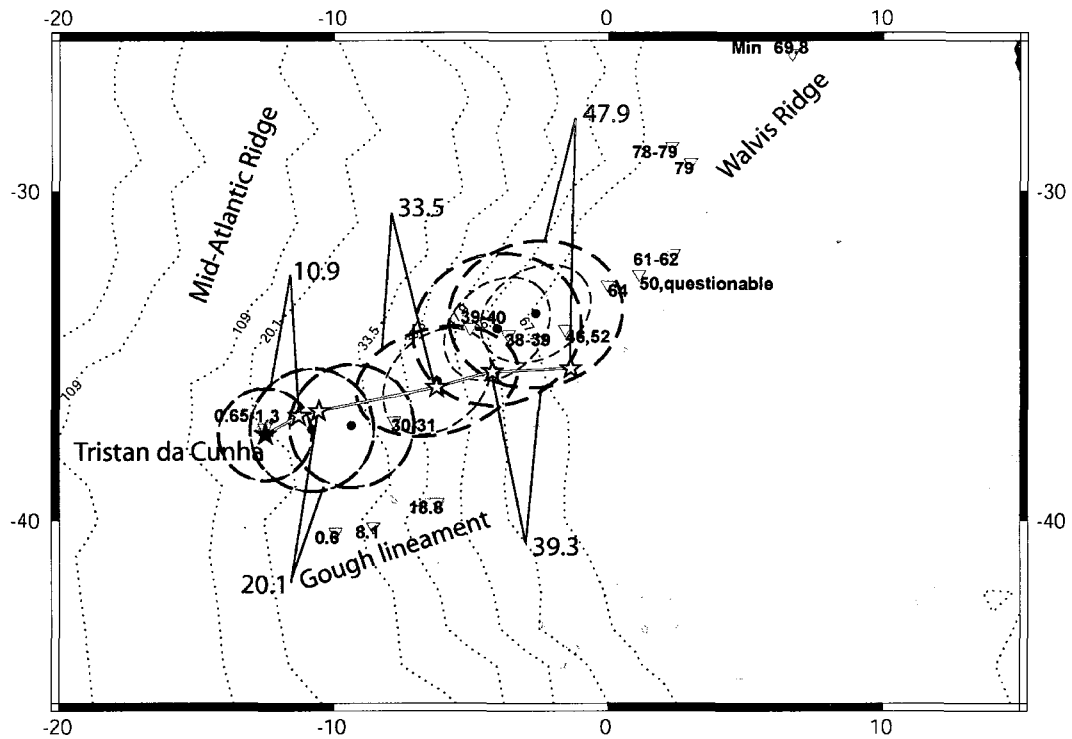


Figure 3.2c. Map showing the Tristan da Cunha hotspot track, input (black small circles with the two-dimensional 95 per cent confidence ellipses shown with stronger dashed line) to the N-hotspot numerical method and resulting model (red stars) obtained using all five hotspot tracks as input. Red inverted triangles accompanied with small numerals show locations of dated igneous rock samples with ages (See references in Table 3.1). Note that since the Indo-Atlantic data needs to be rotated onto the Pacific reference frame, uncertainties in the relative plate motions are added to the initial uncertainties picked along the chains (shown here with lighter dashed uncertainty regions). All uncertainty regions are shown in their original frames of reference. Dotted lines are synthetic isochrons from Mueller et al. (2008) with ages (Ma) as labeled. All ages are in millions of years before present.

3.3.3 Réunion

Many of the intraplate volcanic features in the Indian Ocean are attributed to known hotspots, one of the most impressive features being the Réunion hotspot track which consists of the Chagos-Laccadive Ridge on the India plate, and the Mascarene Plateau-Nazareth Bank-Mascarenen Island group on the Somalia plate (Duncan and Hargraves,

1990). The Deccan flood basalts indicate the arrival of the Réunion plume head beneath India at around 65.5 Ma (e.g. Hoffmann et al., 2000; other estimates by Duncan and Pyle (1988) and Courtillot et al. (1988) span from 64 to 69 Ma).

The current position of the Réunion hotspot is taken as -21.1°N , 55.5°E on Réunion Island. Réunion Island has experienced ongoing volcanism since 2 Ma (Duncan and Hargraves, 1990; McDougall, 1971), and Duncan (1990) notes that a large seamount, currently 160 km west of Réunion, may actually represent the most recent activity of the hotspot. Thus, the present-day location of the Réunion hotspot is assigned a circular uncertainty with a radius of 200 km to include this possible shift of the current location of the hotspot.

We pick the locations for 10.9 Ma (c5), 20.1 Ma (c6), 33.5 Ma (c13) and 39.3 Ma (c18) on the Mascarene Plateau within the Somalia plate, and the location for 47.9 Ma (c21) on the Chagos-Laccadive Ridge on the India plate. Thus, we assume that the Réunion hotspot has stayed under the Somalia plate at least since 39.3 Ma. Age progression on the Mascarene Plateau, however, is somewhat complicated to assess. We believe that the samples dated as 31.5 Ma and 33.2 Ma on the Mascarene Plateau (Duncan and Hargraves, 1990; Table 3.1) may not necessarily reflect age progression along the hotspot track but may actually be age estimates for the seafloor in the locations. Thus, we do not primarily base the age progression on these ages. However, we assign large uncertainty ellipses especially for the 33.5 Ma and 39.3 Ma locations. These uncertainty ellipses also include the dated locations for 31.5 Ma and 33.2 Ma. The 10.9 Ma location is assigned an uncertainty ellipse with a 300-km-long major axis and 150-km-long minor axis. The location for 20.1 Ma is assigned an uncertainty ellipse with a

400-km-long major axis and 150-km-long minor axis. The 33.5 Ma and 39.3 Ma locations are assigned uncertainty ellipses with 550-km-long major axes and 200-km-long minor axes. Finally, the 47.9 Ma location is taken to be slightly south from the 49.3 Ma dated location (Duncan and Hargraves, 1990) and is assigned uncertainty ellipse with a 300-km-long major axis and 200-km-long minor axis. The input locations along with the uncertainties are shown in Fig. 3.2d (and listed in Table 3.2).

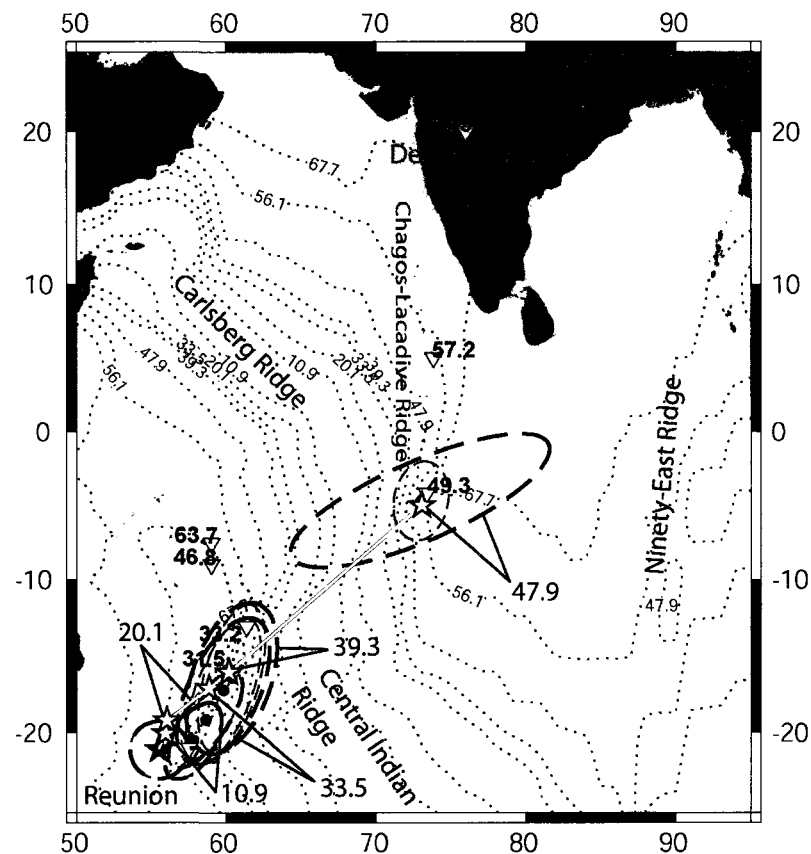


Figure 3.2d. Map showing the Réunion hotspot track, input (black small circles with the two-dimensional 95 per cent confidence ellipses shown with stronger dashed line) to the N-hotspot numerical method and resulting model (red stars) obtained using all five hotspot tracks as input. Red inverted triangles accompanied with small numerals show locations of dated igneous rock samples with ages (See references in Table 3.1). Note that since the Indo-Atlantic data needs to be rotated onto the Pacific reference frame, uncertainties in the relative plate motions are added to the initial uncertainties picked along the chains (shown here with lighter dashed uncertainty regions). All uncertainty regions are shown in their original frames of reference. Dotted lines are synthetic isochrons from Mueller et al. (2008) with ages (Ma) as labeled. All ages are in millions of years before present.

3.3.4 Iceland

Iceland hotspot track comprises anomalously thick and compositionally enriched basaltic oceanic crust at Iceland and at the Greenland-Faeroe and Voring Plateaus. The location of the Iceland hotspot on the axis of the Mid-Atlantic Ridge gives it a unique role. As a consequence of the plume-ridge interaction, the Iceland hotspot lacks a simple time-progressive volcanic track. However, Vink's (1984) simple geometric model with a fixed hotspot, and channeling of asthenosphere to the closest section of the rise crest, uniquely predicts a location, orientation, and age progression for the Greenland-Faeroe and Voring Plateaus. Thus, these features are used to constitute the Iceland hotspot track and the ocean floor isochrons are used to indicate the location of the hotspot at different times.

Widespread initiation of volcanism over the Labrador-Greenland-British Isles region has been documented at ~61-62 Ma, with contemporaneous eruptions occurring over a broad, roughly circular area 2000 km across (Storey et al., 1998; Tegner et al., 1998; 2008; Storey et al., 2007). This has been interpreted to represent the arrival of the Iceland mantle plume. At ~56 Ma, continental thinning focused on the East Greenland margin and continental separation between Europe and Greenland began (Storey et al., 2007). The East Greenland rifted margin has furthermore experienced a prolonged period of volcanic activity, mostly constrained to discrete episodes of magmatism (e.g. Tegner et al., 1998; 2008). The discrete post-breakup episodes are explained first by the crossing of the central East Greenland rifted margin over the axis of the Iceland mantle plume (50-47 Ma) and later by uplift associated with regional plate-tectonic reorganization (37-35 Ma) (Tegner et al., 1998; 2008).

The current position of the Iceland hotspot is taken as 64°N, 344°E (Lawver and Mueller, 1994), under eastern Iceland about 240 km east of the Reykjanes and Kolbeinsey ridges. The present-day location is assigned a circular uncertainty region with a radius of 200 km which includes all the other suggestions for the present-day location (e.g. Mihalfy et al., 2008; Morgan and Morgan, 2007). The location for 10.9 Ma is picked on the Eurasia plate, on the older side of the corresponding seafloor isochron and the 20.1 Ma, 33.5 Ma and 39.3 Ma locations on the older side of the corresponding seafloor isochrons on the Greenland plate. The 47.9 Ma location is taken to be in East Greenland, in the vicinity of the volcanism dated 50-47 Ma (e.g. Tegner et al., 1998; 2008). All these locations are assigned elliptical uncertainties with 200-km-long major semi axes and 150-km-long minor semi axes to include the hotspot related features on the Greenland-Faeroe Plateau. The input locations along with the uncertainties are shown in Fig. 3.2e.

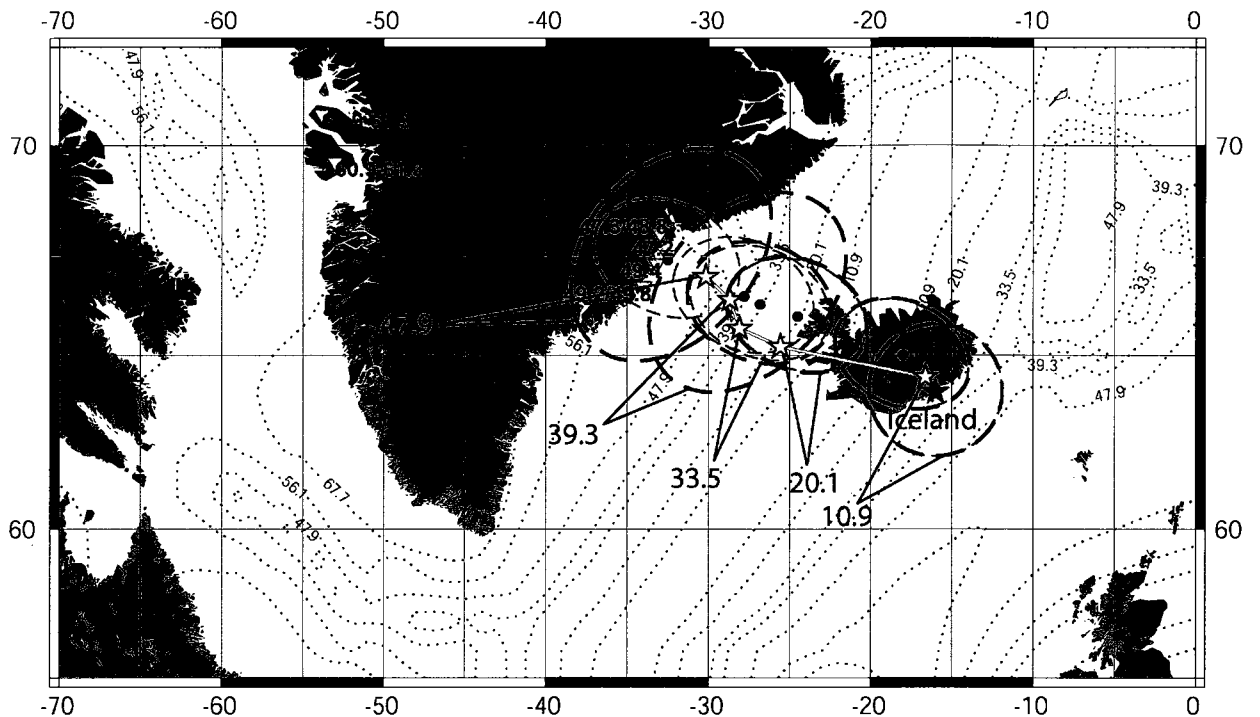


Figure 3.2e. Map showing the Iceland hotspot track, input (black small circles with the two-dimensional 95 per cent confidence ellipses shown with stronger dashed line) to the N-hotspot numerical method and resulting model (red stars) obtained using all five hotspot tracks as input. Red inverted triangles accompanied with small numerals show locations of dated igneous rock samples with ages (See references in Table 3.1). Note that since the Indo-Atlantic data needs to be rotated onto the Pacific reference frame, uncertainties in the relative plate motions are added to the initial uncertainties picked along the chains (shown here with lighter dashed uncertainty regions). All uncertainty regions are shown in their original frames of reference. Dotted lines are synthetic isochrons from Mueller et al. (2008) with ages (Ma) as labeled. All ages are in millions of years before present.

3.4 Results

Fig. 3.3 shows the resulting Pacific-hotspot poles of rotation for all five hotspot tracks as input. The poles are listed in Table 3.5 with sum squared misfits and covariance matrix parameters. The pole positions appear to progress somewhat systematically from 20.1 Ma to 47.9 Ma, with the pole for 33.5 Ma creating a small kink into the pattern. Interestingly, the pole for 10.9 Ma moves further away from the other poles, and closer to the pole of

Morgan and Morgan (2007; at 59.33°N, -85.10°E) as recently suggested for present-day Pacific plate motion relative to global hotspots.

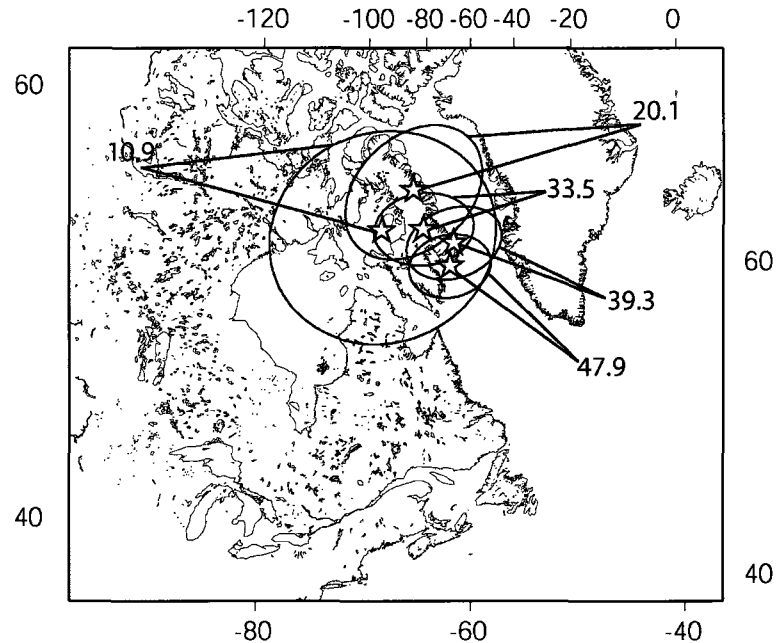


Figure 3.3. Poles of rotation for the Pacific plate motion relative to the global hotspots (red stars). Ellipses are the corresponding two-dimensional 95 per cent confidence regions. Uncertainties seem to get smaller with increasing age. This, however, does not indicate decreasing uncertainty with age but is an artifact caused by projecting uncertainties of rotations onto a spherical surface (Chang et al., 1990).

The model-calculated positions for each track are shown in Figs. 3.2a-e. The model fits the observed volcanism along the Hawaiian-Emperor and Louisville tracks very well (Figs. 3.2a and b). For Tristan da Cunha, the model deviates from the observed track somewhat more for 39.3 Ma and 47.9 Ma (Fig. 3.2c). Overall, the model fits the observed track very well for Réunion, and for 47.9 Ma, the difference between the observed (dated sample for ~49 Ma) and modeled locations is vanishingly small (Fig. 3.2d). The observed and modeled Iceland tracks agree well (Fig. 3.2e), too.

Misfits for 10.9 Ma, 20.1 Ma, 39.3 Ma and 47.9 Ma fall within the acceptable limits, as discussed above in the Section 3.2 on methods, but misfit for 33.5 Ma is smaller

than the lower limit (Table 3.5). This reflects too conservative uncertainty regions as picked along the tracks.

Fig. 3.4 compares the poles of rotation obtained for the Pacific hotspots (Hawaiian and Louisville; Chapter 2 of this thesis) with the poles of rotation estimated in this Chapter for the Indo-Atlantic hotspots (Tristan da Cunha, Réunion and Iceland; the poles listed in Table 3.6). Uncertainty regions for the Indo-Atlantic poles are smaller as we have used more tracks (three tracks as compared to the two tracks in Pacific) for them. The poles for the Pacific hotspots stay within the uncertainty regions of the Indo-Atlantic poles suggesting, within the uncertainties, no significant motion between these two frames of reference.

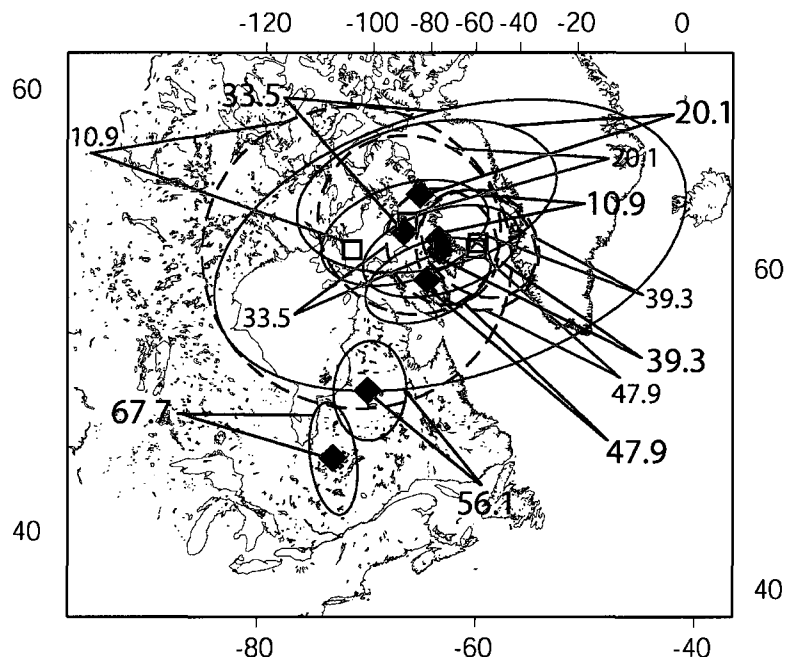


Figure 3.4. Poles of rotation for the Pacific plate motion relative to the Indo-Atlantic hotspots (red squares with dashed ellipses) and poles of rotation for the Pacific plate motion relative to the Pacific hotspots (blue diamonds with solid ellipses; Chapter 2 of this thesis). Ellipses are the corresponding two-dimensional 95 per cent confidence regions.

To investigate these three frames of reference (Pacific, Indo-Atlantic and global hotspots) in closer detail, we tested the motion between them through plate-circuit reconstructions. The relative plate motion data we have used for the predictions is the same as that used to rotate the input onto a common reference frame, and is listed in Table 3.3. To obtain the final uncertainty in the predicted positions, the uncertainties in relative plate motions were accumulated through the plate circuit. Table 3.4 lists the covariance matrix parameters used.

First, we predicted the tracks of each hotspot by obtaining a Pacific-hotspot model, with the use of all the tracks except the one we were about to predict. All the poles of rotation obtained this way are listed in Table 3.6. Figs. 3.5 to 3.9 show the predicted tracks for each hotspot. All the predicted tracks agree with the observed tracks within the uncertainties, thus indicating no significant motion between the hotspots. For the Hawaiian-Emperor track, the fit to the observed track is very good (Fig. 3.5) and only the predicted position for 47.9 Ma deviates notably from the dated volcanism (but, note that these predicted positions are in far better agreement with the observed track than those previously presented for predicting the Hawaiian-Emperor track, for example, by Raymond et al. (2000) and Steinberger et al. (2004)). The predicted Louisville track lies slightly north from the observed track (Fig. 3.6). This may indicate that the current position of the hotspot used to predict the tracks is not viable. If a slightly southern location (as is suggested by some authors, e.g. Wessel and Kroenke (1997)) was used, the predicted track would coincide with the observed track. However, within the uncertainties, the predicted track coincides well with the observed track. For Tristan da Cunha, the biggest differences appear for the predicted 39.3 Ma and 47.9 Ma locations

(Fig. 3.7). The predicted Réunion and Iceland tracks agree with the observed tracks well (Figs. 3.8 and 3.9). Small motions, up to $\approx 10 \text{ mm a}^{-1}$, are allowed within the uncertainties, but this is far less than the earlier suggestions for rapid motion between the hotspots (e.g. Molnar and Stock, 1987).

For comparison, we also predicted the tracks of the Hawaiian and Louisville hotspots from the model of Pacific plate motion relative to the Indo-Atlantic hotspots (Figs. 3.5 and 3.6). These predicted tracks are almost identical to the predictions from the global model. Interestingly, however, the predicted positions from the Indo-Atlantic model agree slightly better with the observed tracks, in particular for the 47.9 Ma predicted locations. In Figs. 3.7 to 3.9 the predictions made in Chapter 2 of this thesis for the Tristan da Cunha, Réunion and Iceland hotspots from the Pacific hotspots are also shown for a comparison. In these cases, the global model agrees with the observed tracks slightly better than the predicted positions from the Pacific hotspots only. For Tristan da Cunha and Iceland, the global model clearly results in smoother predicted tracks. For Réunion, the predicted tracks, however, are almost identical.

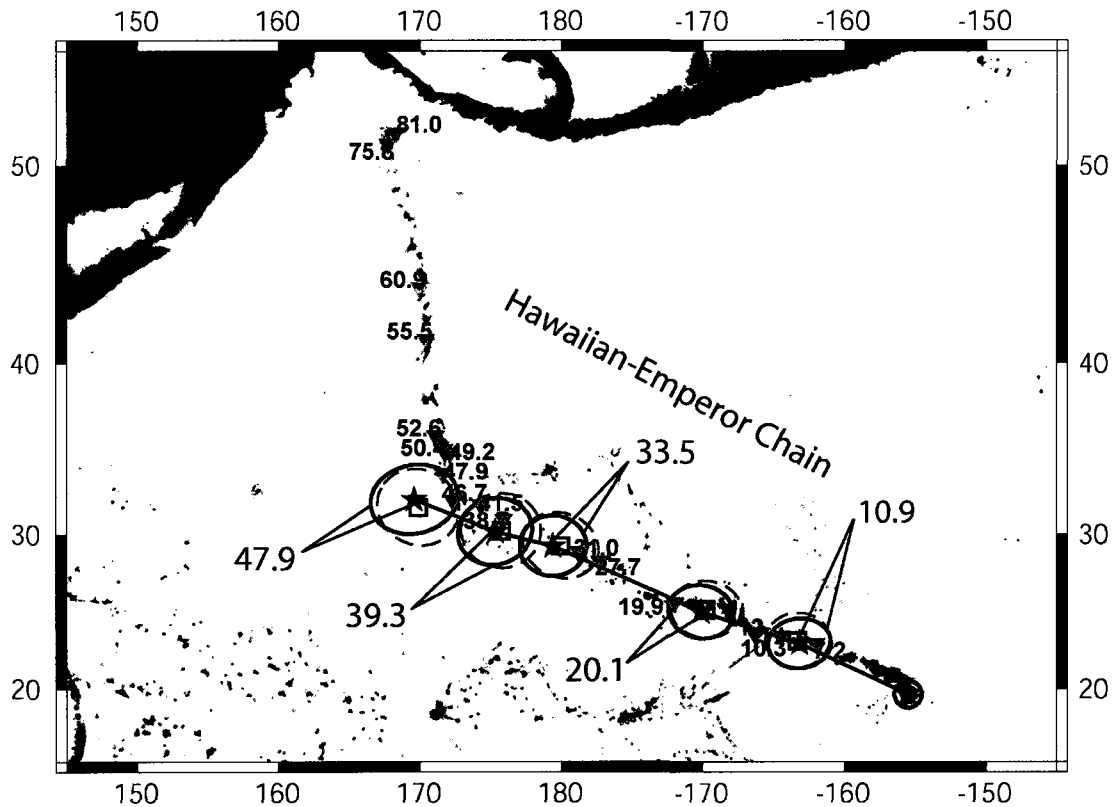


Figure 3.5. Predicted positions of the Hawaiian hotspot relative to the Pacific plate assuming that the Hawaiian hotspot is stationary relative to the Louisville, Tristan da Cunha, Réunion and Iceland hotspots (shown with blue stars) and assuming that the Hawaiian hotspot is stationary relative to the Indo-Atlantic hotspots (black squares). Red inverted triangles accompanied with small numerals show locations of dated igneous rock samples with ages (See references in Table 3.1). Ellipses (two-dimensional 95 per cent confidence regions) show uncertainties propagated from the uncertainties in the motion of the Pacific plate relative to the hotspots and relative plate motion uncertainties, combined with the uncertainty in the current location of the Hawaiian hotspot. The black star shows the current location of the Hawaiian hotspot (at 19.6°N, 204.5°E). All ages are in millions of years before present.

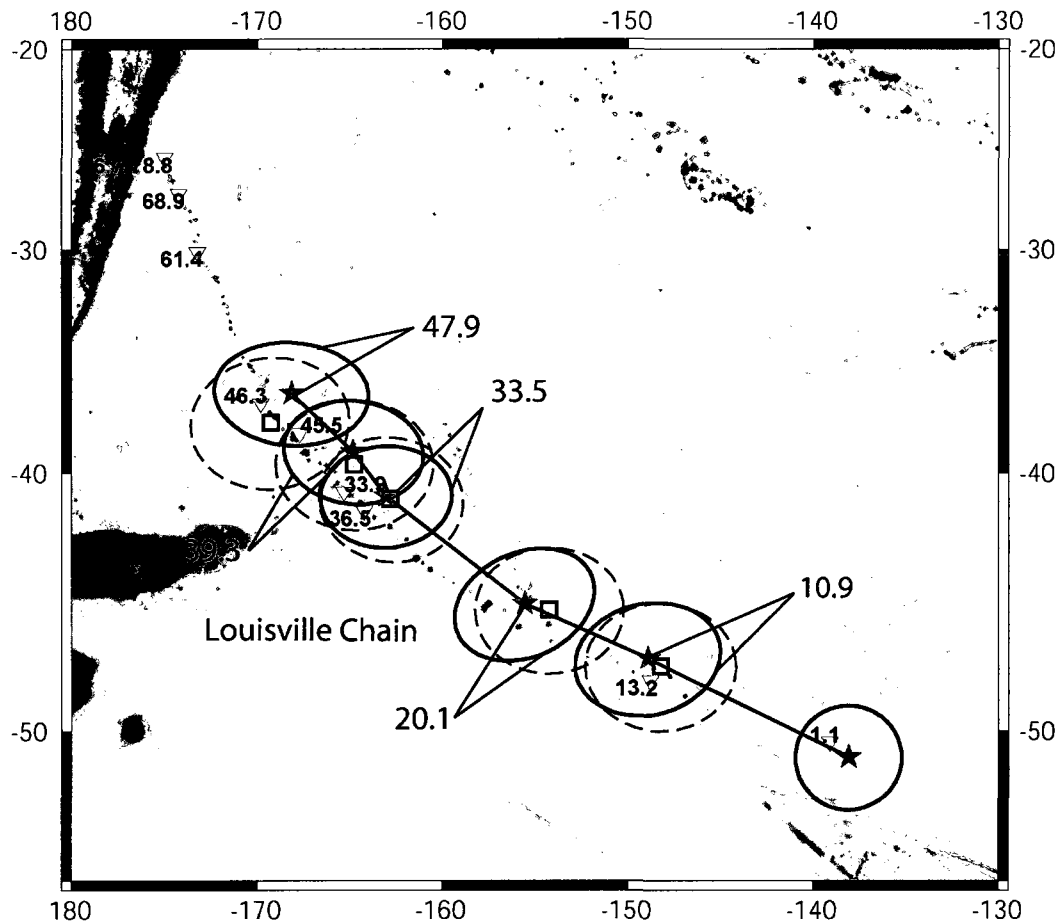


Figure 3.6. Predicted positions of the Louisville hotspot relative to the Pacific plate assuming that the Louisville hotspot is stationary relative to the Hawaiian, Tristan da Cunha, Réunion and Iceland hotspots (shown with blue stars) and assuming that the Louisville hotspot is stationary relative to the Indo-Atlantic hotspots (black squares). Red inverted triangles accompanied with small numerals show locations of dated igneous rock samples with ages (See references in Table 3.1). Ellipses (two-dimensional 95 per cent confidence regions) show uncertainties propagated from the uncertainties in the motion of the Pacific plate relative to the hotspots and relative plate motion uncertainties, combined with the uncertainty in the current location of the Louisville hotspot. The black star shows the current location of the Louisville hotspot (at -50.9°N , 221.9°E). All ages are in millions of years before present.

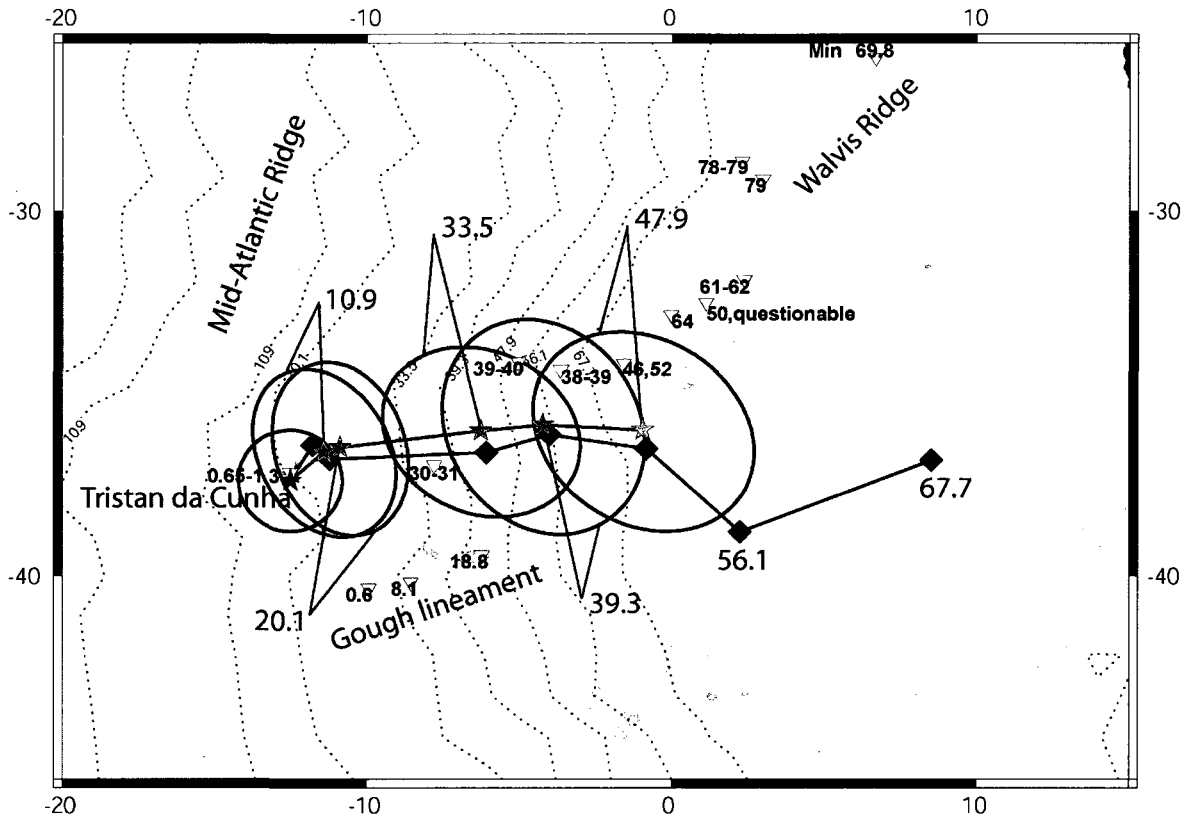


Figure 3.7. Predicted positions of the Tristan da Cunha hotspot relative to the Nubia plate assuming that the Tristan da Cunha hotspot is stationary relative to Hawaiian, Louisville, Réunion and Iceland hotspots (shown with green stars). Predicted positions assuming that the Tristan da Cunha hotspot is stationary relative to the Pacific hotspots (black diamonds) are shown for a comparison (Chapter 2 of this thesis). Red inverted triangles accompanied with small numerals show locations of dated igneous rock samples with ages (See references in Table 3.1). Ellipses (two-dimensional 95 per cent confidence regions) show uncertainties propagated from the uncertainties in the motion of the Pacific plate relative to the hotspots and relative plate motion uncertainties, combined with the uncertainty in the current location of the Tristan da Cunha hotspot. The black star shows the current location of the Tristan da Cunha hotspot (at -37.5°N , 347.5°E). Dotted lines are synthetic isochrons from Mueller et al. (2008) with ages (Ma) as labeled. All ages are in millions of years before present.

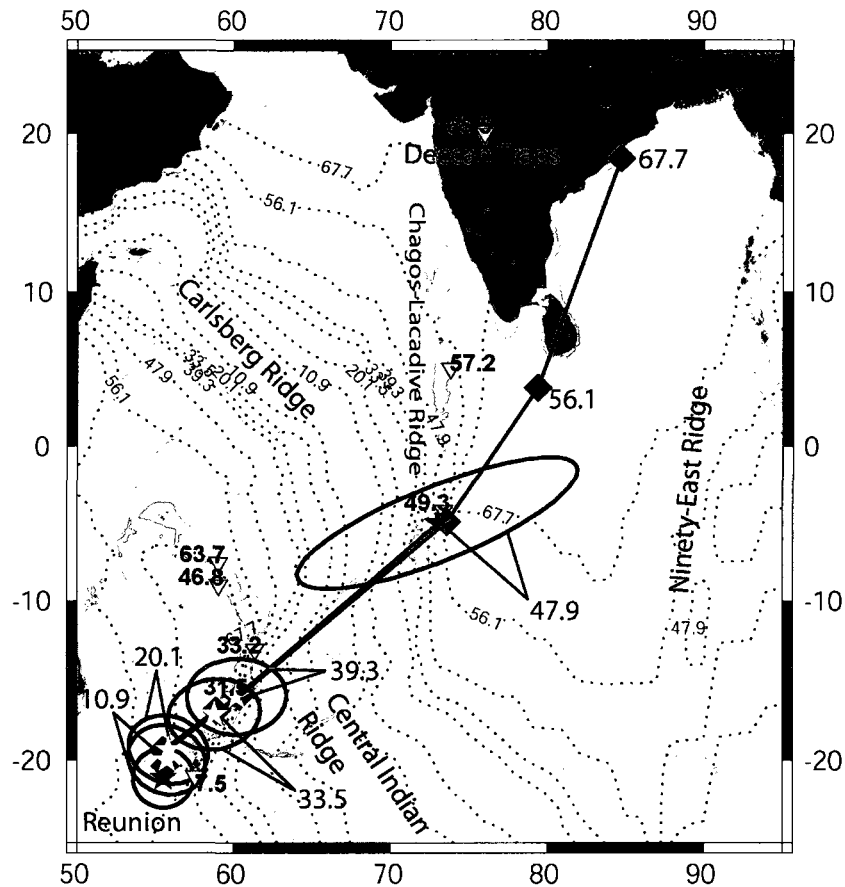


Figure 3.8. Predicted positions of the Réunion hotspot relative to the Somalia plate for times 10.9 Ma through 39.3 Ma (yellow stars) and relative to the India plate for older times (purple stars) assuming that the Réunion hotspot is stationary relative to the Hawaiian, Louisville, Tristan da Cunha and Iceland hotspots. Predicted positions assuming that the Réunion hotspot is stationary relative to the Pacific hotspots (black diamonds) are shown for a comparison (Chapter 2 of this thesis). Red inverted triangles accompanied with small numerals show locations of dated igneous rock samples with ages (See references in Table 3.1). Ellipses (two-dimensional 95 per cent confidence regions) show uncertainties propagated from the uncertainties in the motion of the Pacific plate relative to the hotspots and relative plate motion uncertainties, combined with the uncertainty in the current location of the Réunion hotspot. The black star shows the current location of the Réunion hotspot (at -21.1°N , 55.5°E). Dotted lines are synthetic isochrons from Mueller et al. (2008) with ages (Ma) as labeled. All ages are in millions of years before present.

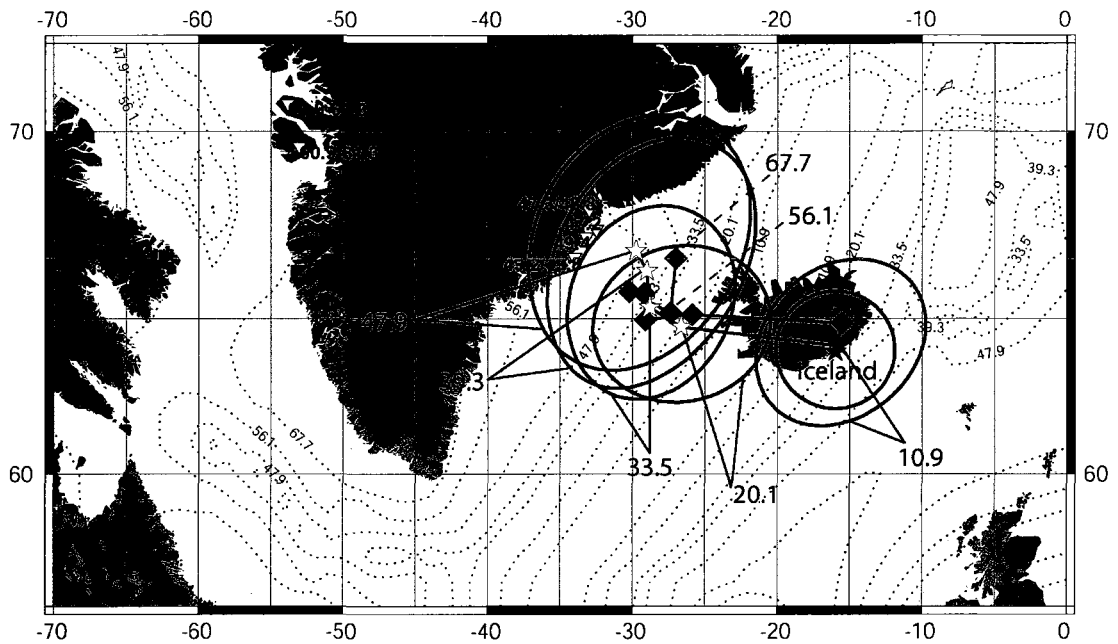


Figure 3.9. Predicted positions of the Iceland hotspot relative to the Eurasia plate for 10.9 Ma (blue star) and relative to the Greenland plate for older times (turquoise stars) assuming that the Iceland hotspot is stationary relative to the Hawaiian, Louisville, Tristan da Cunha and Réunion hotspots. Predicted positions assuming that the Réunion hotspot is stationary relative to the Pacific hotspots (black diamonds) are shown for a comparison (Chapter 2 of this thesis). Red inverted triangles accompanied with small numerals show locations of dated igneous rock samples with ages (See references in Table 3.1). Reconstructed points are made with the constraint that they always lay on a seafloor older than the reconstruction age. The black star shows the current location of Iceland hotspot (at 64°N , 344°E). Dotted lines are synthetic isochrons from Mueller et al. (2008) with ages (Ma) as labeled. All ages are in millions of years before present.

3.5 Discussion

Recently, Morgan and Morgan (2007) presented a model of current motions of the plates relative to the hotspots. They found no difference from the pole of non-Pacific hotspots and the pole using all the hotspot tracks and concluded that for the present-day motion, a single reference frame fits the entire world. In this work, we have shown that also for the past 48 million years, a globally self-consistent set of rotations can be found. All the hotspot frames of reference investigated herein (global, Pacific and Indo-Atlantic) agree

within the uncertainties for the past 48 million years. Small motions (up to $\approx 10 \text{ mm a}^{-1}$), however, are acceptable within the uncertainties.

An interesting implication of the model presented here is that it allows direct inferences of the plate motions relative to the hotspots. The model shows that, within the uncertainties, the Nubia and Somalia plates have remained stationary relative to the hotspots for the past ≈ 20 million years (Figs. 3.7 and 3.8), but that the plates have moved significantly relative to the hotspots since 30 Ma. Also, it was found that, within the uncertainties, the Eurasia plate has remained stationary relative to the hotspots for the past 48 million years (the predicted locations for Eurasia not shown in Fig. 3.9). Pacific plate has moved relative to the hotspots throughout the past 48 million years (Figs. 3.5 and 3.6).

3.6 Conclusions

It is possible to find a set of rotations of all plates relative to the hotspots for the past 48 million years that is both constrained to and consistent with known relative plate motions and is further consistent with fixed hotspots within uncertainties.

An uncertainty in the location of the reconstructed points of up to $\approx \pm 4^\circ$ (95 per cent confidence limits) is found. This allows up to $\approx 10 \text{ mm a}^{-1}$ of motion between hotspots within the uncertainties.

The new set of plate reconstructions presented here provide a firm basis for estimating absolute plate motions for the past 48 million years. They can be used to separate paleomagnetically determined apparent polar wander into the part due to plate

motion and the part due to true polar wander. Furthermore, they can be used to determine the net rotation of the lithosphere over the past 48 million years.

Tables

Table 3.1. Radiometric age dates used along the Hawaiian-Emperor, Louisville, Tristan da Cunha, Réunion and Iceland tracks.

HAWAII				
Age (Ma)	Lat (°N)	Lon (°E)	Source	Comments
0 ^{al}	19.6	204.5		At Kilauea
7.2	23.0	198.0	Darlympe et al. 1974	*
10.3	23.5	195.5	Darlympe et al. 1974	*
12	23.6	193.7	Darlympe et al. 1974	*
19.9	25.7	188.0	Darlympe et al. 1981	*
27.7	28.3	182.7	Darlympe et al. 1977	*
31	28.9	181.2	Sharp and Clague 2006	Unnamed seamount; Shield and postshield stage
38.7	30.9	175.9	Sharp and Clague 2006	Colahan seamount; Shield stage
41.5	31.8	174.3	Sharp and Clague 2006	Abbott seamount; Postshield stage
46.7	32.1	172.3	Sharp and Clague 2006	Diakakuji seamount; Postshield stage
47.9	33.7	171.6	Sharp and Clague 2006	Kimmei seamount; Shield stage
50.4	35.1	171.7	Sharp and Clague 2006	Koko (south); Shield stage
52.6	35.9	171.1	Sharp and Clague 2006	Koko (north); Rejuvenated
60.9	44.0	170.0	Sharp and Clague 2006	Suiko seamount; Postshield stage
49.2	34.9	172.2	Duncan and Keller 2004	Site 1206; Koko Seamount; Shield stage
55.5	41.3	170.4	Duncan and Keller 2004	Site 1205; Nintoku seamount; Shield stage
75.8	51.0	167.7	Duncan and Keller 2004	Site 1203; Detroit seamount; Shield stage
81	51.5	168.3	Keller et al. 1995	Detroit north
*Age dates for the younger part of the chain are not comparable in quality to the newer ages along the older part of the chain.				
LOUISVILLE				
Age (Ma)	Lat (°N)	Lon (°E)	Source	Comments
0 ^{al}	-50.9	221.9	Lonsdale 1988	
1.11	-50.4	220.9	Koppers et al. 2004	Sample MTHN-7D1
13.2	-48.2	211.2	Koppers et al. 2004	Sample MTHN-6D1
36.5	-41.6	195.8	Koppers et al. 2004	Sample VG-3a/MSN110-1; Valerie seamount
33.9	-40.8	194.7	Koppers et al. 2004	Sample VM36-02
45.5	-38.3	192.3	Koppers et al. 2004	Sample VM36-03
46.3	-37.0	190.2	Koppers et al. 2004	Sample VM36-04
61.4	-30.1	186.8	Koppers et al. 2004	Sample SOTW-9-48-2; Currituck seamount
68.9	-27.3	185.8	Koppers et al. 2004	Sample SOTW-9-52-1
76.7/78.7	-25.5	185	Koppers et al. 2004	Samples SOTW-9-58-1a and SOTW-9-58-7; Osbourn seamount

TRISTAN DA CUNHA

Age (Ma)	Lat (°N)	Lon (°E)	Source	Comments
0 ^{a)}	-37.5	347.5	O'Connor and le Roex 1992	On Tristan da Cunha island; best age estimate ranges 0.64-1.3 Ma
Walvis Ridge				
30*	-37.1	-7.8	O'Connor and Duncan 1990	Comments from O'Connor and Duncan (1990): Best estimate for the age of this site is 30-31 Ma
39-40	-34.3	-5.0	O'Connor and Duncan 1990	Best estimate for the crystallization age is 39-40 Ma
38-39	-34.5	-3.6	O'Connor and Duncan 1990	Best estimate for the age of this volcano is 38-39 Ma
46,52/~50**	-34.3	-1.6	O'Connor and Duncan 1990	Total fusion age of 52 Ma and plateau age of 46.2
64	-33.0	0.0	O'Connor and Duncan 1990	Apparent age of this sample is 64 Ma
50	-32.6	1.1	O'Connor and Duncan 1990	Questionable sample V29-9-1; we omit this age
61-62	-32.0	2.4	O'Connor and Duncan 1990	Crystallization age of this site is between 61-62 Ma
79	-29.1	3.0	O'Connor and Duncan 1990	Best estimate for the age of the basement is 79 Ma Best estimate of the crystallization age at this site is between 78-79 Ma
78-79	-28.5	2.3	O'Connor and Duncan 1990	
Min 69.8	-25.4	6.7	O'Connor and Duncan 1990	Questionable sample, minimum age provided

*concordant sample with 30 Ma average

**Baksi (1999) estimates ~50 Ma based on high temperature step ages

We omit the ages along the Gough Lineament

REUNION

Age (Ma)	Lat (°N)	Lon (°E)	Source	Comments
0 ^{a)}	-21.1	55.5	McDougall 1971	on Réunion Island
7.5	-21.0	57.5	Duncan and Hargraves 1990; McDougall 1971	
31.5*	-16.0	60.5	Duncan and Hargraves 1990	Industry well NB-1
33.2*	-13.1	61.4	Duncan and Hargraves 1990	ODP site 706
49.3*/50	-4.2	73.4	Duncan and Hargraves 1990	ODP site 713; Baksi (2005) estimates 50±2 Ma
57.2*	5.1	73.8	Duncan and Hargraves 1990	ODP site 715
~65.5	~20.0	~76.0	Hoffmann et al. 2000	Deccan traps, within 1 Ma

*age is the average of weighted isochron and plateau ages

ICELAND

Age (Ma)	Lat (°N)	Lon (°E)	Source	Comments
0 ^{a)}	64.0	344.0	Lawver and Muller 1994	

West Greenland

Storey et al. 1998 estimate that 80% of the lavas erupted between 60.9 and 61.3 Ma

East Greenland

49.4	67.3	-33.2	Tegner et al. 2008	Sample SA-1; Plateau age
47.2	67.5	-32.5	Tegner et al. 2008	Sample P-175; Total fusion age
49.2/49.8	66.7	-34.0	Tegner et al. 1998	Samples 416822 and 416804; Plateau and isochron age
47.3/48.8	68.0	-33.0	Tegner et al. 1998	Samples PCT-75 and KEH-302; Plateau ages

^{a)}Current location of the hotspot

Table 3.2. Locations and uncertainties used as input into the N-hotspot method. Azimuth is the azimuth of the major axis of the uncertainty ellipse associated with the input location.

HAWAII					
Age (Ma)	Lat (°N)	Lon (°E)	Major axis (km)	Minor axis (km)	Azimuth (CW from N)
0	19.6	204.5	100	100	0
10.9	23.7	195.6	200	100	-75
20.1	25.8	187.9	200	100	-80
33.5	29.5	179.5	200	100	-70
39.3	31.1	175.6	200	100	-70
47.9	33.7	171.6	200	100	-35
LOUISVILLE					
Age (Ma)	Lat (°N)	Lon (°E)	Major axis (km)	Minor axis (km)	Azimuth (CW from N)
0	-50.9	221.9	200	200	0
10.9	-48.6	213.0	300	100	-70
20.1	-46.3	204.3	300	100	-60
33.5	-40.9	195.0	300	100	-50
39.3	-39.6	193.6	300	100	-45
47.9	-36.3	189.8	300	100	-25
TRISTAN DA CUNHA					
Age (Ma)	Lat (°N)	Lon (°E)	Major axis (km)	Minor axis (km)	Azimuth (CW from N)
0	-37.5	347.5	150	150	0
10.9	-37.4	349.2	200	200	0
20.1	-37.2	350.7	200	200	0
33.5	-35.9	-6.2	200	150	45
39.3	-34.3	-4.0	200	150	45
47.9	-33.9	-2.6	200	150	55
REUNION					
Age (Ma)	Lat (°N)	Lon (°E)	Major axis (km)	Minor axis (km)	Azimuth (CW from N)
0	-21.1	55.5	200	200	0
10.9	-20.5	57.8	300	150	30
20.1	-19.2	58.6	400	150	35
33.5	-17.3	59.9	550	200	20
39.3	-16.5	60.4	550	200	15
47.9	-4.7	73.0	300	200	10
ICELAND					
Age (Ma)	Lat (°N)	Lon (°E)	Major axis (km)	Minor axis (km)	Azimuth (CW from N)
0	64.0	344.0	200	200	0
10.9	65.0	342.0	200	150	-65
20.1	66.0	335.5	200	150	-65
33.5	66.3	333.2	200	150	-65
39.3	66.5	332.2	200	150	-65
47.9	67.4	327.5	200	150	-65

Table 3.3. Preferred rotations used to quantify the global plate circuit in making the hotspot track predictions and to rotate the input data onto a common reference frame attached to the Pacific plate. pa refers to the Pacific plate, wa is the West Antarctica, ea East Antarctica, lw Lwandle, sm Somalia, nb Nubia, na North America, eu Eurasia, gr Greenland and in India plate. The ages are shown in the timescale of Cande and Kent (1995). The rotations for the plate pairs are given as motion of the first plate relative to the second.

Plate pair	Source age	Age (Ma)	Lat (°N)	Lon (°E)	Angle (°)	Source
pa-wa	C5n.2n(o)	10.9	70.36	-77.81	9.48	Croon et al. 2008
pa-wa	C6n(o)	20.1	74.00	-70.16	16.73	Croon et al. 2008
pa-wa	C13n(o)	33.6	74.48	-64.02	27.40	Croon et al. 2008
pa-wa	C18n.1n(y)	38.4	74.86	-56.21	31.41	Croon et al. 2008
pa-wa	C18n.2n(o)	40.1	74.87	-54.46	32.62	Croon et al. 2008
pa-wa	C20n(o)	43.8	74.78	-51.61	35.29	Croon et al. 2008
pa-wa	C21n(o)	47.9	74.52	-50.19	37.64	Cande et al. 1995
Plate pair	Source age	Age (Ma)	Lat (°N)	Lon (°E)	Angle (°)	Source
ea-wa	C8n.2n(o)	26.6	0.00	0.00	0.00	Cande et al. 2000
ea-wa	C13n(o)	33.5	-18.15	-17.85	-0.70	Cande et al. 2000
ea-wa	C20n(o)	43.8	-18.15	-17.85	-1.70	Cande et al. 2000
Plate pair	Source age	Age (Ma)	Lat (°N)	Lon (°E)	Angle (°)	Source
ea-lw	C5n.2n(o)	10.9	14.6	-49.1	1.53	Lemaux et al. 2002
ea-lw	C6n(o)	20.1	10.8	-46.0	2.70	Patriat et al. 2008
ea-lw	C13n(m)	33.3	16.2	-44.7	5.66	Patriat et al. 2008
ea-lw	C26n(o)	57.9	8.8	-42.6	10.83	Royer & Chang 1991
Plate pair	Polarity Chron	Age (Ma)	Lat (°N)	Lon (°E)	Angle/Ma (°/Ma)	Source
nb-lw	angular velocity vector		-37.20	-23.10	0.04	Horner-Johnson et al. 2007
lw-nb		30	-37.20	-23.10	1.20	
Plate pair	Source age	Age (Ma)	Lat (°N)	Lon (°E)	Angle (°)	Source
nb-na	C6n(m)	19.6	81.1	56.5	-5.21	McQuarrie et al. 2003
nb-na	C13n(m)	33.3	76.3	2.2	-9.96	McQuarrie et al. 2003
nb-na	C18n(m)	39.3	-74.8	177.1	12.48	McQuarrie et al. 2003
nb-na	middle of anomaly 20	43.2	-74.3	175.4	13.87	McQuarrie et al. 2003
nb-na	C21n(m)	47.1	73.7	-6.1	-15.46	McQuarrie et al. 2003
nb-na	C25n(m)	56.1	80.0	-0.7	-18.11	McQuarrie et al. 2003
Plate pair	Source age	Age (Ma)	Lat (°N)	Lon (°E)	Angle (°)	Source
na-eu	c5n.2n(o)	10.9	67.75	133.17	2.62	Merkouriev and DeMets 2008
na-eu	c6n(o)	20.1	68.62	131.76	5.03	Merkouriev and DeMets 2008
Plate pair	Source age	Age (Ma)	Lat (°N)	Lon (°E)	Angle (°)	Source
gr-na		35	0.00	0.00	0.00	Roest & Srivastava 1989
gr-na	C21n	48	62.80	-91.95	-2.61	Roest & Srivastava 1989
gr-na	C24n.3n	54	55.86	-104.55	-4.44	Roest & Srivastava 1989
Plate pair	Source age	Age (Ma)	Lat (°N)	Lon (°E)	Angle/Ma (°/Ma)	Source
sm-lw	angular velocity vector		-27.9	52.2	0.066	Horner-Johnson et al. 2007
lw-sm		30	-27.9	52.2	1.98	

Plate pair	Source age	Age (Ma)	Lat (°N)	Lon (°E)	Angle (°)	Source
sm-in	c5n.2n(o)	10.9	23.98	29.71	4.34	Demets et al. 2004
sm-in	c6n(o)	20.1	24.52	31.20	8.59	Demets et al. 2004
sm-in	c13n(m)	33.3	21.80	35.00	14.39	Royer & Chang 1991
sm-in	c21n(y)	46.3	18.64	43.37	22.56	Royer et al. 2002
sm-in	c22n(y)	49.0	18.94	39.62	23.20	Royer et al. 2002

Table 3.4. Covariance matrix values used for the relative plate motions. Covariance matrix values are given in the reference frame fixed to the second plate in the plate pair.

Plate pair	Used for	Source	Source	a	b	c	d	e	f	g
pa-wa	c5	c5	Croon et al. 2008	2.52	0.662	3.49	2.72	3.92	10.6	8
pa-wa	c6	c6	Croon et al. 2008	2.00	0.848	2.37	1.13	1.54	4.65	8
pa-wa	c13	c13	Croon et al. 2008	5.29	3.16	0.72	2.68	3.37	6.19	8
pa-wa	c18	c18	Croon et al. 2008	1.48	1.04	1.61	0.982	1.34	2.24	7
pa-wa	c21	c24	*	49.5	4.10	75.1	2.10	4.60	119	7
Plate pair	Used for	Source	Source	a	b	c	d	e	f	g
ea-wa	c13-c21	c13	Cande et al. 2000	2.19	0.0039	5.74	0.0041	0.0083	15.1	5
Plate pair	Used for	Source	Source	a	b	c	d	e	f	g
ea-lw	c5	c5	Lemaux et al. 2002	0.221	0.236	-0.092	0.304	-0.167	0.245	6
ea-lw	c6	c6	Patriat et al. 2008	1.028	0.883	-0.234	1.759	-1.347	2.237	6
ea-lw	c13	c13	Patriat et al. 2008	0.856	0.673	-0.166	0.690	-0.374	0.582	5
ea-lw	c18, c21	c26	Royer and Chang 1991	0.150	0.120	-0.090	0.110	-0.070	0.110	3
Plate pair	Used for	Source	Source	a	b	c	d	e	f	g
lw-nb	c5-c21	**	Horner-Johnson et al. 2007	73.116	49.887	-95.766	41.736	-67.68	132.657	8
Plate pair	Used for	Source	Source	a	b	c	d	e	f	g
nb-na	c5, c6	c6	***	0.5773	-0.4609	0.4223	0.4724	-0.3969	0.3577	5
nb-na	c13	c13	***	0.5686	-0.4835	0.433	0.5206	-0.434	0.3841	5
nb-na	c18	c18	***	0.1231	-0.1092	0.0959	0.1207	-0.0987	0.0884	4
nb-na	c21	c21	***	0.1119	-0.1155	0.0822	0.1484	-0.0991	0.0694	4
Plate pair	Used for	Source	Source	a	b	c	d	e	f	g
na-eu	c5	c5	Merkouriev and DeMets 2008	0.0779	-0.0133	0.0925	0.0572	-0.1141	0.2978	5
na-eu	c6	c6	Merkouriev and DeMets 2008	0.5661	-0.1278	0.6896	0.0758	-0.2358	0.9895	5
Plate pair	Used for	Source	Source	a	b	c	d	e	f	g
gr-na	c18, c21	c21	****	0.1574	-0.1967	0.3899	0.2499	-0.4923	0.9775	4
Plate pair	Used for	Source	Source	a	b	c	d	e	f	g
lw-sm	c5-c21	**	Horner-Johnson et al. 2007	65.004	63.732	-79.782	78.783	-80.493	114.321	8
Plate pair	Used for	Source	Source	a	b	c	d	e	f	g
sm-in	c21	c23	Royer & Chang 1991	42900	77300	19900	139400	35800	93000	7

*Personal communication with Stock 1997

**Extrapolated from the values for angular velocity vector

***Calculated from partial uncertainty rotations of McQuarrie et al. 2003

****Calculated from Acton's unpublished partial uncertainty rotations

$$\text{Covariance matrix} = \begin{pmatrix} a & b & c \\ b & d & e \\ c & e & f \end{pmatrix} \times 10^{-8} \text{ radians}^2$$

Table 3.5. Rotations and uncertainties of the Pacific plate relative to the hotspots as obtained using all the 5 hotspot tracks. ‘r’ is the sum squared normalized misfit. Input into the N-hotspot method is listed in Table 3.2 (initially picked uncertainties along the chains) and shown in Figs. 2a-e (shown with the full uncertainty as obtained after accumulating the uncertainties in relative plate motions through the circuit).

AGE (Ma)	Best-fit rotation				Covariance matrix values					
	Lat (°N)	Lon (°E)	Angle (°)	r	a	b	c	d	e	f
10.9	66.99	-76.59	9.48	5.03	0.0810	0.0197	-0.0211	0.0656	0.0226	0.1195
20.1	70.42	-72.44	16.89	7.06	0.0811	0.0371	-0.0153	0.1011	0.0427	0.1110
33.5	67.73	-69.00	26.22	1.82	0.1181	0.0357	-0.0287	0.0764	0.0069	0.0874
39.3	66.93	-63.03	29.67	2.25	0.1326	0.0510	-0.0225	0.0996	0.0201	0.0880
47.9	65.24	-63.43	34.07	6.07	0.1524	0.0311	0.0137	0.0722	0.0291	0.1589

$$\text{Covariance matrix} = \begin{pmatrix} a & b & c \\ b & d & e \\ c & e & f \end{pmatrix} \times 10^{-3} \text{ radians}^2$$

Table 3.6. Rotations of the Pacific plate relative to the hotspots as obtained using 4 hotspot tracks at a time (indicated which one is left out), using the three Indo-Atlantic tracks and using the two Pacific hotspot tracks. ‘r’ is the sum squared normalized misfit. Input into the N-hotspot method is listed in Table 3.2 (initially picked uncertainties along the chains) and shown in Figs. 2a-e (shown with the full uncertainty as obtained after accumulating the uncertainties in relative plate motions through the circuit).

Best-fit rotation				
AGE (Ma)	Lat (°N)	Lon (°E)	Angle (°)	r
Without Tristan da Cunha				
10.9	67.67	-73.22	9.46	4.52
20.1	70.57	-69.33	17.01	5.37
33.5	67.65	-69.33	26.25	1.78
39.3	66.53	-64.45	29.82	0.54
47.9	64.96	-66.33	34.12	1.57
AGE (Ma)	Lat (°N)	Lon (°E)	Angle (°)	r
Without Réunion				
10.9	68.00	-76.65	9.62	2.93
20.1	70.42	-71.05	17.07	4.09
33.5	67.76	-68.81	26.28	1.55
39.3	67.01	-63.08	29.66	2.22
47.9	65.23	-63.41	34.08	6.05
AGE (Ma)	Lat (°N)	Lon (°E)	Angle (°)	r
Without Iceland				
10.9	64.28	-75.25	9.38	4.00
20.1	70.48	-78.55	17.17	5.54
33.5	67.88	-71.52	26.42	0.69
39.3	67.13	-63.55	29.69	2.13
47.9	64.94	-63.46	34.08	5.45

AGE (Ma)	Lat (°N)	Lon (°E)	Angle (°)	r
Without Hawaii				
10.9	66.32	-80.74	8.65	2.67
20.1	69.58	-77.48	15.77	2.47
33.5	67.93	-68.76	26.23	1.76
39.3	67.84	-61.84	29.67	1.41
47.9	66.9	-60.27	35	1.97
AGE (Ma)	Lat (°N)	Lon (°E)	Angle (°)	r
Without Louisville				
10.9	66.01	-79.25	9.66	3.52
20.1	69.93	-70.99	16.87	6.49
33.5	67.18	-66.15	25.89	0.37
39.3	66.10	-60.27	29.37	1.15
47.9	64.53	-60.79	33.72	4.51
AGE (Ma)	Lat (°N)	Lon (°E)	Angle (°)	r
Indo-Atlantic hotspots				
10.9	65.46	-81.41	8.89	1.97
20.1	68.46	-73.19	15.35	1.34
33.5	67.13	-66.26	25.59	0.19
39.3	67.05	-59.90	29.18	0.61
47.9	67.46	-59.53	34.61	0.81
AGE (Ma)	Lat (°N)	Lon (°E)	Angle (°)	r
Pacific hotspots				
10.9	67.55	-66.85	9.56	1.50
20.1	70.55	-71.89	17.49	0.93
33.5	67.70	-73.53	26.58	0.04
39.3	66.77	-66.49	29.90	0.10
47.9	64.56	-67.99	34.29	0.005

Conclusions

In this thesis, a high-quality paleomagnetic pole for chron 32 (72 Ma), tests in inter-hotspot motion between the Pacific and Indo-Atlantic hotspots since 68 Ma and a globally self-consistent model of plate motions relative to the global hotspots for the past 48 million years are presented. The main results are as follows:

- (1) An updated paleomagnetic skewness pole for chron 32 (72 Ma) successfully corrects for the spreading-rate dependence of anomalous skewness (Dyment and Arkani-Hamed, 1995), a correction which hasn't been applied to Pacific skewness poles before. The results validate the model for spreading-rate-dependent anomalous skewness of Dyment and Arkani-Hamed (1995). Previously, anomalous skewness has been considered as one of the main factors limiting the accuracy of Pacific paleomagnetic poles determined from the skewness data. And thus, successfully correcting for the anomalous skewness, as was done in this study, significantly improves the reliability of the Pacific skewness poles.
- (2) The earlier assertions of a $13^{\circ} \pm 3^{\circ}$ (95 per cent confidence limit) southward shift of the Hawaiian hotspot relative to the spin axis since ≈ 72 Ma (Petronotis and Gordon, 1999) are strongly supported by the revised paleomagnetic pole determined using a spreading-rate-dependent correction for anomalous skewness.
- (3) Plate-circuit reconstructions from a new Pacific-hotspot motion model show that the Indo-Atlantic hotspots have had no significant motion relative to the Pacific hotspots

since 48 Ma. However, prior to 48 Ma, the apparent inter-hotspot drift rates increase to about $45\text{--}55 \pm 20 \text{ mm a}^{-1}$. Uncertainties allow some motion between Pacific and Indo-Atlantic hotspots (up to $\approx 10 \text{ mm a}^{-1}$) for the past 48 million years. Based on this study, however, the fixed hotspot approximation cannot be excluded.

(4) A possible cause for the pre-48 Ma apparent motion is a systematic error in the global plate circuits used to make the predictions. Potential candidate for the error is pre-48 Ma motion across Antarctica. If the observed discrepancy can be shown to correspond to an error in the plate circuit, the southward motion of the Hawaiian hotspot of 13° since ≈ 72 Ma can likely be attributed to true polar wander.

(5) As the motion between the Pacific and Indo-Atlantic hotspots is shown to be insignificant for the past 48 million years, a globally self-consistent model of plate motion relative to the global hotspots is presented to serve as a global hotspot frame of reference for the absolute plate motions, and true polar wander, for the past 48 million years. The data sets (Pacific and Indo-Atlantic) are consistent and the internally consistent plate motion model relative to the hotspots does not indicate major motion between the hotspots within the time span of the analysis.

Appendix A

SUPPLEMENTARY MATERIAL PACIFIC-HOTSPOT MODEL AND PLATE CIRCUIT CONSIDERATIONS

Pacific-hotspot models

Fig. A.1 shows both the Pacific-hotspot poles of rotation found in this study (Chapter 2), and the poles of Andrews et al. (2006) for comparison. The two sets of poles are somewhat similar. The biggest difference is to be seen for 20.1 Ma. Our 20.1 Ma pole moves closer (than the pole of Andrews et al. (2006)) to the rest of the poles for the past 50 million years. But, the 33.5 Ma pole, on the other hand, moves further away, breaking the general pattern Andrews et al. (2006) observed from 33.5 Ma to 47.9 Ma.

In this study, we have used an updated age progression along the Hawaiian-Emperor and Louisville tracks, the ages of Sharp and Clague (2006) and Duncan and Keller (2004) for the Hawaiian-Emperor track and the ages of Koppers et al. (2004) for the Louisville chain. In comparison, Andrews et al. (2006) relied on the age data of Watts et al. (1988) for the Louisville chain and while they used the updated ages of Sharp and Clague (2002) for the Hawaiian-Emperor chain, they didn't include the age data of Duncan and Keller (2004). It should be noted, though, that for the past 30 million years, the age data used along the Hawaiian-Emperor chain is the same for both sets of poles.

The new age data used in this study, in particular the significantly older ages for the oldest part of the Louisville chain, lead to a worse fit to Pacific hotspot tracks (Table 2.5) than found by Andrews et al. (2006). Koppers et al. (2004) reanalyzed the samples of Watts et al. (1988) used to establish the age progression along the Louisville trail and reported up to 10-12 Ma (15 %) older ages than originally proposed by Watts et al. (1988), within the oldest part of the track (other than this, the ages of Koppers et al. (2004) are similar to those estimated by Watts et al. (1988)). Furthermore, Duncan and Keller (2004) recently reported a new age of 75.8 Ma for the Detroit seamount (south) in the tip of the Emperor chain. Earlier 81 Ma has been reported and used for Detroit (this age is for Detroit north by Keller et al. (1995)).

Our large misfit for 56.1 Ma and 67.7 Ma (Table 2.5) might indicate southward motion of the Hawaiian hotspot relative to the Louisville hotspot (or northward motion of the Louisville hotspot relative to the Hawaiian hotspot). If we would, however, allow 100-150 km longer major axes for the uncertainty ellipses at the input locations for 56.1 Ma and 67.7 Ma, we would obtain an acceptable misfit at the 5 per cent significance level. Another option to consider is the current location of the Louisville hotspot. Here we take the current location to be at -50.9°N , 221.9°E (Lonsdale, 1988) at a seamount which is in the close vicinity of seamount with recent volcanism (dated 1.1 Ma by Koppers et al. (2004); 0.5 Ma by Watts et al. (1988)). This location is commonly used in Pacific-hotspot reconstructions. However, Louisville hotspot has not left an easily traceable track for the recent past and considerably different present-day locations have

been suggested (e.g. Morgan and Morgan, 2007; Epp, 1978; Wessel and Kroenke, 1997). Within all the suggested locations for Louisville, the misfit problem could be made to disappear simply by changing the current location of the hotspot.

For comparison, we tested how these changes in the Pacific-hotspot model affect the predicted tracks (Figs. A.2-4).

Choices for the plate circuit

Before making the final choices for our plate circuit rotations, we went through numerous published studies to find the most up-to-date rotations (preferably with uncertainty estimates) for each plate pair and tested how different available rotations would affect the final predicted positions. In general, the tests resulted in similar predicted positions than our preferred rotations and all the different predicted positions remained within the 95 per cent uncertainty limits of our preferred model. Thus, the choice between all these particular rotations available is arbitrary. Our preferred plate circuit is listed in Table 2.1 in Chapter 2 and Table A.1 herein lists the tests shown in this document.

In particular, we wanted to test how different estimates of motion within Africa (e.g. Royer et al., 2006; Horner-Johnson et al., 2007 etc.) change the predicted tracks. The exact timing of motion between the Nubia (West Africa) and Somalia (East Africa) plates is still an open question and the boundary between these two plates has not been fully resolved. The suggested existence of the Lwandle plate (Hartnady, 2002; Horner-Johnson et al., 2007) between the Nubia and Somalia plates adds to the puzzle. Horner-Johnson et al. (2007) found that their data is better fit assuming that two plates, not just the Somalia plate, spread away from the Antarctic plate east of the Andrew Bain Transform Complex. They refer to the eastern of the two plates as the Somalia plate and the western plate as the Lwandle plate. If this is the case, published rotations for “Africa-Antarctica” motion need to be used with caution as they may represent neither Nubia-Antarctic nor Somalia-Antarctic motion (Horner-Johnson et al., 2007), but may also possibly be estimates of Lwandle-Antarctic motion. Following the suggestion of Horner-Johnson et al. (2007), we account for the Lwandle plate. We have chosen to account for 30 million years of motion, as this is a likely end member for the timing of the motion (e.g. Burke, 1996). By incorporating the Lwandle plate, we take the estimates for East Antarctic-Africa motion (e.g. Royer and Chang, 1991; Molnar et al., 1988; Bernard et al., 2005) to represent East Antarctic-Lwandle motion because most of the data used to constrain these estimates of motion actually come from the portion of the Southwest Indian Ridge on the boundary of the East Antarctic and hypothesized Lwandle plates. Even if the Lwandle plate wouldn’t actually exist, this part of the Southwest Indian Ridge would in that case likely link East Antarctica directly to the Nubia plate (e.g. Patriat et al., 2008), not to the Somalia plate. We also tested how this scenario would play out (Figs. A.2-4) by neglecting the motion between the Nubia and Lwandle plates. As this boundary has earlier been believed to belong to Somalia and East Antarctica, we also tested how correcting for the motion between the Nubia and Somalia plates affects the predicted tracks.

In general, all the other choices for motion within Africa resulted in very similar predicted tracks (Figs. A.2-4) but if 30 million years of motion between the Nubia and Somalia plates was accounted for (the last option discussed above), the predicted tracks shifted $\sim 2^\circ$ further away from the observed tracks, thus resulting in poorer fit. However, it should be noted that we think this scenario is unlikely. Our preferred model accounts for the Lwandle plate, but in the other likely scenario of linking East Antarctica directly to Nubia, the predicted tracks are very close to our preferred model (Figs. A.2-4).

Our preferred rotations for describing the motion between East Antarctica and Africa are those of Royer and Chang (1991) for >33.3 Ma motion, combined with the rotation of Molnar et al. (1988) for c31. For the more recent past, we use the estimate of Lemaux et al. (2002) for c5 and the estimates of Patriat et al. (2008) for c6 and c13. The data used to constraint these rotations is superior to the data used by Royer and Chang (1991) for these times. For times > 33 Ma, our choices were between those listed above and the rotations of Bernard et al. (2005). The predicted positions from the rotations of Bernard et al. (2005) are very similar to our preferred rotations (Figs. A.2-4), but result in somewhat different predicted locations for 67.7 Ma, in particular for Iceland hotspot (Fig. A.4).

Sources for the other links in our preferred plate circuit are as follows: For Pacific-West Antarctica we use the rotations of Croon et al. (2008) for the past ≈ 44 Ma and a combination of the rotations of Cande et al. (1995) and Stock et al. (as listed in Eagles et al. (2004)) for older times. For the motion between East and West Antarctica, the best estimate up-to-date comes from Cande et al. (2000). For reconstructing Nubia relative to North America, we use the rotations of McQuarrie et al. (2003). And, for North America to Eurasia, we use the recent detailed study of Merkuriev and DeMets (2008) for c5 and c6, and rotations by McQuarrie et al. (2003) for earlier times (the predicted positions for c5 and c6 from the model of McQuarrie et al. (2003) would have been almost identical. Also, the rotations of Gaina et al. (2002) resulted in very similar predicted positions as our preferred model; these tests are not shown here). For the motion between Greenland and North America, we rely on the work of Roest and Srivastava (1989) and for reconstructing the India plate relative to the Somalia plate for the chrons c21, c25 and c31, a combination of rotations from Royer et al. (2002) and Molnar et al. (1988).

For the motion between Greenland and North America, we also tested the rotations of Gaina et al. (as listed in Torsvik et al. (2008)) and found that the predicted locations from their rotations are very close to the positions predicted from the rotations of Roest and Srivastava (1989) (Fig. A.5).

Predicted tracks

Tristan da Cunha

Fig. A.2 shows the different tests for Tristan da Cunha. All tests remain within the uncertainty limits of the preferred predicted positions. Biggest discrepancy (from the preferred model) is seen for the choice to account for Nubia-Somalia motion. This shifts the predicted track up to $\sim 2^\circ$ southward, further away from the observed track. The

predicted positions for the preferred model, and for neglecting the motion between the Nubia and Lwandle plates, are almost identical. Moreover, prior estimate of Royer et al. (2006) for the Nubia-Somalia motion (which also corresponds to Nubian-Lwandle motion when the Lwandle plate is introduced) since 11 Ma results in predicted positions very close to the positions obtained using the estimate of Horner-Johnson et al. (2007) for Nubian-Lwandle motion since 30 Ma (this test not shown here).

For Tristan da Cunha, the choice between our Pacific-hotspot rotations and those of Andrews et al. (2006) does not make much of a difference (Fig. A.1). Rotations of Andrews et al. (2006), however, result in predicted positions slightly closer to the Walvis Ridge.

Predicted positions from the East Antarctic-Africa rotations of Bernard et al. (2005) (for ages >33 Ma; for earlier times we use the same rotations for both models) are very similar to those of our preferred model.

Réunion

Fig. A.3 shows the tests for the Réunion hotspot. All the different rotations tested in the plate circuit resulted very similar predicted tracks for the Réunion hotspot.

Iceland

Figs. A.4 and A.5 show the tests for the Iceland hotspot. Fig. A.4 shows the different predicted positions of the Iceland hotspot relative to the Eurasia and Greenland plates. The preferred model is chosen relative to the Eurasian plate for 10.9 Ma and relative to the Greenland plate for later times, with the constraint that predicted positions always lay on seafloor older than the reconstruction age. As seen for Tristan da Cunha, accounting for Nubia-Somalia motion over the past 30 million years shifts the predicted track southwards. For Iceland, accounting for motion between the Nubia and Lwandle plates, and neglecting the motion, result in somewhat different predicted positions. Neglecting the motion shifts the pattern of the predicted positions more toward Iceland.

Our Pacific-hotspot poles of rotation and those of Andrews et al. (2006) result in similar tracks. The predicted positions of Andrews et al. (2006) are slightly closer to the observed track for 56.1 Ma and 67.7 Ma.

Use of the rotations of Bernard et al. (2005) for East Antarctic-Africa motion, instead of the rotations of Royer and Chang (1991) and Molnar et al. (1988) for > 33 Ma, results in slightly different predicted positions, in particular for 67.7 Ma (only shown relative to the Greenland plate in Fig. A.4), moving the predicted position ~130 km north-eastwards. The rotations of Gaina et al. (as listed in Torsvik et al. (2008)) for Greenland-North America don't change the predicted position much at all (Fig. A.5).

Figures

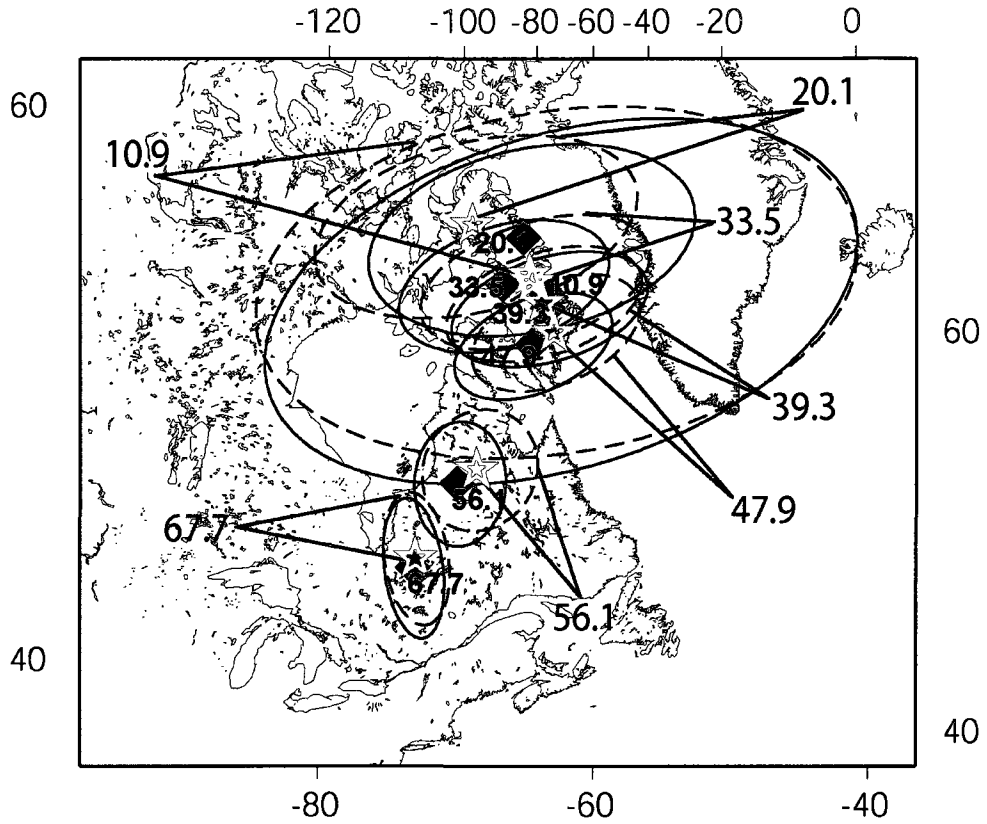


Figure A.1. Pacific-hotspot poles of rotation determined with the N-hotspot method (Andrews et al., 2006). Blue diamonds show pole locations found in this study with the use of updated age data (see Chapter 2 for more). Red stars show the poles of Andrews et al. (2006). Ellipses are the corresponding two-dimensional 95 per cent confidence regions.

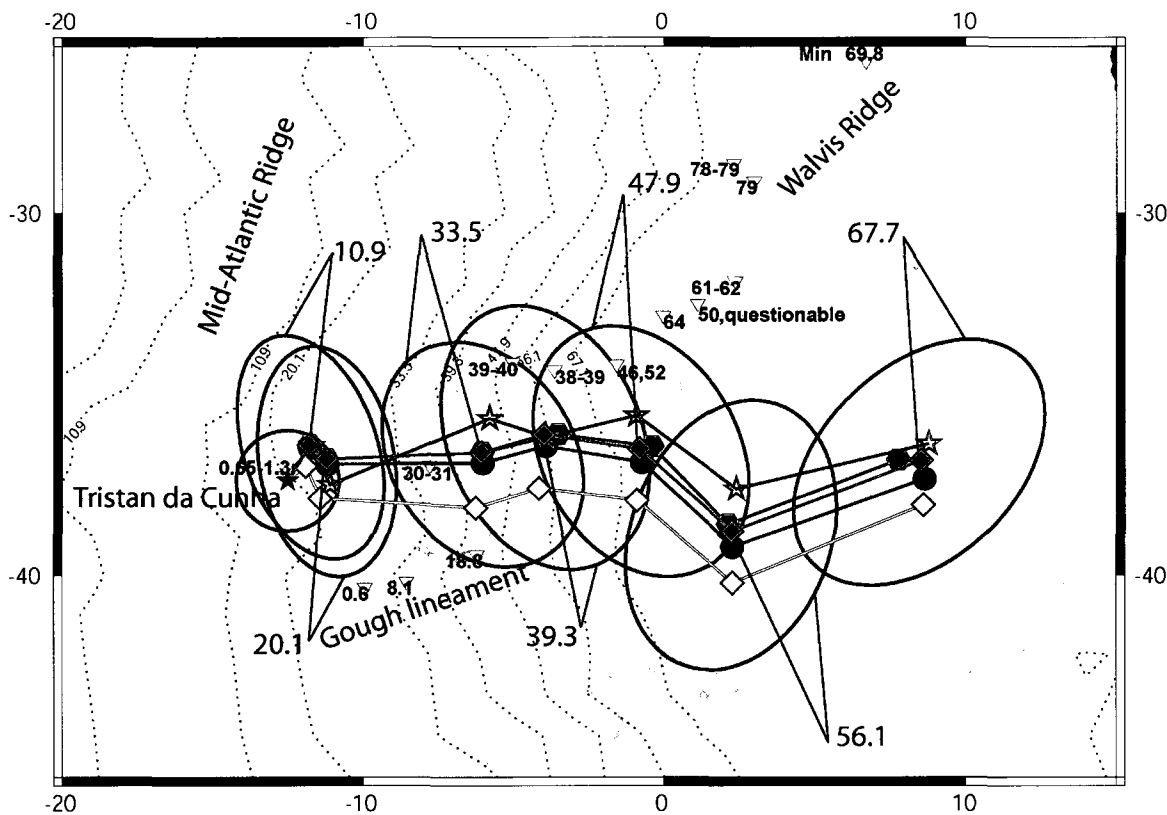


Figure A.2. Predicted positions of the Tristan da Cunha hotspot relative to the Nubia plate, for different relative plate motion models, assuming the Tristan da Cunha hotspot is stationary relative to Pacific hotspots. Blue diamonds show the preferred model (relative plate motion data used for the preferred model is listed in Table 2.1 in Chapter 2) with the updated Pacific-hotspot rotations and relative motion between the Nubia and Lwandle plates since 30 Ma (Horner-Johnson et al., 2007). Red diamonds show the predicted positions for relative motion between the Nubia and Somalia plates for the past 30 Ma (Horner-Johnson et al., 2007) and black circles for neglecting the motion between the Nubia and Lwandle (or Somalia) plates. Black hexagons with red outline test the East Antarctica-Somalia relative motion model of Bernard et al. (2005), otherwise, the same rotations as for the preferred model were used. Blue stars are otherwise the same as our preferred model, but, obtained with the Pacific-hotspot rotations from Andrews et al. (2006). Ellipses (two-dimensional 95 per cent confidence regions) show uncertainties for the preferred model propagated from the uncertainties in the motion of the Pacific plate relative to the Hawaiian and Louisville hotspots and relative plate motion uncertainties, combined with the uncertainty in the current position of the Tristan da Cunha hotspot. Inverted triangles show locations for age dates of O'Connor and Duncan (1990) and O'Connor and le Roex (1992) and the black star shows the current location of the Tristan da Cunha hotspot (at -37.5°N , 347.5°E). Dotted lines are synthetic isochrons from Mueller et al. (2008) with ages as labeled. All ages are in millions of years before present.

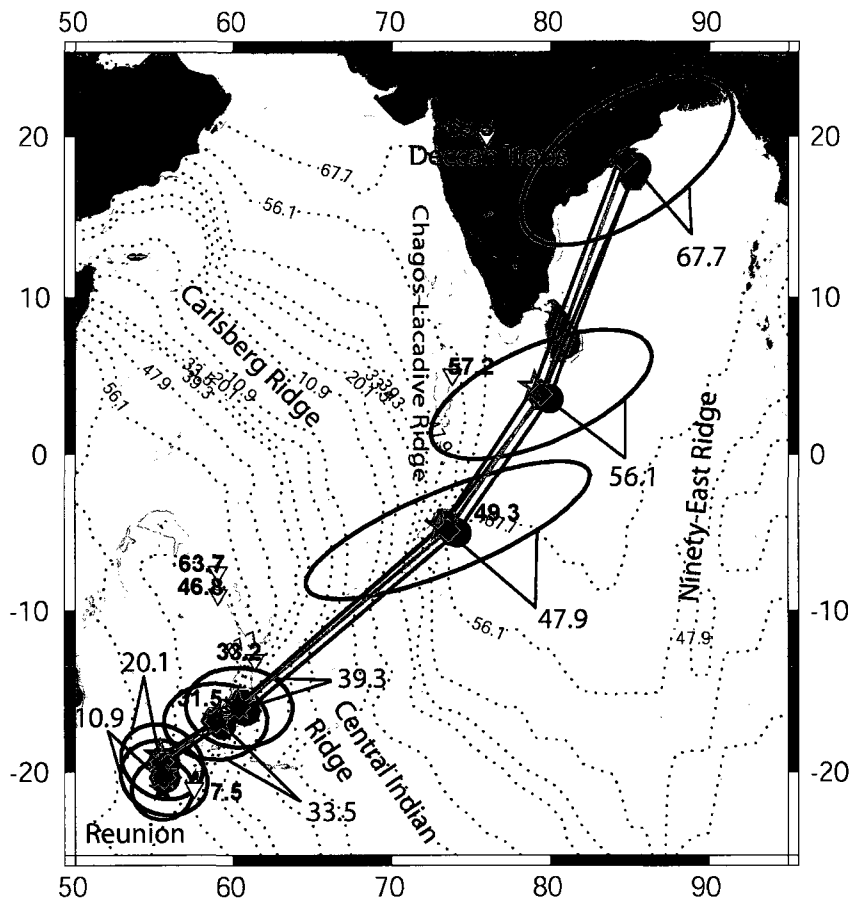


Figure A.3. Predicted positions of the Réunion hotspot relative to the Somalia plate for times 10.9 Ma through 39.3 Ma and relative to the India plate for older times assuming that the Réunion hotspot is stationary relative to Pacific hotspots. Blue diamonds show the preferred model (relative plate motion data used for the preferred model is listed in Table 2.1 in Chapter 2). Black circles are otherwise same but for neglecting motion within Africa. Black hexagons with red outline test the East Antarctica-Somalia relative motion model of Bernard et al. (2005). Otherwise, the same rotations as for the preferred model were used. Blue stars are otherwise the same as the preferred model but obtained with the Pacific-hotspot rotations from Andrews et al. (2006). Ellipses (two-dimensional 95 per cent confidence regions) show uncertainties propagated for the preferred model from the uncertainties in the motion of the Pacific plate relative to the Hawaiian and Louisville hotspots and relative plate motion uncertainties, combined with the uncertainty in the current position of the Réunion hotspot. Inverted triangles show locations for age dates of Duncan and Hargraves (1990). The black star shows the current location of the Réunion hotspot (at -21.1°N , 55.5°E). Dotted lines are synthetic isochrons from Mueller et al. (2008) with ages as labeled. All ages are in millions of years before present.

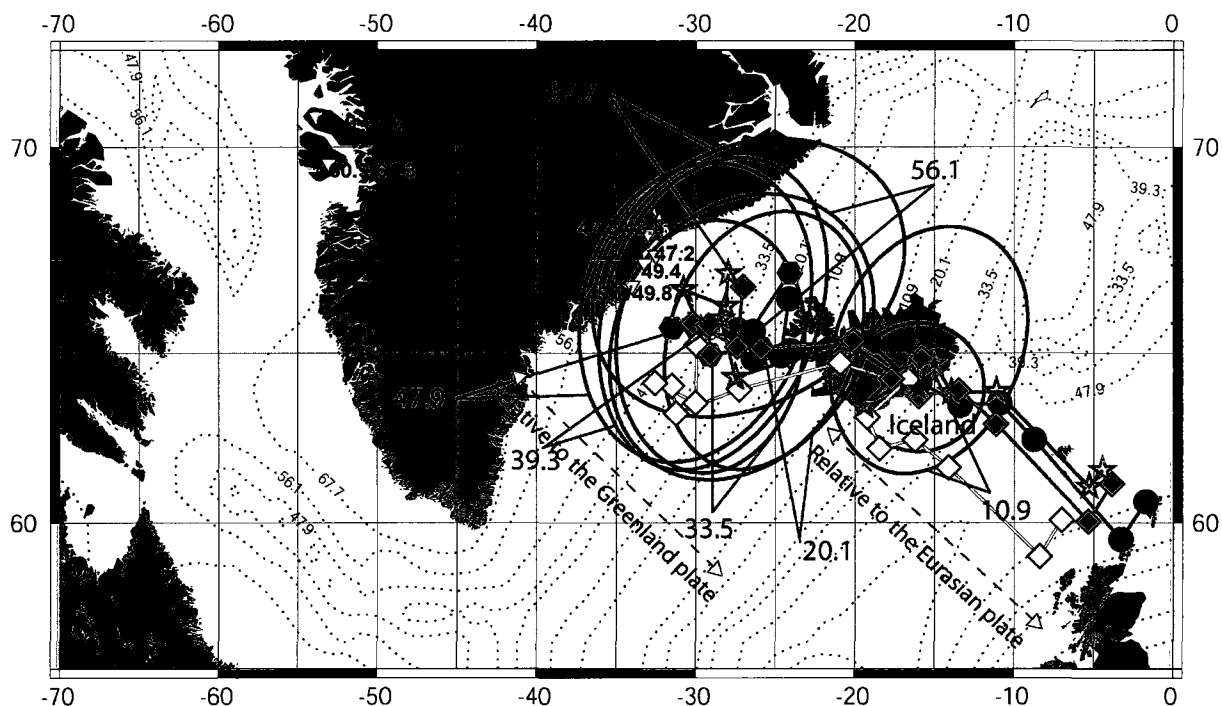


Figure A.4. Predicted positions of the Iceland hotspot relative to the Eurasia and Greenland plates for different relative plate motion models assuming that the Iceland hotspot is stationary relative to Pacific hotspots. Blue diamonds show the preferred model (relative plate motion data used for the preferred model is listed in Table 2.1 in Chapter 2) with the updated Pacific-hotspot rotations and relative motion between the Nubia and Lwandle plates since 30 Ma (Horner-Johnson et al., 2007). Red diamonds show the predicted positions for relative motion between Nubia and Somalia plates for the past 30 Ma (Horner-Johnson et al., 2007). Black circles are for neglecting motion between the Nubia and Lwandle (or Somalia) plates. Black hexagons with red outline test the East Antarctica-Somalia relative motion model of Bernard et al. (2005), otherwise, the same rotations as for the preferred model were used. Blue stars are otherwise the same as the preferred model but obtained with the Pacific-hotspot rotations from Andrews et al. (2006). Ellipses (two-dimensional 95 per cent confidence regions) show uncertainties propagated for the preferred model from elliptical uncertainties in the motion of the Pacific plate relative to the Hawaiian and Louisville hotspots and relative plate motion uncertainties, combined with the uncertainty in the current location of the Iceland hotspot. The preferred model is chosen relative to the Eurasian plate for 10.9 Ma and relative to the Greenland plate for later times, with the constraint that predicted positions always lay on seafloor older than the reconstruction age. The black star shows the current location of Iceland hotspot (at 64°N, 344°E). Inverted triangles show locations for age dates of Tegner et al (1998), Tegner et al. (2008) and Storey et al, (1998). Dotted lines are synthetic isochrons from Mueller et al. (2008) with ages as labeled. All ages are in millions of years before present.

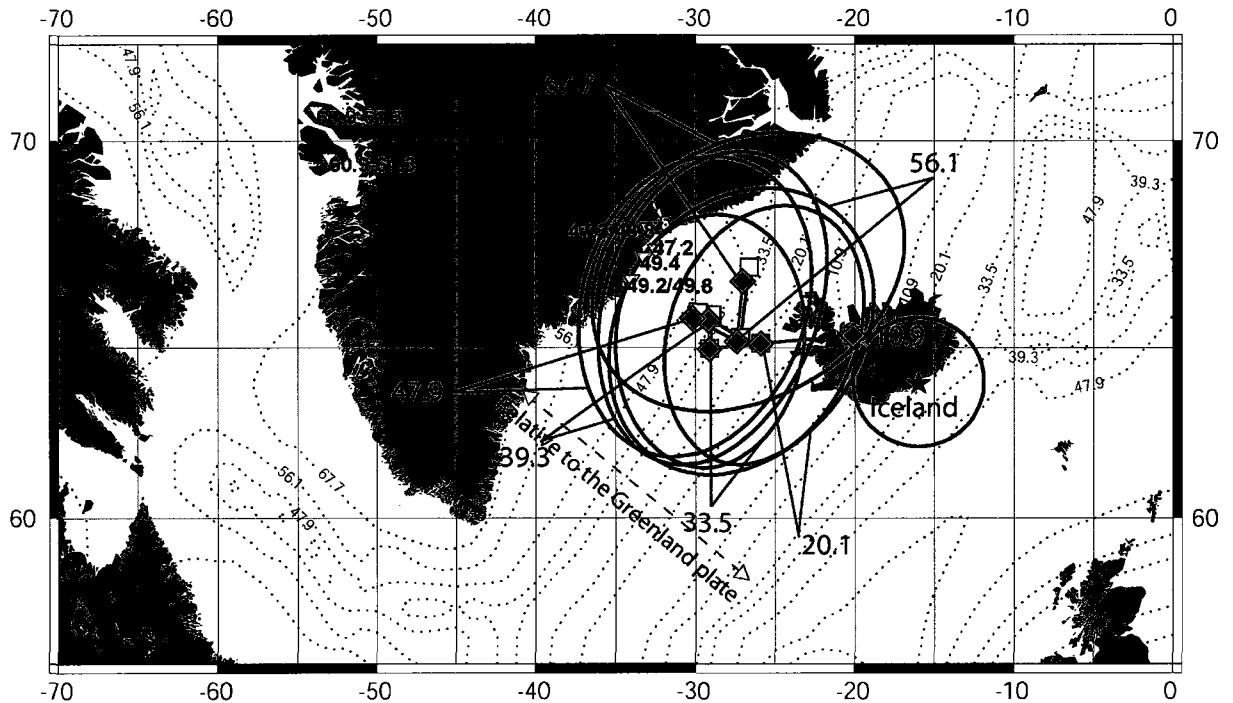


Figure A.5. Predicted positions of the Iceland hotspot relative to the Greenland plate for different relative plate motion models between North America and Greenland, and assuming that the Iceland hotspot is stationary relative to Pacific hotspots. Blue diamonds show the preferred model with the rotations of Roest and Srivastava (1989) for Greenland-North America motion. Green squares show otherwise the same but for the Greenland-North America relative motion model of Gaina et al. (as listed in Torsvik et al. (2008)). Ellipses (two-dimensional 95 per cent confidence regions) show uncertainties propagated for the preferred model from elliptical uncertainties in the motion of the Pacific plate relative to the Hawaiian and Louisville hotspots and relative plate motion uncertainties, combined with the uncertainty in the current location of Iceland hotspot (at 64° N, 344° E). Uncertainties are not shown for the 10.9 Ma predicted position on the Greenland plate because, for the preferred model, the predicted position is chosen to lie on the Eurasia plate, with the constraint that predicted positions always lay on seafloor older than the reconstruction age. Inverted triangles show locations for age dates of Tegner et al (1998), Tegner et al. (2008) and Storey et al. (1998). Dotted lines are synthetic isochrons from Mueller et al. (2008) with ages as labeled. All ages are in millions of years before present.

Tables

Table A.1. Alternative rotations used in the tests. pa refers to the Pacific plate, ha to the Pacific hotspot reference frame, ea East Antarctica, sm Somalia, lw Lwandle, nb Nubia, na North America and gr Greenland. Rotations for the plate pairs are given as motion of the first plate relative to the second. (y), (o), and (m), young and old ends and middle of Polarity Chron, respectively. Ages are given in the timescale of Cande and Kent (1995).

Plate pair	Polarity Chron	Age (Ma)	Lat (°N)	Lon (°E)	Angle (°)	Source
pa-hs	C5n.2n(o)	10.9	68.54	-69.85	9.61	Andrews et al. 2006
pa-hs	C6n(o)	20.1	70.52	-80.83	18.02	Andrews et al. 2006
pa-hs	C13n(o)	33.5	68.19	-69.26	25.80	Andrews et al. 2006
pa-hs	C18n(m)	39.3	67.03	-67.32	29.96	Andrews et al. 2006
pa-hs	C21n(o)	47.9	65.43	-65.30	33.95	Andrews et al. 2006
pa-hs	C25n(m)	56.1	57.01	-72.12	37.22	Andrews et al. 2006
pa-hs	reversed polarity interval between 30/31 (m)	67.7	51.36	-76.16	41.26	Andrews et al. 2006
Plate pair	Mag. An.	Age (Ma)	Lat (°N)	Lon (°E)	Angle (°)	Source
ea-af*	18o	40.1	13.6	-41.4	7.47	Bernard et al. 2005
ea-af*	23o	51.7	8.50	-40.8	10.01	Bernard et al. 2005
ea-af*	28	63.1	11.3	-49.6	11.11	Bernard et al. 2005
ea-af*	32y	71.1	-1.20	-42.4	12.38	Bernard et al. 2005
Plate pair	Source age	Age (Ma)	Lat (°N)	Lon (°E)	Angle/Ma (°/Ma)	Source
nb-lw	angular velocity vector		-37.2	-23.1	0.04	Horner-Johnson et al. 2007
lw-nb		30	-37.2	-23.1	1.2	
Plate pair	Source age	Age (Ma)	Lat (°N)	Lon (°E)	Angle/Ma (°/Ma)	Source
nb-sm	angular velocity vector		-37.0	27.1	0.092	Horner-Johnson et al. 2007
sm-nb		30	-37.0	27.1	2.76	
Plate pair	Source age	Age (Ma)	Lat (°N)	Lon (°E)	Angle/Ma (°/Ma)	Source
sm-lw	angular velocity vector		-27.9	52.2	0.066	Horner-Johnson et al. 2007
lw-sm		30	-27.9	52.2	1.98	
Plate pair		Age (Ma)	Lat (°N)	Lon (°E)	Angle (°)	Source
gr-na		33.1	0	0	0	**
gr-na		47.9	62.80	260.9	-2.80	**
gr-na		53.3	40.64	243.1	-3.62	**
gr-na		55.9	20.30	221.8	-3.00	**
gr-na		68.7	52.86	223.6	-6.28	**

*Depending on the model tested af refers to Lwandle, Nubian or Somalia

**Torsvik et al. 2008 from Gaina et al. (manuscript in preparation)

References

Acton, G. D., and R. G. Gordon (1991), A 65 Ma Palaeomagnetic pole for the Pacific Plate from the skewness of magnetic anomalies 27r-31, *Geophys. J. Int.*, 106, 407-420.

Acton, G. D., and R. G. Gordon (1994), Paleomagnetic tests of Pacific plate reconstructions and implications for motion between hotspots, *Science*, 263, 1246-1254.

Anderson, D. L. (2000), The thermal state of the upper mantle: no role for mantle plumes, *Geophys. Res. Lett.*, 27, 3623-3626.

Andrews, D. L., Gordon, R. G., and B. C. Horner-Johnson (2006), Uncertainties in plate reconstructions relative to the hotspots; Pacific-hotspot rotations and uncertainties for the past 68 million years, *Geophys. J. Int.*, 166, 939-951.

Arkani-Hamed, J. (1988), Remanent magnetization of the oceanic upper mantle, *Geophys. Res. Lett.*, 15, 48-51.

Arkani-Hamed, J. (1989), Thermoviscous remanent magnetization of oceanic lithosphere inferred from its thermal evolution, *J. Geophys. Res.*, 94, 17421-17436.

Baksi, A. K. (1999), Reevaluation of plate motion models based on hotspot tracks in the Atlantic and Indian Oceans, *Journal of Geology*, 107, 13-26.

Baksi, A. K. (2005), Evaluation of radiometric ages pertaining to rocks hypothesized to have been derived by hotspot activity, in and around the Atlantic, Indian and Pacific Oceans, in *Plates, plumes and paradigms*, *Geological Society of America Special Paper 388*, edited by G. R. Foulger, J. H. Natland, D. C. Presnall and D. L. Anderson, D.L., pp. 55-70, GSA, Boulder, Colorado.

Berggren, W. A., D. V. Kent, J. J. Flynn, and J. A. van Couvering (1985), Cenozoic geochronology, *Geol. Soc. Am. Bull.*, 96, 1407-1418.

Bernard, A., M. Munsch, Y. Rotstein, and D. Sauter (2005), Refined spreading history at the Southwest Indian Ridge for the last 96 Ma, with the aid of satellite gravity data, *Geophys. J. Int.*, 162, 765-778.

Beske-Diehl, S. J. (1989), Comment on "Magnetization of the oceanic crust: thermoremanent magnetization or chemical remanent magnetization?" by C. A. Raymond and J. R. LaBrecque, *J. Geophys. Res.*, 94, 3046-3048.

Blakely, R. J. and A. Cox (1972), Identification of short polarity events by transforming marine magnetic profiles to the poles, *J. Geophys. Res.*, 77, 4339-4349.

Blakely, R. J. (1976), An age-dependent, two-layer model for marine magnetic anomalies, in *The geophysics of the Pacific Ocean basin and its margin*, *Geophys. Monograph 19*, edited by G.H. Sutton, M.H. Manghnani, R. Moberly and E.U. McAfee, pp. 227-234, AGU, Washington, D. C.

Cande, S. C. (1976), A Palaeomagnetic Pole from Late Cretaceous Marine Magnetic Anomalies in the Pacific, *Geophys. J. R. Astr. Soc.*, 44, 547-566.

Cande, S.C. (1978), Anomalous behavior of the paleomagnetic field inferred from the skewness of anomalies 33 and 34, *Earth planet. Sci. Lett.*, 40, 275-286.

Cande, S. C., and D. Kent (1992), A new geomagnetic polarity time scale for the late Cretaceous and Cenozoic, *J. Geophys. Res.*, 97, 13,917-13,951.

Cande, S. C., and D. Kent (1995), Revised calibration of the geomagnetic polarity timescale for the Late Cretaceous and Cenozoic, *J. Geophys. Res.*, 100, 6093-6095.

Cande, S. C., E. M. Herron, and B. R. Hall (1982), The early Cenozoic tectonic history of the Southwest Pacific, *Earth Planet. Sci. Lett.*, 57, 63-74.

Cande, S. C., C. A. Raymond, J. Stock, and W. F. Haxby (1995), Geophysics of the Pitman fracture zone and Pacific-Antractic plate motions during the Cenozoic, *Science*, 270, 947-953.

Cande, S. C., J. M. Stock, R. D. Muller, and T. Ishihara (2000), Cenozoic motion between East and West Antarctica, *Nature*, 404, 145-150.

Cannat, M. (1993), Emplacement of mantle rocks in the seafloor at mid-ocean ridges, *J. Geophys. Res.*, 98, 4163-4172.

Chang, T. (1988), Estimating the relative motion of two tectonic plates from boundary crossings, *J. Am. Stat. Assoc.*, 83, 1178-1183.

Chang, T., J. Stock, and P. Molnar (1990), The rotation group in plate tectonics and the presentation of uncertainties of plate reconstructions, *Geophys. J. Int.*, 102, 649-661.

Clague, D. A., and R. D. Jarrard (1973), Tertiary Pacific plate motion deduced from the Hawaiian-Emperor Chain, *Geol. Soc. Am. Bull.*, 84, 1135-1154.

Courtillot, V., A. Davaille, J. Besse, and J. Stock (2003), Three distinct types of hotspots in the Earth's mantle, *Earth Planet. Sci. Lett.*, 205, 295-308.

Courtillot, V. E., and P. R. Renne (2003), On the ages of flood basalt events, *C. R. Geoscience*, 335, 113-140.

Croon, M. B., S. C. Cande, and J. M. Stock (2008), Revised Pacific-Antarctic plate motions and geophysics of the Menard Fracture Zone, *Geochem. Geophys. Geosyst.*, 9, Q07001, doi:10.1029/2008GC002019.

Dalrymple, G. B., M. A. Lamphere, and E. D. Jackson (1974), Contributions to the petrography and geochronology of volcanic rocks from the Leeward Hawaiian Island, *GSA Bull.*, 85, 727-738.

Dalrymple, G. B., D. A. Clague, and M. A. Lamphere (1977), Revisited age for Midway volcano, Hawaiian volcanic chain, *Earth Planet. Sci. Lett.*, 2, 107-116.

Dalrymple, G. B., D. A. Clague, M. O. Garcia, and S. W. Bright (1981), Petrology and K-Ar ages of dredged samples from Laysan Island and Northhampton Bank volcanoes,

Hawaiian Ridge, and evolution of the Hawaiian Emperor chain, Part II, *GSA Bull.*, 92, 315-318.

Duncan, R.A. (1981), Hotspots in the Southern oceans-an absolute frame of reference for motion of Gondwana continents, *Tectonophysics*, 74, 29-42.

Duncan, R. A. (1990), The volcanic record of the Réunion hotspot, *Proc. Ocean Drill. Program Sci. Results*, 115, 3-10.

Duncan, R. A., and R. B. Hargraves (1990), $^{40}\text{Ar}/^{39}\text{Ar}$ Geochronology of Basement Rocks from the Mascarene Plateau, The Chagos Bank, and the Maldives Ridge, *Proc. Ocean Drill. Program Sci. Results*, 115, 43-52.

Duncan, R. A., and R. A. Keller (2004), Radiometric ages for basement rocks from the Emperor Seamounts, ODP Leg 197, *Geochem. Geophys. Geosyst.*, 5, Q08L03, doi:10.1029/2004GC000704.

Dyment, J., S. C. Cande, and J. Arkani-Hamed (1994), Skewness of marine magnetic anomalies created between 85 and 40 Ma in the Indian Ocean, *J. Geophys. Res.*, 99, 24121-24134.

Dyment, J., and J. Arkani-Hamed (1995), Spreading-rate-dependent magnetization of the oceanic lithosphere inferred from the anomalous skewness of marine magnetic anomalies, *Geophys. J. Int.*, 121, 789-804.

Dyment, J., J. Arkani-Hamed, and A. Ghods (1997), Contribution of serpentinitized ultramafics to marine magnetic anomalies at slow and intermediate spreading centres: insights from the shape of the anomalies, *Geophys. J. Int.*, 129, 691-701.

Eagles, G., K. Gohl, and R. D. Larter (2004), High-resolution animated tectonic reconstruction of the South Pacific and West Antarctic Margin, *Geochem. Geophys. Geosyst.*, 5, Q07002, doi:10.1029/2003GC000657.

Engelbretson, D. C., A. Cox, and R. G. Gordon (1984), Relative motions between oceanic plates of the Pacific basin, *J. Geophys. Res.*, 89, 10291-10310.

Gaina, C., W. R. Roest, and R. D. Müller (2002), Late Cretaceous-Cenozoic deformation of northeast Asia, *Earth Planet. Sci. Lett.*, 197, 273-286.

Gordon, R. G. (1982), The late Maastrichtian palaeomagnetic pole of the Pacific plate, *Geophys. J. R. astr. Soc.*, 70, 129-140.

Harada, Y., and Y. Hamano (2000), Recent progress on the plate motion relative to hotspots, in *History and Dynamics of Global Plate Motions, AGU Monograph Series*, edited by M.A. Richards, R.G. Gordon and R.D. van der Hilst, pp. 327-338, AGU, Washington, D. C.

Harland, W. B., A. V. Cox, P. G. Llewellyn, C. A. G. Pickton, A. G. Smith, and R. Walters (1982), *A geologic time scale*, Cambridge University Press, New York, 128pp.

Harrison, C. G. A. (1987), Marine magnetic anomalies—the origin of the stripes, *Annu. Rev. Earth planet. Sci.*, 15, 505-543.

Hartnady, C. J. H. (2002), Earthquake hazard in Africa: Perspectives on the Nubia-Somalia boundary, *South. Afr. J. Sci.*, 98, 425-428.

Hellinger, S. J. (1981), The uncertainties of finite rotations in plate tectonics, *J. Geophys. Res.*, 86, 9312-9318.

Hofmann, C., G. Feraud, and V. Courtillot (2000), $^{40}\text{Ar}/^{39}\text{Ar}$ dating of minerals separates and whole rocks from the Western Ghats lava pile: Further constraints on the duration and age of the Deccan Traps, *Earth Planet. Sci. Lett.*, 180, 13-27.

Horner-Johnson, B. C., R. G. Gordon, and D. F. Argus (2007), Plate kinematic evidence for the existence of a distinct plate between the Nubian and Somalian plates along the Southwest Indian Ridge, *J. Geophys. Res.*, 112, B05418, doi:10.1029/2006JB004519.

Kirkwood, B. H., J. Y. Royer, T. C. Chang, and R. G. Gordon (1999), Statistical tools for estimating and combining finite rotations and their uncertainties, *Geophys. J. Int.*, 137(2), 408-428.

Keller, R., R. Duncan, R., and M. Fisk (1995), Geochemistry and $^{40}\text{Ar}/^{39}\text{Ar}$ geochronology of basalts from ODP Leg 145 (North Pacific Transect), *Proc. Ocean Drill. Program Sci. Results*, 145, 333-344.

Koppers, A. A., R. A. Duncan, and B. Steinberger, (2004), Implications of a nonlinear $^{40}\text{Ar}/^{39}\text{Ar}$ age progression along the Louisville seamount trail for models of fixed and moving hotspots, *Geochem. Geophys. Geosyst.*, 5, Q06L02, doi:10.1029/2003GC000671.

Larsen, L. M., A. K. Pedersen, G. K. Pedersen, and S. Piasecki (1992), Timing and duration of Early Tertiary volcanism in the North Atlantic: New evidence from West Greenland, in *Magmatism and the causes of continental break-up*, *Geological Society of London Special Publication 68*, edited by B. Storey et al., pp. 321-333.

Lawver, L. A. and R. D. Müller (1994), Iceland hotspot track, *Geology*, 22, 311-314.

Lemaux, J., R. G. Gordon, and J.-Y. Royer (2002), Location of the Nubia-Somalia boundary along the Southwest Indian Ridge, *Geology*, 30, 339-342.

Lonsdale, P. (1988), Geography and History of the Louisville Hotspot Chain in the Southwest Pacific, *J. Geophys. Res.*, 93, 3078-3104.

McDougall, I. (1971), The geochronology and evolution of the young oceanic island of Réunion, Indian Ocean, *Geochim. Cosmochim. Acta*, 35, 261-170.

McQuarrie, N., J. M. Stock, C. Verdel, and B. P. Wernicke (2003), Cenozoic evolution of Neotethys and implications for the causes of plate motions, *Geophys. Res. Lett.*, 30, 2036, doi:10.1029/2003GL017992.

Merkouriev, S., and C. DeMets (2006), Constraints on Indian plate motion since 20 Ma from dense Russian magnetic data: Implications for Indian plate dynamics, *Geochem. Geophys. Geosyst.*, 7, Q02002, doi:10.1029/2005GC001079.

Merkouriev, S. and C. DeMets (2008), A high-resolution model for Eurasia-North America plate kinematics since 20 Ma, *Geophys. J. Int.*, 173, 1064-1083.

Mihalfy, P., B. Steinberger, and H. Schmeling (2008), The effect of the large-scale mantle flow field on the Iceland hotspot track, *Tectonophysics*, 447, 5-18.

Molnar, P., F. Pardo-Casas, and J. Stock (1988), The Cenozoic and Late Cretaceous evolution of the Indian Ocean Basin: uncertainties in the reconstructed positions of the Indian, African and Antarctic plate, *Basin Research*, 1, 23-40.

Molnar, P., and J. M. Stock (1985), A method for bounding uncertainties in combined plate reconstructions, *J. Geophys. Res.*, 90(B14), 12,537-12,544.

Molnar, P., and J. M. Stock (1987), Relative motions of hotspots in the Pacific, Atlantic and Indian Oceans since late Cretaceous time, *Nature*, 327, 587-591.

Morgan, W. J. (1971a), Convection plumes in the lower mantle, *Nature*, 230, 42.43.

Morgan, W. J. (1971b), Plate motions and deep mantle convection, *Geol. Soc. Am. Mem.*, 132, 7-22.

Morgan, W. J. (1978), Rodriguez, Darwin, Amsterdam..., A second type of hot spot island, *J. Geophys. Res.*, 83, 5355-5360.

Morgan, W. J., and J. P Morgan (2007), Plate velocities in the hotspot reference frame, in *Plates, plumes, and planetary processes*, *Geological Society of America Special Paper 430*, edited by G. R. Foulger and D. M. Jurdy, pp. 65-78, GSA, Boulder, Colorado.

Müller, R. D., J.-Y. Royer, and L. A. Lawver (1993), Revised plate motions relative to the hotspots from combined Atlantic and Indian ocean hotspot tracks, *Geology*, 21, 275-278.

Müller, R. D., W. R. Roest, J.-Y. Royer, L. M. Gahagan, and J. G. Sclater (1997), Digital Isochrons of the World's Ocean Floor. *J. Geophys. Res.*, 102, 3211-3214.

Müller, R. D., M. Sdrolias, C. Gaina, and W. R. Roest (2008), Age, spreading rates, and spreading asymmetry of the world's ocean crust., *Geochem. Geophys. Geosyst.*, 9, Q04006, doi:10.1029/2007GC001743.

O'Conner, J. M., and R. A. Duncan (1990), Evolution of the Walvis Ridge-Rio Grande Rise Hot Spot System: Implications for African and South American Plate Motions Over Plumes, *J. Geophys. Res.*, 95, 17,475-17,502.

O'Connor, J.M., and A. P. le Roex (1992), South Atlantic hot spot-plume systems: 1. Distribution of volcanism in time and space, *Earth Planet. Sci. Lett.*, 113, 343-364.

O'Neill, C., D. Müller, and B. Steinberger (2005), On the uncertainties in hot spot reconstructions and the significance of moving hot spot reference frames, *Geochem. Geophys. Geosyst.*, 6, Q04003, doi:10.1029/2004GC000784.

Patriat, P., H. Sloan, and D. Sauter (2008), From slow to ultraslow: A previously undetected event at the Southwest Indian Ridge at ca. 24 Ma, *Geology*, 36, 207-210.

Petronotis, K. P., and R. G. Gordon (1989), Age dependence of skewness of magnetic anomalies above seafloor formed at the Pacific-Kula spreading center, *Geophys. Res. Lett.*, 16, 315-318.

Petronotis, K. E., and R. G. Gordon (1999), A Maastrichtian palaeomagnetic pole for the Pacific plate from a skewness analysis of marine magnetic anomaly 32, *Geophys. J. Int.*, 139, 227-247.

Petronotis, K. P., R. G. Gordon, and G. D. Acton (1992), Determining palaeomagnetic poles and anomalous skewness from marine magnetic anomaly skewness data from a single plate, *Geophys. J. Int.*, 109, 209-224.

Petronotis, K. E., R. G. Gordon, and G. D. Acton (1994), A 57 Ma Pacific plate palaeomagnetic pole determined from a skewness analysis of crossings of marine magnetic anomaly 25r, *Geophys. J. Int.*, 118, 529-554.

Raymond, C. A., and J. L. LaBrecque (1987), Magnetization of the oceanic crust: thermoremanent magnetization or chemical remanent magnetization?, *J. Geophys. Res.*, 92, 8077-8088.

Raymond, C. A., J. M. Stock, and S. C. Cande (2000), Fast Paleogene motion of the Pacific hotspots from revised global plate circuit constraints, in *History and Dynamics of Global Plate Motions, AGU Monograph Series*, edited by M.A. Richards, R.G. Gordon and R.D. van der Hilst, pp. 359-376, AGU, Washington, D. C.

Renne, P. R., M. Ernesto, I. G. Pacca, R. S. Coe, J. Glen, M. Prevot, and M. Perrin (1992), The age of Parana flood volcanism, rifting of Gondwanaland, and the Jurassic-Cretaceous boundary, *Science*, 258, 975-979.

Renne, P. R., J. M. Glen, S. C. Milner, and R. A. Duncan (1996), Age of Etendeka flood volcanism and associated intrusions in southwestern Africa, *Geology*, 24(7), 659-662.

Roest, W. R., and S. P. Srivastava (1989), Sea-floor spreading in the Labrador Sea: A new reconstruction, *Geology*, 17, 1000-1003.

Roest, W. R., J. Arkani-Hamed, and J. Verhoef (1992), The sea-floor spreading rate dependence of the anomalous skewness of marine magnetic anomalies, *Geophys. J. Int.*, 109, 653-669.

Rosa, J., and P. Molnar (1988), Uncertainties in reconstructions of the Pacific, Farallon, Vancouver, and Kula plates and constraints on the rigidity of the Pacific and Farallon (and Vancouver) plates between 72 and 35 Ma, *J. Geophys. Res.*, 93, 2997-3008.

Royer, J.-Y., and T. Chang (1991), Evidence for Relative Motions Between the Indian and Australian Plates During the Last 20 m.y. From Plate Tectonic Reconstructions: Implications for the Deformation of the Indo-Australian Plate, *J. Geophys. Res.*, 96, 11,779-11,802.

Royer, J.-Y., A. K. Chaubey, J. Dymant, G. C. Bhattacharya, K. Srinivas, V. Yatheesh, and T. Ramprasad (2002), Paleogene plate tectonic evolution of the Arabian and Eastern Somali basins, in *The tectonic and climatic evolution of the Arabian Sea Region*, edited by P. D. Clift, pp. 7-24, Geological Society of London.

Royer, J.-Y., R. G. Gordon, and B. C. Horner-Johnson (2006), Motion of Nubia relative to Antarctica since 11 Ma: Implications for Nubia-Somalia, Pacific-North America, and India-Eurasia motion, *Geology*, 34, 501-504.

Schouten, H., and K. McCamy (1972), Filtering marine magnetic anomalies, *J. Geophys. Res.*, 77, 7089-7099.

Schouten, H., and S. C. Cande (1976), Palaeomagnetic poles from marine magnetic anomalies, *Geophys. J. R. Astr. Soc.*, 44, 567-575.

Sharp, W. D., and D. A. Clague (2006), 50-Ma Initiation of Hawaiian-Emperor Bend Records Major Change in Pacific Plate Motion, *Science*, 313, 1281-1284.

Steinberger, B., R. Sutherland, and R. J. O'Connell (2004), Prediction of Emperor-Hawaii seamount locations from a revised model of global plate motion and mantle flow, *Nature*, 430, 167-173.

Stock, J., and P. Molnar (1988), Uncertainties and implications of the late Cretaceous and Tertiary position of North America relative to the Farallon, Kula, and Pacific plates, *Tectonics*, 7, 1339-1384.

Storey, M., R. A. Duncan, and C. Tegner (2007), Timing and duration of volcanism in the North Atlantic Igneous Province: Implications for geodynamics and links to the Iceland hotspot, *Chem. Geol.*, 241, 264-281.

Tegner, C., R. A. Duncan, S. Bernstein, C. K. Brooks, D. K. Bird, and M. Storey (1998) $^{40}\text{Ar}/^{39}\text{Ar}$ geochronology of Tertiary mafic intrusions along the East Greenland rifted margin: Relation to flood basalts and the Iceland hotspot track, *Earth Planet. Sci. Lett.*, 156, 75-88.

Tegner, C., C. K. Brooks, R. A. Duncan, L. E. Heister, and S. Bernstein (2008), $^{40}\text{Ar}/^{39}\text{Ar}$ ages of intrusions in East Greenland: Rift-to-drift transition over the Iceland hotspot, *Lithos*, 101, 480-500.

Torsvik, T. H., R. Van der Voo, J. G. Meert, J. Mosar, and H. J. Walderhaug (2001), Reconstructions of the continents around the North Atlantic at about the 60th parallel. *Earth Planet. Sci. Lett.*, 187, 55-69.

Torsvik, T. H., R. D. Müller, R. Van der Voo, B. Steinberger, C. Gaina (2008), Global plate motion frames: Toward a unified model, *Rev. Geophys.*, 46, RG3004, doi:10.1029/2007RG000227.

Vink, G. E. (1984), A hotspot model for Iceland and the Vøring Plateau, *J. Geophys. Res.*, 89, 9949-9959.

Watts, A. B., R. A. Weissel, R. A. Duncan, and R. L. Larson (1988), The origin of Louisville Ridge and its relationship to the Eltanin fracture zone system, *J. Geophys. Res.*, 93, 3051-3077.

Wessel, P., and L. W. Kroenke (1997), A geometric technique for relocating hotspots and refining absolute plate motions, *Nature*, 387, 365-369.

Wessel, P., and L. W. Kroenke (2008), Pacific absolute plate motion since 145 Ma: An assessment of the fixed hot spot hypothesis, *J. Geophys. Res.*, 113, B06101, doi:10.1029/2007JB005499.

Wessel, P., Y. Harada, and L. W. Kroenke (2006), Towards a self-consistent high-resolution absolute plate motion model for the Pacific, *Geochem. Geophys. Geosyst.*, 7, Q03L12, doi:10.1029/2005GC001000.

Whittaker, J. M., R. D. Müller, G. Leitchenkov, H. Stagg, M. Sdrolias, C. Gaina, A. Goncharov (2007), Major Australian-Antractic plate reorganization at Hawaiian-Emperor Bend Time, *Science*, 318, 83-86.